ABSTRACT

Title of Document: LINEAR AND NON-LINEAR FREQUENCY DOMAIN TECHNIQUES FOR PROCESSING IMPACT ECHO SIGNALS TO EVALUATE DISTRIBUTED DAMAGE IN CONCRETE.

Nicolas McMorris, Doctor of Philosophy, 2009

Directed By: Professor, Amde M. Amde, Department of Civil and Environmental Engineering

The condition evaluation of in-situ concrete with non-destructive testing is difficult at best. The concrete deterioration processes of alkali-silica reaction (ASR), delayed ettringite formation (DEF) and freeze-thaw cycles all produce distributed damage in the form of micro-cracking which results in loss of strength or stiffness. Presently, a suitable field applicable method for determining the degree of micro-cracking does not exist. The impact echo test is potentially the best candidate if improvements can be made in the signal processing techniques which are crucial for accurately interpreting the data retrieved from concrete with distributed damage.

In this research, two batches of concrete specimens were prepared in accordance with standard procedures. A portion of each batch was subjected to either the Modified Duggan cycle or to Freeze Thaw cycles, both proven methods of inducing DEF and micro-cracking respectively. Curing techniques and materials were also chosen to accelerate distributed damage in the concrete specimens. In addition to

the impact echo, a number of secondary tests were employed to monitor the progress of distributed damage in the concrete specimens.

Previous research efforts utilizing the impact echo method have attempted to characterize damage in terms of P-wave attenuation or pulse velocity. This involves signal processing in the time domain. These are inherently linear dynamics methods whereas the development of micro-cracks in concrete, an inhomogeneous material, gives rise to non-linear dynamics. Non-linear approaches to signal processing in the frequency domain are proposed herein. One involves calculating the deviation of the peak of the response spectrum from the shape of an ideal Lorentzian function model. The other calculates the second order non-linear harmonic coefficient.

The results showed that the potassium content, the curing methods and the Duggan and Freeze Thaw cycles had the desired effect of inducing distributed damage. The results of the signal processing of the impact echo data yielded more reasonable results for the specimens subjected to Freeze Thaw testing than for the specimens subjected to the Duggan Cycle. The results of the Freeze Thaw specimens suggest that the non-linear analysis of impact echo signals is capable of accurately quantifying distributed damage in concrete.

LINEAR AND NON-LINEAR FREQUENCY DOMAIN TECHNIQUES FOR PROCESSING IMPACT ECHO SIGNALS TO EVALUATE DISTRIBUTED DAMAGE IN CONCRETE.

By

Nicolas McMorris

Dissertation submitted to the Faculty of the Graduate School of the
University of Maryland, College Park, in partial fulfillment
of the requirements for the degree of
Doctor of Philosophy
2009

Advisory Committee:
Professor Amde M. Amde, Chair
Professor Mohamad S. Aggour
Professor Sung Lee
Dr. Chung C. Fu
Dr. Yunfeng Zhang

© Copyright by
Nicolas McMorris
2009

Dedication

To Michael and Mary, and Nakia and Nasir.

Acknowledgements

I would like to thank Professor Amde, my advisor, for his thorough supervision of my work. I would also like to thank Dr. Richard Livingston for the insight and time he contributed to this research. I would like to thank Dr. Jorgormai Ceesay and Cintia Lijeron for their contributions during this research. Also, I would like to thank the people at the FHWA Turner Fairbank Highway Research Facility in Mclean, Virginia, especially Jussara Tanesi and Clay Ormsby.

Thank You.

Table of Contents

List of Tables

List of Figures

Chapter 1: Introduction

1.1 Problem Statement

To be sure, the non-destructive determination of deterioration in in-situ concrete is difficult at best. The concrete deterioration processes of alkali-silica reaction (ASR), delayed ettringite formation (DEF) and freeze-thaw cycles all produce distributed damage in the form of micro-cracking which results in loss of strength or stiffness. Replacing or repairing, and maintaining such concrete is costly and will incur delays in access to and use of such structures. Presently, a suitable field applicable method for determining the degree of micro-cracking does not exist. The potential benefits that non-destructive testing holds for filling this void, pardon the pun, are incalculable.

Many researchers consider the impact echo test as the best overall technique presently available for achieving this goal because it is robust, one sided and yields a good signal to noise ratio. Currently, commercial interests have pioneered the use of impact echo for myriad of uses. However, the state of art, especially concerning signal processing, still needs to be improved if the impact echo method is to be used to achieve this goal.

Previous research utilizing the impact-echo method has characterized the damage in terms of changes in the attenuation factor, or pulse velocity, which are obtained by processing the signal in the time domain. However, these are inherently linear dynamics method while the development of micro-cracks gives rise to nonlinear dynamics. In recent years non-linear acoustic techniques have been

successfully employed for the assessment of cracks and damage in metals. The results of these assessments have demonstrated that non-linear acoustics is more sensitive than linear ultrasonics for monitoring the development of damage.

1.2 Background

This research stems from a previous research effort that was focused on Delayed Ettringite Formation (DEF) as the primary source of distributed damage. The present research seeks to encapsulate other sources of damage while developing signal processing techniques for the impact echo method to accurately quantify distributed damage as a whole.

Delayed ettringite formation (DEF) is a term used to describe a physicochemical process that may lead to the premature deterioration of concrete. Concrete deterioration due to delayed ettringite formation and alkali silica reactions have been identified as a cause of premature cracking and deterioration in concrete structures in many parts of the world since the early 1980's. This distributed damage mechanism is a matter of controversy among researchers. Many contrasting hypotheses have been suggested for explaining the mechanism; one such research suggests that for DEF induced damage to occur three essential components must be present. These are micro-cracking, exposure to moisture and late or delayed sulphate release.

During the past two decades, many research advances have been made to upgrade infrastructure, from new materials and innovative structural systems to total quality management principles and improved organizational effort. Yet major barriers

still exist. Perhaps the most important of these is the lack of reliable in-place non-destructive testing methods for the condition evaluation of concrete structures.

The study of the spectral response and damping of concrete started in the 1930's and most of the fundamental research was carried out before the 1970's (Amick and Monteiro, 2006). This was before the dawn of computerized data acquisition and signal processing. Much of that earlier work was hampered by the limitations of the measurement technology available. The ultrasonic inspection of concrete has traditionally been limited to rather simple measurements conducted in the time domain, such as the pulse velocity which is the backbone ASTM C597. This test is leaned upon to correlate the concrete properties of existing structures based on the P-wave velocity. However, with distributed damage and the inhomogeneous nature of concrete, signal processing is required to be performed in the frequency domain.

1.3 Objectives and Scope

1. Perform a literature review to understand and evaluate the various ultrasonic non-destructive testing methods available and their respective signal processing techniques.
2. Prepare concrete specimens based on proven techniques for initiating distributed damage. These techniques will be based around the selection of materials and additives, the curing method of the concrete and processes to accelerate distributed damage; namely the UMD Modified Duggan Cycle and Freeze Thaw cycles.

3. Apply advanced material testing methods to monitor the process and progress of distributed damage in the concrete specimens. These tests include expansion, weight change, fundamental frequency, compressive strength and SEM images.
4. Perform impact echo tests on the concrete specimens to gather data on the condition of the specimens over time.
5. Apply advanced linear and non-linear signal processing techniques in an attempt to quantify distributed damage in the concrete specimens. This includes but is not limited to cutting edge and novel non-linear signal processing techniques.

1.4 Research Significance

Non-destructive testing methods are needed to determine damage in its early state and to evaluate the condition of existing concrete structures. Destructive methods such as taking core samples alter the integrity of the structure and induce damage to the core samples by extraction. Non-destructive test methods are commercially available for determining large fractures in concrete. However, the state of the art needs to be improved in order to detect micro-cracking associated with distributed damage.

1.5 Thesis Structure

This thesis consists of nine (9) chapters. The first chapter introduces the subject and provides background, objectives and research significance. Chapter 2 discusses the major distributed damage mechanisms and the cement chemistry related to them. Chapter 3 provides a comprehensive literature review of the major and current non-destructive tests available for concrete inspection. Chapter 4 outlines the sample preparation methods for the concrete specimens and explains the tests employed to monitor said concrete specimens. Chapter 5 presents the results of the tests used to monitor specimens subjected to the Duggan cycle. Chapter 6 presents the results of the tests used to monitor specimens subjected to the Freeze-Thaw cycles. Chapter 7 provides the methods and results of signal processing techniques used to evaluate specimens subjected to the Duggan cycle. Chapter 8 provides the methods and results of signal processing techniques used to evaluate specimens subjected to the Freeze-Thaw cycles. Chapter 9 summarizes and provides conclusions for the research.

Chapter 2: Cement Chemistry and DEF

2.1 Introduction

Premature deterioration of concrete in structures is a worldwide phenomenon. Replacing or repairing, and maintaining such concrete is costly and will incur delays in access to and use of such structures. Well designed Portland cement concrete is typically a durable material. However, material-related distresses can occur which affect the concrete durability. The deterioration of concrete in the field is a combination of corrosion, alkali-aggregate reaction, delayed ettringite formation (DEF), sulphate attack, alkali-silica reaction (ASR), alkali-carbonate reaction (ACR) and the freeze/thaw cycle.

Concrete deterioration due to delayed ettringite formation and alkali silica reactions have been identified as a cause of premature cracking and deterioration in concrete structures in many parts of the world since the early 1980's. This distributed damage mechanism is a matter of controversy among researchers. Many contrasting hypotheses have been suggested for explaining the mechanism; one such research suggests that for DEF induced damage to occur three essential components must be present. These are micro-cracking, exposure to moisture and late or delayed sulphate release.

Throughout all the varying researches it is apparent that there exists a very close relationship between DEF and ASR. For this reason this chapter will be focusing on presenting the results of a literature review into the causes of both mechanisms. A more detailed analysis of DEF will be presented because it is the

focus of this research and it is naturally more complex and because it is less clearly understood in the concrete industry. Review of the ASR mechanism will provide primarily background information.

The goal of this chapter is to provide an explanation of how these mechanisms occur, and to document how they produce distributed cracking in concrete structures. This chapter will provide useful information for subsequent chapters in order to develop a method for the detection and quantification of damage caused by DEF. Suggestions for preventative schemes will conclude the chapter.

2.2 General

Ettringite is a term used to denote a number of minerals that have similar crystal structures. Using the term Ettringite without qualification refers to sulphate Ettringite. Ettringite is a naturally occurring mineral that forms in concrete both at the mixture stage and later in the life (after months or years) of the hardened concrete, known as 'Delayed Ettringite Formation'(DEF). Ettringite is a complex mineral that forms naturally in concrete, while the concrete is still plastic, during the early hydration process. This formation is due to reaction between gypsum and other sulphate compounds with calcium aluminates. Gypsum is added to the concrete mixture as a clinker to retard the hydration of calcium aluminates. The early formation benevolently influences application properties of concrete such as setting, durability and strength. In fact, this early form of Ettringite works as a skeleton providing the principal source of early stage strength. It is generally believed that DEF can cause expansion of concrete. Examination of deteriorated concrete by

optical microscopy and scanning electron microscopy (SEM) has shown that Ettringite filled cracks, cavities and formed around aggregates.

Another cause of premature concrete deterioration is the alkali silica reaction (ASR). When sodium and/or potassium (alkali) from the cement, or other sources, attack the silica rich components in the aggregate, gels are produced that expand and crack the concrete. A dark rim around the aggregate particle and cracking of the aggregate particle with the ASR gel in the cracks may characterize the distress of concrete due to ASR. Severe ASR can lead to extensive map cracking of the concrete.

The resulting deterioration of concrete from DEF and ASR is very similar as both produce internal pressures within the brittle concrete. Both ASR and DEF are associated with expansion, extensively distributed cracking and reduced service life of concrete.

2.3 Background – Delayed Ettringite Formation

In 1965 Kennerly was one of the first to report possible problems with DEF. He examined exudations at a cold joint in the Roxburgh Dam, Otago, New Zealand. Analysis indicated that the white deposit was ettringite. Then, in the 1980's, definitive reports were made identifying DEF as a major contributor to concrete deterioration in Germany and the United States (Heinz and Ludwig, 1987). Deterioration by DEF is characterized by the presence of extensive map cracking on the surface of the concrete. The interior channels (air voids, cracks etc.) in the concrete are typically filled with deposits of ettringite. Ettringite and calcium aluminates may dissolve and be transported through permeable channels to areas high

in lime; these compounds will then precipitate as ettringite in lime rich regions. The presence of ettringite crystals in concrete generally results in a separation of the large aggregates from the cement paste (Mielenz et al.,1995).

The chemical process that occurs in DEF is essentially similar to the traditional sulphate attack on concrete (Mehta 1986). In sulphate attack, sulphates from the soil or water in contact with the concrete react with C_3A hydration products to from ettringite. The formation of ettringite results in expansion of concrete and deterioration of the surfaces exposed to the sulphates. Because of the external nature of the sulphate source, this form of concrete deterioration will not be considered as DEF.

In the 1980's the DEF phenomena resulting from internal sulphate attack became a favourite explanation of concrete deterioration whether or not this was actually the case. In Finland, in 1980, the original distress diagnosis was assumed to be the freeze thaw cycle. In a Cement Industry Research Institute document (268), problems prior to 1984 are reported to have occurred in Germany with heat treated prefabricated concrete elements. The report notes that heat treatment has two important effects to initiate these problems: (1) an inadequate pre-treatment allows internal de-bonding between aggregate particles and the paste matrix, and through cracking, (2) heat treatment interrupts the normal formation of ettringite; this formation continues later in the hardened concrete with undesirable effects. It was noted that the solution to the problem is to provide an adequate period for pre-curing. In 1980, Ghorab et al performed the first important work related to DEF. He found expansions when specimens were cured at temperatures greater than 80° C. He

reported that the time at which the treatment occurred was not important but the heat treatment was found to be an important component if expansion during soaking was to occur. His view was later confirmed by work done at the Research Institute and other researchers such as Ozol, 2000.

The standard method for the identification of DEF is done by petrographically examining samples taken from the distressed concrete. The use of high power microscopes and X-ray diffraction techniques are frequently required to verify the presence of ettringite crystals in concrete (Mielenz, et al. 1995). Several researchers have attempted to develop a laboratory test method to evaluate the potential of a concrete to exhibit DEF related distress in service (Grabowski, et al., 1992). By 1997, these efforts have not produced an accepted standard test method to evaluate the potential for development of DEF in a particular concrete. However, there exists a test method initially created to measure the potential alkali-silica susceptibility of concrete. This is the Duggan Test. Some researchers believe this test is satisfactory for measuring the susceptibility of concrete to DEF. The details of this test will be discussed later in this chapter. There is no accepted test method for the in-situ identification and verification of DEF available at this time.

At the present time there is no consensus about the exact mechanism(s) of expansion that occur as a result of DEF or about, the mechanism by which ettringite reforms in hardened concrete. There is also considerable disagreement among researchers about the correct term for the distress (Day, 1992). Various researchers have described the phenomena as secondary ettringite formation, late ettringite

formation, and delayed ettringite formation. The term delayed ettringite formation (abbreviated DEF) will be used exclusively in this text.

2.4 Portland Cement and Ettringite

The notation of cement chemists is adopted in this report and the relevant notations are described in Table 2.1. Portland cement is basically a mixture of calcium silicates and consists predominately of tri-calcium silicate and di-calcium silicate, which are abbreviated as C_3S and C_2S respectively. Tri-calcium Aluminate (C_3A) and alumino ferrites (C_4AF) are also present. Typical weight proportions for normal Portland cement are as follows; 60% C_3S, 15% C_2S, 8% C_3A, and 10% C_4AF. Several other compounds are also present in smaller quantities including; sulphate, manganese dioxide, magnesium oxide and alkalis (K_2O, Na_2O).

Table 2.1 – Relevant chemical notations

Compound	Chemical Notation	Cement Chemist Notation
Calcium Oxide	CaO	C
Silicate	SiO_2	S
Sulphate	SO_3	Š
Aluminum Oxide	Al_2O_3	A
Water	H_2O	H

Gypsum is added to Portland cement the, otherwise fast setting, reaction that occurs in the presence of water. Gypsum also influences the volume stability, the strength, and strength development. Since the addition of large amounts of gypsum can lead to expansion and cracking, limits were placed on the amount that can be added to cement. The finer the cement the more gypsum needed for proper hydration (Mehta, 1986). The optimum gypsum content for a Portland cement can be determined using ASTM C-563, which determines the optimum sulfate content based upon the strength at 24 hours of cement mortar cube specimens.

The chemical requirements for Portland cement are regulated by ASTM C150-90 “Standard Specifications for Portland Cement”.

The two silicate compounds (C_2S and C_3S) are the most important compounds in Portland cement. They are the primary contributors to the strength of the hydrated cement paste. Tricalcium aluminate (C_3A) and tetracalcium alumino ferrite (C_4AF) provide only a small percentage of Portland cement's ultimate strength. C_3A and C_4AF occur in Portland cement as a result of the addition of iron and aluminum oxides to the calcareous raw materials used in the manufacture of cements. Iron and aluminum oxides act as a flux to facilitate the combination of the lime and silica in the manufacture of Portland cements. Their addition increases the percentage of C_3S in a Portland cement (Neville and Brooks, 1987). C_3S is preferable over C_2S because it hydrates more rapidly (Taylor, 1990).

2.4.1 Primary Ettringite Formation

Primary ettringite formation is a necessary step in the hydration of Portland cement. Ettringite formation occurs as a by-product of the hydration of the C_3A component of the Portland cement. In the absence of Gypsum, the reaction of C_3A with water is very violent, where C_3A is converted to calcium aluminate hydrate. This leads to the immediate and irreversible hardening of the paste (flash set). Gypsum is added to the cement to slow the reaction of the C_3A. This retardation is attributed to the formation of a coating of ettringite on the surface of C_3A particles. When mixed with water, Gypsum reacts with C_3A to form fine-grained ettringite crystal, $C_6AS_3H_{32}(3CaO.Al_2O_3.3CaSO_4.32H_2O)$, coatings on the surface of C_3A particles. Initially these ettringite crystals are too small to bridge the gap between the cement particles and the mix therefore remains plastic. Ettringite crystal continues to grow eventually bridging the gap between the cement particles. At this stage setting occurs.

X-ray peaks that are associated with ettringite are detectable within a few hours and the quantity increases during the first day. After this time the ettringite peaks normally weaken, but depending on the chemical composition of the cement and the environmental conditions, ettringite may persist indefinitely. It is generally believed that if all the gypsum is consumed through the ettringite reaction, ettringite then reacts with more C_3A and water to form monosulphate hydrate. In average cement this process starts at about one day and can be monitored as a reduction of the ettringite X-ray peaks.

When the amount of active alumina C_3A in cement is low, 5% or less, the amount of gypsum usually present in Portland cement (5-6%) is sufficient to convert

all the C_3A to ettringite. Ordinary Portland cement contains more than 5% C_3A. When the C_3A content is about 8% the product of hydration with 5% gypsum content would be monosulphate hydrate.

Chemical formula for Ettringite:

$C_3A + 3C\check{S}H_2 + H_{26} => C_6A\check{S}_3H_{32}$ (ettringite)

It is apparent that ettringite has a large number of water molecules in its structure. During crystallization of the ettringite this can create significant expansive stresses. This primary ettringite forms during the first few minutes of the cement hydration process and acts as a skeleton, providing the principal source of early stage strength. Later in the cement hydration process, after the depletion of the sulfate in the solution, and the increase in aluminate concentration due to the hydration of C_3A, the ettringite becomes unstable and is gradually converted into monosulfate (calcium aluminate monosulfate hydrate). The reaction is shown below:

$$C_6A\check{S}_3H32 + 2C_3A + H_4 => 3C_4A\check{S}H_{18} \text{ (monosulfate)}$$

Monosulfate is the final hydration product in Portland cements containing less than 5% C_3A (Mehta, 1986). This is a highly idealized representation of the reactions involved. In a real system, three products - ettringite, monosulfate and C_3A hydrate (C_4AH) will be present, in varying quantities, after the completion of the hydration reactions (Day, 1992). Monosulphate has a much lower number of water molecules than ettringite and therefore should be less expansive.

2.5 Delayed Ettringite Formation

Ettringite crystals are produced by the normal chemical reactions of sulphates, calcium aluminates and water during the early Portland cement hydration. These needles are harmless to concrete since they are largely formed before the final set time of concrete.

The formation and expansion of ettringite, in a sulphate free environment, after the concrete has hardened is referred to as delayed ettringite formation, DEF. The exact reason for the reformation of ettringite after the initial hardening of the concrete is not known or understood clearly. Currently several researchers worldwide are investigating the mechanisms that could cause DEF.

2.5.1 Mechanisms of DEF

Although early reports have suggested that DEF is confined to steam cured concretes, damage associated with DEF in non-steam cured concretes has also been reported. The exact mechanism for the breakdown and reformation of ettringite has not yet been determined. Several researchers have reported that insoluble sulfate present in the Portland cement clinker[1] may contribute to DEF. (Mielenz, et al.,1995 and Hime, 1996)

Sulphate Attack

Sulphates can exist in concrete either from an external or internal source. External sulphate attack is a destructive process that has been widely recognized for a long time. Internal sulphate attack has been reported in the last two decades. The

1. Cement clinker is the term used for Portland cement after firing of the raw materials in the kiln, but prior to final grinding.

presence of insoluble sulfate in the cement clinker has been reported as a potential cause for DEF by many researchers.

Portland cement contains sulfur compounds from the cement clinker and from the added gypsum. Sulfates from gypsum dissolve fast and participate in retarding the setting of cement while sulfate in the clinker is slowly soluble and unavailable for this reaction. Previous research has attributed the presence of insoluble or slowly soluble sulfate in the clinker to DEF. DEF is reported to occur as a result of the sulfate materials slowly entering into solution after the initial setting and hardening of the concrete. Ettringite forms when the sulfate entering solution reacts with C_4AH and water. The chemical reaction is similar to traditional sulfate attack on concrete (Mehta, 1986). Cracking and concrete deterioration occur as a result of the expansive reformation of ettringite crystals.

The changes in fuels used at cement manufacturing plants were suggested as a possible source for the clinker sulfates. The sulfur content of different fuels can change daily and cause variations in the sulfate content of the clinker.

The issue of slowly soluble sulfates has also been addressed in research by Klemm and Miller. Their research focused on determining the end products of the hydration of cements made with high sulfate clinkers. Thirty-three different clinkers with a wide variety of sulfate contents were included in the study. Laboratory testing using differential scanning calorimetry showed that all of the sulfate in the cement was incorporated into ettringite within 24 hours of hydration. Ettringite formation was determined to occur prior to the hardening of the cement paste. Additionally, the

sulfate materials in the clinkers dissolve in the presence of excess aluminate which allows for the immediate formation of primary ettringite (Klemm and Miller, 1997).

The subject of slowly soluble sulfates in cement clinkers is controversial at this time. A recent report released by the Portland Cement Association (PCA) indicates that the sulfate content of cements has risen over the past fifty years (PCA, 1996). The increased fineness of modern day cements is generally cited as the reason for the increase. Finer cement grinding requires higher sulfate contents to adequately control the hydration of the C_3A (Mehta, 1986). Because of the reliance of the cement industry on relatively short term tests, as discussed in Section 2.2, the presence of slowly soluble sulfates could result in cements being produced with sulfate contents in excess of that needed for the retardation of C_3A hydration.

The presence of sulfate materials in the cement clinker is difficult to verify. Neither the AASHTO M-84 nor the ASTM C-150 standards require the testing of the clinker phase of the cement (AASHTO M-84 and ASTM C-150-95). Chemical analysis - to determine composition - of Portland cements is conducted after the addition of sulfate to the ground clinker. This specification could allow for cements with large clinker sulfate contents to remain undetected by the end user of the material.

Effects of High Temperature Curing

Concrete distress caused by DEF has been associated with concrete elements that were cured at high temperatures. High temperatures usually occur during steam curing or due to concrete's heat of hydration in the case of large mass concrete

placement. Heat treatments are commonly used in precast concrete production to accelerate the strength gain of concrete. Several researchers have found that at temperatures above 140 F (60 C), the ettringite formed during hydration can decompose and later reform (Day, 1992). The value of 140 F (60 C) represents the lower bound of temperatures that have been associated with DEF. Note that DEF has also been reported in concrete pavements and precast elements which have not been cured at elevated temperatures. (Wolter, 1997, and Gress, 1997)

Aggressive steam curing may cause defective hydration of the cement which initially weakens the concrete by the formation of microcracks in the cement paste, poor bond between the aggregate and the cement paste, and the formation of inhomogeneous microstructure. Such weakening makes concrete vulnerable to cracking and premature deterioration caused by ASR, sulfate attack, freezing and thawing, and DEF.

Steam curing is usually used to minimize the time required to cure new concrete members. Steam curing is used in conjunction with high early strength cement (type III) in the production of precast concrete members of high early strength. It will be useful to note here that most of problems caused by DEF results from the use of cement type III in the mix design.

Steam curing is also known to dissolve ettringite in the pore liquid of the hardened concrete if the concrete temperature exceeds 70° C. In concrete structure exposed to water or humidity ettringite recrystallizes inducing high tensile stresses in the hardened concrete causing expansion, cracking and premature deterioration.

Researchers have also reported that relative humidity at elevated temperatures can affect the breakdown of ettringite. High temperatures in dry environments are reported to aggressively break down ettringite (Fu et al. 1994). The exact mechanism that causes the breakdown of the ettringite is not clearly understood (Day, 1992). The breakdown is probably related to the instability of the crystalline ettringite at elevated temperatures. The possibility of competing chemical reactions has also been reported as a potential cause for DEF (Fu and Beaudoin, 1996).

Heinz et al [1987] argued that at elevated temperatures primary ettringite is broken down to monosulfate. Later when the concrete is exposed to moisture at normal temperature, the monosulfate is reconverted to ettringite. Heinz et al. considered the SO_3/Al_2O_3 (Š/A) ratio to be the critical parameter in assessing the susceptibility of a cement to potential DEF problems. Cements with Š/A ratios greater than 0.67 or $Š^2/A$ ratios greater than 2.0 have been determined to be susceptible to DEF (Heinz and Ludwig, 1987 and Grabowski, et al. 1992).

Other research into DEF supports a different mechanism for the breakdown of primary ettringite at high temperatures. Bothe and Brown have reported that ettringite is still present after high temperature curing, and the breakdown product (monosulfate) was not observed in X-ray diffraction studies. Their research found that ettringite is still present in samples made in an alkaline environment at high temperatures.

Expansion and cracking caused by DEF associated with steam curing have been attributed to uniform paste expansion which results in cracks around the aggregate particles, subsequently the cracks are filled with ettringite. Other

researchers suggest that the damage is caused by pressure exerted by the growing ettringite crystals (Fu and Beaudoin, 1996). It is also important to note that many researchers have reported DEF in concrete pavements and precast elements, which have not been cured at elevated temperatures (Wolter, 1997).

Concrete Properties

Almost all of the problems caused by the formation of ettringite occur when using cement type III in the mix design. Cement Type III is used in concrete mixture, especially in pavements, because of its higher early strength. The fineness of type III is almost three times that of other cements. It is well known that as fineness increases, the hydration rate and the heat of hydration increase, all of which is associated with the formation of ettringite (Kelham, 1996). Type III is more susceptible to DEF because it may contain more C_3A and SO_3 in the form of calcium sulfate (Fu and Beaudoin, 1996). It contains more C_3A to promote high early strength. Many researchers support the idea that only type III cement is susceptible to DEF.

As stated previously, one of the essential components for DEF is microcracks. Concrete, even of the best quality, should not be considered completely impermeable. With freshly placed concrete, there are visible cracks such as plastic cracks, early-age thermal cracks and drying shrinkage cracks. Also there are cracks between the aggregate and the cement paste, called bond cracks. The permeability of concrete rather than the cement chemistry appears to be the most important factor in sulfate attack. Sulfate is manifested as loss of adhesion and strength associated with chemical decomposition of cement hydration products and the formation of ettringite.

2.5.2 Mechanisms of Expansion Associated with DEF

The cause of concrete expansion and cracking due to DEF is not well understood. Crystal growth and swelling are reported as the two possible mechanisms for the formation of ettringite crystals and their subsequent expansion (Day, 1992).

The "crystal growth" theory is based upon the theory that expansion is caused by the formation of ettringite at the surface of reactive cement grains. Expansion is the result of pressures created by the growth of crystals in a confined space. Growth of the inner layer on the surface of the reactive cement grain pushes out other particles resulting in expansion. The presence of calcium hydroxide is required for expansion to occur. When calcium hydroxide is present, the ettringite crystal growth is topochemical and expansion occurs. A topochemical reaction refers to the reaction between the reactive site and the surrounding solution, where the reaction products are formed on the surface of the reactive particle. In the absence of calcium hydroxide, ettringite forms from solution without expansion (Cohen, 1983). Crystal growth theory is the result of research into the expansion mechanism associated with Type K expansive cements. The destructiveness of ettringite formation is related to where the reaction occurs, because only growth in confined spaces will produce damage. Crystal formation at an aggregate, results in maximum expansion due to the rigid nature of the aggregate. Formation near air voids or other cavities allows the cavity to act as an expansion chamber, relieving the stress caused by the formation of crystals (Day, 1992).

"Swelling" is another generally accepted mechanism for ettringite formation. Ettringite forms from a "through solution mechanism". Through solution refers to the formation of crystals in a saturated solution. In a saturated calcium hydroxide solution, ettringite crystals are gel-like and colloidal in nature. The large surface area of the colloidal ettringite crystals results in adsorption of significant quantities of water and the generation of swelling pressures (Day, 1992). Small ettringite crystals, colloidal in size, and formed in an alkaline environment, will possess a negative charge. The large surface area of the colloidal molecules combined with the negative charge results in a large attraction for water. Tests performed by Mehta confirmed the swelling hypothesis (Metha, 1982).

Research by Fu et al. suggests another possible mechanism for the formation of ettringite crystals in hardened concrete. The research focused on the formation of ettringite crystals in pre-formed cracks in cement pastes. Heat treatments were used to produce conditions favorable to DEF. The formation of ettringite in the cracks was determined to be caused by the preferred nucleation of crystals in cracks which are optimally sized for crystal formation. The formation of ettringite crystals in cracks results in a decrease in the free energy in the system. The presence of ettringite in cracks was verified by the use of scanning electron microscopes (SEM) and energy dispersion x-ray analysis (EDXA) (Fu et al., 1994). After the ettringite crystals form in the cracks, expansion and ultimately concrete cracking will likely be caused by crystal growth as described above (Fu and Beaudoin, 1996).

In the research by Fu, et al. crystal formation was determined to preferentially occur in crack tip zones rather than on plane solid surfaces in concrete. In the heat

cured specimens the cracking occurs due to drying and cooling shrinkage (Fu, et al., 1994). Other possible sources of cracking, as a potential surface for ettringite formation include alkali silica reactivity and freeze thaw deterioration.

It is unlikely that one mechanism is solely responsible for the expansion associated with DEF. Rather, expansion is likely the result of several mechanisms acting, with environmental conditions determining which mechanism is dominant. It should be noted that both the crystal growth and swelling mechanisms require an alkaline environment saturated with calcium hydroxide for ettringite formation and expansion to occur.

2.5.3 Holistic approach to DEF

This approach considers concrete construction as a whole including environmental conditions and loading in service rather than concrete as a laboratory specimen. The mechanism of DEF has been addressed from the holistic standpoint by Collepardi in a paper in Concrete International in 1999. In this mechanism it is suggested that some factors are essential for DEF related damage. In the absence of one of these factors, DEF does not occur. These factors are: the presence of micro-cracks, exposure to wetting-drying cycles, late sulfate release from the cement clinker or other sources, and the migrations of reactant ions through the pore aqueous solution of concrete exposed to water or saturated air. Ettringite deposits into the existing cracks and subsequently the cracks are opened by ettringite swelling or crystal growth.

2.6 Alkali Silica Reactivity

Alkali-silica reactivity (ASR) is a type of distributed damage mechanism that occurs when the alkalis contained in Portland cement react with siliceous materials in the aggregates in the concrete. In the presence of water, the reaction products swell, resulting in expansion and cracking of the concrete. The cracking pattern in unrestrained concrete takes on the appearance of a random network of fine cracks. In restrained concrete, cracks tend to form perpendicular to the axis of minimum restraint to cracking (Taylor, 1990). The problem of ASR has been extensively studied since it was first documented by Stanton in 1940.

2.6.1 Alkali-Silica Reaction Chemistry

The conditions necessary for ASR to occur in a Portland cement concrete are a sufficient content of alkali oxides in the cement, a reactive aggregate, and a supply of water. Alkalis (typically Na^+ and K^+) occur in Portland cement as a result of the raw materials used in the manufacture of the cement. Alkalis can also be present from external sources such as contaminated deicing salts and environmental pollution (Taylor, 1990). All aggregates that contain silica are potentially susceptible to alkali-silica related reactions. Typically, only aggregates with a loosely bound or amorphous silica structure are involved in reactions. These potentially reactive materials include opals, chalcedony, cherts, flints, certain forms of strained quartz, and other materials (Mehta, 1996).

The ASR reaction starts with the breakdown of the silica structures in the aggregates due to exposure to hydroxide ions. The hydroxides are present as a result of the alkali products entering the pore solution. The damaged elements of the silica structure are

then free to react with alkalis (Na^+ and K^+) to form a water-soluble alkali silicate. The alkali silicate material occurs as a dense gel (secondary deposit) surrounding the reaction site on the surface of the reactive aggregate. The gel material then attracts moisture from the surrounding cement paste. The resulting osmotic pressure may cause some of the expansion and cracking attributed to ASR (Czernin, 1980). The cracking will have the external appearance of randomly oriented cracks on the concrete surface. Frequently the cracks will have a mottled or wet appearance on the concrete surface.

2.6.2 Relationship with Delayed Ettringite Formation

The simultaneous occurrence of ASR gel products and ettringite in deteriorated concrete has been reported by several investigators (Meilenz, et al., 1995, Shayan and Quick, 1992, and Johansen et al. 1993). There are several factors that suggest that concrete experiencing distress due to alkali-silica reactivity may be more susceptible to DEF. The results of research by Brown and Bothe suggest that the decrease in alkali content in the pore water of concrete due to ASR, resulting in a lower pH, may create a favorable environment for DEF. Using this hypothesis, ettringite should form at locations where the pH is lowest. This will correspond to the paste aggregate interface where ASR gel products are present. The investigations by Mielenz, et al. and Shayan and Quick both report the occurrence of ettringite adjacent to alkali-silica gel products in deteriorated concrete railroad ties (Mielenz, et al., 1995 and Shayan and Quick, 1992).

In their investigation into concrete railroad tie deterioration, originally attributed to DEF, Shayan and Quick concluded that the damage was the result of

ASR. Ettringite was reported to have formed as a secondary product after the creation of cracks by ASR. This conclusion is based upon examination of railroad ties with varying amounts of deterioration. Only minimal signs of ettringite were found in railroad ties without visible cracking. In contrast, ASR gel products were observed in all of the examined railroad ties (Shayan and Quick, 1992).

Research by Shayan and Ivanusec has shown that steam curing of mortars prepared with excess sulfate may not lead to DEF in the absence of alkali reactive aggregates that produce expansion and microcracking. The research showed, in steam cured mortars containing reactive aggregates and alkali, the addition of sulfate increases the amount of observed expansion. This indicates that DEF may contribute to expansion in this case. In mortars prepared with reactive aggregates and alkali, cured at 40 C, the addition of sulfate did not increase the amount of observed expansion. This research indicates that elevated temperatures (greater that 60 C) may be necessary for the simultaneous observation of DEF products with ASR products (Shayan and Inanusec, 1996). This finding has not been reported by other researchers.

Growth of ettringite crystals, after the initial formation of cracks, may have contributed to the extent of cracking in the railroad ties. The formation of ettringite could result in the release of hydroxyl ions from $Ca(OH)_2$, which will enhance the ASR (Shayan and Quick, 1992). The finding of ettringite in cracks formed by ASR is consistent with the research by Fu et al. which found that ettringite prefers to form in preexisting cracks (Fu et al., 1994).

2.7 Factors Affecting Delayed Ettringite Formation

For expansion and cracking due to DEF to happen, some researchers suggest that several chemical and environmental conditions have to be all satisfied. These conditions have been identified as; heat treatment temperature higher than 70°C, high SO_3/ Al_2O_3 ratio in the cement i.e. 0.5–0.6, and that concrete or mortar be stored in water or a nearly saturated environment. Also, the rate and expansion due to DEF has been found to be affected by other factors as well including; ASR, cement composition, the aggregate type used, crack inducing treatment and storage or service conditions. These factors will not determine whether DEF is formed but will hasten the process.

2.7.1 Cement Chemistry

Mortar samples made of 40 different cements were used to study the effect of cement composition on expansion and cracking due to DEF. The samples were cured in a cycle that included heat treatment for 3 hours at 100°C then stored in water at 20°C. Expansions were monitored during a period of 2-4 years. A significant relationship between expansion at ages 400-800 days and the contents of SO_3, MgO, and Na_2O was observed (Taylor, 1993).

To understand the effect of SO_3 content and the curing method on the strength and expansion of concrete, two different clinkers of high C_3A and C_3S content, were blended with gypsum to give cements of SO_3 content from 2.0 – 7.5%. The concrete samples were then heat cured. The expansion and strength of concrete were monitored for 182 days. Large expansions were observed for samples having SO_3 content above 3.8%.

2.7.2 High Temperature Curing

Day has reported that heat treatment of concrete has been a significant cause of DEF. Changes in heat treatment procedures have been found to eliminate the DEF problem in concrete railroad ties manufactured in Finland. (Tepponen and Eriksson, 1992). Many European concrete associations have amended their specifications for concrete curing to mitigate the problems associated with steam curing. This mainly deals with limiting the range of temperature increase during curing and limiting the maximum temperature of the specimens (Day, 1992).

2.7.3 Poor Quality Construction

Air entrained concrete is beneficial to increase the durability of the structure to the freeze – thaw cycle. Air entrainment consists of the addition of chemical agents to the concrete during mixing that stabilize small air voids in the hardened concrete. The air voids act as relief areas for absorbed water when the concrete is exposed to freezing temperatures. Water that is present in the pore spaces of the concrete is able to diffuse into the air voids and freeze without damaging the concrete.

Several possible sources of ettringite in pavements have been reported. They include:

1. Ettringite occurring due to DEF
2. Use of deicing salts contaminated with gypsum
3. Freeze-thaw deterioration due to an inadequate air void system, with ettringite crystals forming after crack initiation.

An adequate air void system is the simplest and most economical method of ensuring the long-term durability of a concrete pavement exposed to freeze-thaw conditions. The small cracks created by freeze-thaw deterioration allow the concrete to become more permeable, allowing water access, and thus significantly contributing to other distress mechanisms. Proper quality control is the best way to achieve this.

2.7.3 Poor Quality Materials

To ensure high quality concrete, the Portland cement, aggregates, and any supplementary cementitious materials such as fly ash, blast furnace slag, or silica fume need to be satisfactory. Test methods are available that allow for the detection of reactive aggregates and cements. These test methods must be used throughout the construction process. Several researchers have recommended improvements in the current standard specification for Portland cement. These changes are recommended to prevent the occurrence of DEF and ASR. Specification changes are also being considered by the Texas Department of Transportation. The proposed changes are summarized below:

1. Limit the total alkali content in a concrete mix to a maximum of 5 lbs/yd^3. The current specification classifies cements with alkali contents below 0.6% alkali, expressed as equivalent Na_2O, as low alkali cements. (ASTM C-150,1995) Use of the 5 lbs/yd^3 maximum alkali content has been successful in both Germany and Canada in reducing the prevalence of ASR related problems (Gress, 1997).

Limit the sulfate content of Portland cements to the amount required for hydration of the C_3A component of the cement. A limit of 3% by weight of cement has been recommended by Gress (Gress, 1997). This recommendation is made without consideration that finer cements, as discussed in Section 2.4, require higher sulfate contents.

The use of pozzolanic materials such as fly ash, blast furnace slag, and silica fume, as supplementary cementitious materials has increased significantly in recent years (Mehta, 1996). Prior to their use in concrete, these materials should be chemically tested to identify potentially deleterious materials. The presence of Al_2O_3 and SO_3 should be of particular concern. Tests methods need to be developed to ensure the compatibility of these supplementary materials with Portland cement.

2.8 Identifying Ettringite

Understanding the processes by which ettringite forms and the reasons for forming have proven a formidable task for researchers. Furthermore, finding a simplified field test by which ettringite can be readily detected is even further from discovery. It is one of the goals of this thesis to define a testing technique that will accomplish this task.

Delayed ettringite formation is usually associated with cracks and expansion. The external cracks that are associated with DEF are randomly oriented surface cracks. These cracks vary from one or two to extensive map cracking. On the other hand, internal cracking is accompanied by ring cracking around the aggregate particles. It has been suggested that without the presence of these ring cracks, ettringite should not be diagnosed as the cause of cracking

Ettringite can be detected using X-ray diffraction, of a finely powdered sample. However, this method may not detect it if it is present only in small quantities. Alternatively, the scanning electron microscope (SEM) has been used. In SEM a beam of electrons with an accelerated voltage of 10-20 kV is trained at the concrete sample. As a result, three signals are produced; secondary electrons (SE), backscattered electrons (BE), and X-ray. The SE are used to obtain the morphology of the microstructure of the samples while BE are used reflect the differences in atomic number. Energy dispersive X-ray analysis (EDAX) is used to obtain the elemental composition of a point on the image produced. Each element is identified by its position of its peak and a quantitative analysis by weight of elements is calculated by a computer. This process must take place in a laboratory.

Visually distinguishing between ASR and DEF in concrete is not a simple task. Both distress mechanisms produce distributed cracking. In cracks, secondary deposits, the results of the ettringite reformation or ASR, are generally observed. The secondary deposits (ettringite or ASR gel) from both ASR and DEF will have a whitish appearance under a light microscope. Figures 2.1 and 2.2 show polished concrete specimens under a light microscope at 100 to 150x magnification. The specimen with cracking due to DEF is shown in Figure 2.1, which is virtually indistinguishable from the specimen with cracking due to ASR shown in Figure 2.2. The use of higher magnifications (418x) does not improve the ability to distinguish between the distress mechanisms. This can be seen in Figure 2.3 and 2.4 which show the same specimens at higher magnification. The image is focused on the cracks at the cement paste/aggregate interface. In Figures 2.3 and 2.4, the secondary deposits

in the cracks have the same whitish appearance as the specimens at lower magnifications.

2.9 Summary

A thorough literature review has been performed as to the causes and effects of delayed ettringite formation. This revealed that the exact reason for DEF is not well understood. The reason for ASR is more clearly understood, however it is apparent that more research is necessary first to investigate DEF and then the relationship between DEF and ASR.

Specific suggestions for further research and conclusions based on existing research are summarized below:

1. Given the current cement production and concrete construction practices there appears to be a potential for a delayed ettringite formation problem in North America and around the world. It is highly probable that DEF can lead to deterioration of heat treated concrete. There is some evidence that non-heat treated concrete may be subject to deterioration from DEF.
2. Three main reasons lead to DEF. High permeability of concrete, exposure to moist conditions and concentration of sulfate ions. Also, it is clear that heat treated concretes are more susceptible to DEF.
3. The effect of DEF is substantially reduced by inclusion of an adequate air-entrainment void system in the concrete.
4. The alkali content in a concrete should be limited to 5 lbs/yd^3.

5. Utilize the recommendations of the European Committee for Standardization for the heat treatment of concrete. The specifications limit the rate of temperature rise during curing, the maximum curing temperature, the cooling rate and the required protection against moisture loss (European Committee for Standardization, Concrete, 1989).
6. Modification of the test procedure contained in ASTM C-1038 to include a longer storage period in water may be considered. A minimum period of 90 days is recommended.
7. Modification of ASTM C-150 to require testing in accordance with ASTM C-1038 for all cements manufactured with sulfate content greater than 3%.
8. Further improvement of the Duggan Test may result in the development of a useful standard to assess long term dimensional stability and durability of concrete.

Based upon the results of the literature review, both ASR and DEF will produce similar forms of internal cracking in concrete structures. Because of this, distinguishing between damage mechanisms using transient stress waves will not be possible. Other techniques such as Autoradiography have to be used to clearly determine the presence of ettringite.

Chapter 3: Non-Destructive Testing

3.1 Introduction

The importance of the in-place evaluation of concrete's material integrity cannot be overstated. The potential benefits that non-destructive testing holds for achieving this goal are incalculable. Many avenues of non-destructive testing have been explored in order to detect and characterize distributed damage in concrete. Visual inspection, sounding, core taking, radiography, nuclear methods and petrographic analysis are some of the more typical examples. Other methods such as spectral analysis of surface waves (SASW) are generally more expensive and are just finding application to concrete. Generally, ultrasonic methods hold the most potential for providing an in-place non-destructive testing method for the condition evaluation of concrete structures.

The present research effort is focused on identifying more practical, cost effective and reliable methods. These methods will be constrained by four criteria: (a)Nondestructive, (b) local i.e. Provide information about the existing condition at a specific locality rather than about the average condition between two locations; (c) One sided, i.e. the test can be performed when there is access to only one side of the concrete (d) inexpensive.

Currently no single test meets all of the above requirements with acceptable reliability. Some researchers, including the author, consider the impact echo test as the best overall technique presently available because it is robust to noise and yields

better signal to noise ratio. However, when the discontinuities are not parallel to the surface their detection is limited by this method.

From the outset more common and potentially useful nondestructive methods were examined. Also, the analysis techniques commensurate with these methods were appraised in order to highlight the advantages and disadvantages.

3.2 Distributed Damage

Distributed damage is usually manifested as map cracking or micro-cracking in concrete. Micro-cracking in concrete is caused by many types of damage mechanisms. For example, DEF, ASR and sulphate attack are all examples of deterioration in concrete.

Damage in concrete first develops as micro-cracking when curing, due to shrinkage and the resulting stresses. The micro-cracks form at the weakest parts of the concrete, that is, at the boundaries between the aggregate and paste matrix. This boundary is referred to by some researchers as the interfacial transition zone (ITZ). It is weakest due to the disparities between material properties such as elastic modulus, density and moisture content. Micro-cracks eventually combine in the form of strain localization, where evenly distributed micro-cracks coalesce to form a major crack. This hazardous potential underscores the importance of developing non-destructive techniques for the condition evaluation of concrete.

3.3 Pulse Velocity Method

Presently, only a few non-destructive tests are established that detect and quantify early damage in concrete. One of these is governed by ASTM C 597, "Standard Test Method for Pulse Velocity Through Concrete." The pulse velocity method uses linear ultrasound to detect internal cracking in concrete.

In this method the through transmission ultrasonic time of flight in a known thickness of concrete is measured with a simple timing unit. For best results, two opposing sides of the member should be accessible. Frequencies between 25 - 250 Hz are typically used. If higher frequencies are attempted this results in significant losses of wave energy. Concrete bulk L-wave velocities vary from 3500 m/s to 4500 m/s, depending on the concrete composition, age and condition.

One of the reasons for the poor results offered by this method is due to the assumption that the bulk pulse velocity is independent of ultrasonic frequency used. This implies that concrete is a non-dispersive, linear material. This is not the case. A 525% increase in measured velocity has been reported for a frequency increase of 25 kHz to 2.25 MHz. (Shah and Chandra, 1970)

3.4 Spectral Analysis of Surface Waves (SASW)

Spectral-Analysis-of-Surface waves (SASW) method is a non-destructive and non-intrusive method that by means of measuring Rayleigh wave dispersion can determine the vertical variation of material stiffness. The spectral analysis of surface waves technique (SASW) was developed initially for geotechnical applications such as the evaluation of pavement sub-grades. More recently, attempts have been made to adapt the technique to concrete structures.

SASW is a surface wave method used for determination of layer thickness, velocity (stiffness), and integrity of concrete, asphalt, timber and masonry structures. This method is based on the propagation of mechanically induced Rayleigh waves. By striking the concrete surface with a light hammer, a transient stress wave is created (surface or Rayleigh), which is registered by two transducers placed in line with the impact point on the ground surface at fixed separations. The transducers, which may be small accelerometers, register the passage of the waves. The receiver outputs are plots of the phase difference between the two transducers as a function of frequency. A profile of Rayleigh wave velocity versus wavelength, or so-called dispersion curve, is calculated from the phase plot. The ratio of Rayleigh wave velocity to shear wave velocity is approximately 0.9:1; thus, the shear wave velocity can be estimated. The shear stiffness (G) of the concrete can be calculated from the shear velocity if the material density is known, and a plot of ground stiffness as a function of depth from the surface can be obtained.

Rayleigh waves have velocities that depend on their wavelength, a phenomenon called dispersion. Waves having different wavelengths sample to different depths, with the longer wavelengths sampling to greater depths. Figure 6 illustrates the sampling depths and particle motion of two Rayleigh waves having different wavelengths.

This principle can be used to locate and roughly delineate in-homogeneities such as voids.

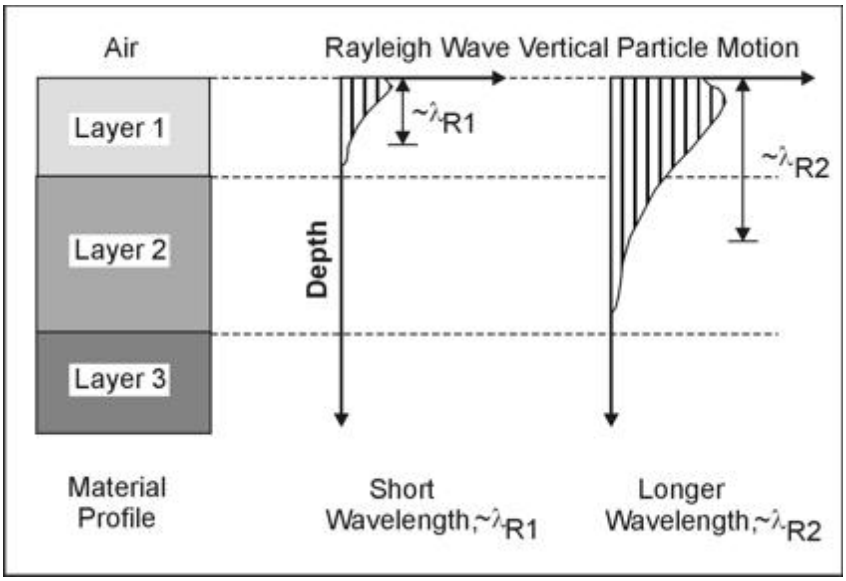

Figure 3.1 - Variation of Rayleigh wave particle motion with depth.

The surface wave dispersion curve can be measured using an active source and a linear array of receivers. The dispersion curve is then inverted to determine the corresponding shear wave velocity profile.

In the SASW method, a Fast Fourier Transform (FFT) analyzer or PC-based equivalent is used to calculate the phase data from the input time-voltage signals. Typically, only the cross power spectrum and coherence are recorded. Coherent signal averaging is used to improve the signal-to-noise ratio. The availability of

either two- or four-channel analyzers has traditionally limited the number of receivers used. Because of the initial processing done by the analyzer in the field, the effectiveness of the survey can be assessed and modified if necessary. An initial estimate of the surface wave velocity (V_S) profile can be made quickly.

Interpretation consists of modeling the surface wave dispersion to determine a layered V_S profile that is compatible. Interpretation can be done on a personal computer.

The acquisition and processing techniques of SASW methods do not separate motions from body wave, fundamental mode Rayleigh waves, and higher modes of Rayleigh waves. Most often, it is assumed that fundamental mode Rayleigh wave energy is dominant and forward modeling is used to build a 1-D surface wave velocity (V_S) profile whose fundamental mode dispersion curve is a good fit to the data.

Advantages

This method provides for layer thickness profiles as well as stiffness. For slabs and pavements, velocity profiles including the surface layer, base and subgrade materials within 5% accuracy. Only one-sided access is required for this method.

Limitations

This method is utilized primarily for the determination of strength properties of concrete rather than the detection of micro cracks. For investigations of thin concrete structures, the presence of rebar will probably influence the data.

Ultrasonic-seismic methods, like impact-echo and SASW used in combination, are very useful at identifying already-damaged locations in a bridge deck. Unlike chain dragging and hammer sounding, these geophysical methods identify this damage at early, moderate, and late stages of development. The common "NDT" methods of chain dragging and hammer sounding only detect those flaws that have developed to an advanced stage, and they finally become audible to the human ear.

3.5 Non-Linear Ultrasonic Testing

Important contrasts exist between linear and non-linear ultrasonic methods. Non-linear methods have the added benefit of increased sensitivity over linear methods. This increased sensitivity enables the detection of micro-cracks of a size undetectable by linear methods. Non-linear methods are also very applicable to inhomogeneous materials such as concrete.

Basically, the objective of ultrasonic methods is to measure the changes in characteristics of the ultrasonic signals propagating through the tested concrete. For linear methods these characteristics may be the P-wave velocity, the amplitude attenuation and the frequency shift. For non-linear methods these may be the shape of the frequency spectrum and the harmonics generated by the internal discontinuities of the material.

Non-linear behavior of ultrasonic waves may be due to several different mechanisms. Classical material non-linearity is the term often used to describe non-linear behavior due to the effects of higher order elastic moduli and dislocations in crystalline materials. Classical material non-linearity results in second order harmonic

generation. Larger discontinuities such as defects, voids and micro-cracks result in increased non-linear behavior as compared to that of classical material non-linearity. In concrete, non-linearity is associated with micro-cracks and the interfacial transition zone. Therefore, non-linear ultrasound is capable, in theory, of detecting and evaluating the degree of micro-cracking occurring in concrete. As the amount of micro-cracking increases, a larger portion of the fundamental wave is expected to be converted to higher harmonics.

3.5.1 Nonlinear Ultrasonic Pulser Receiver

A toneburst pulser capable of supplying an output voltage of up to 1400v is typically used. Unlike conventional ultrasonic pulsers that generate broadband output, the toneburst pulser's output is concentrated at one frequency. This concentration of energy at one frequency is necessary to drive the response of the specimen into the nonlinear range. Two transmitting and two receiving transducers are used when a larger volume of concrete needs to be evaluated than would be with the use of only one transmitting and one receiving transducer.

3.5.2 Pitch Catch

This system consists of a tone burst transmitter and a superheterodyne receiver that allows for the reception of harmonics as well as the fundamental frequency. This non-linear system creates a high power tone burst UT signal that can be varied over a range of frequencies in incremental steps. The UT pulse is initiated in the direction of casting.

3.6 Impact Echo

The impact-echo method is a technique for flaw detection in concrete based on stress wave propagation. The principle of the impact-echo method is illustrated in Figure 3.2. A transient stress wave is introduced into the test object by means of a mechanical impact on the surface. The mechanical impact is generated by tapping a small steel ball, of ranging diameters (though usually less than 15mm), against the testing surface. The stress wave generated propagates into the test medium along spherical wavefronts as compression (P-) and shear (S-) waves. Additionally, a surface wave is generated, which is called a Rayleigh (R-) wave, and travels along the surface away from the point of impact. The P- and S- waves are reflected by internal discontinuities and external boundaries. The reflected waves returning to the surface of impact generate displacements which can be measured by a receiving transducer placed near the point of impact. If the receiver is placed close to the impact point then the displacement waveform is dominated by the arrival of the P- waves. The displacement waveform is used to determine the travel time, t, from the time of impact to the arrival of the first P- wave reflection. If the P- wave speed, C_p, in the test medium is known then the distance, T, to the reflecting interface can be calculated.

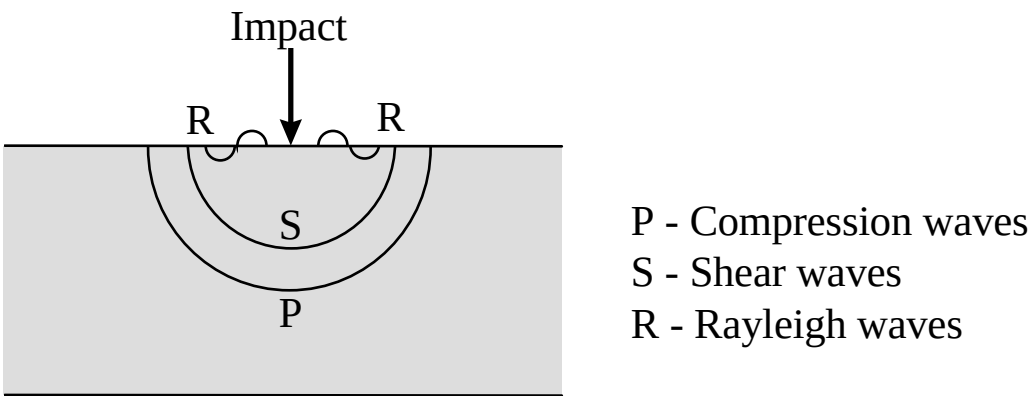

Figure 3.2 - Schematic illustration of wave-fronts generated by impact on a solid.

The first wave to reach the transducer is an R- wave. The R-wave causes a large initial downward displacement of the transducer. The P- wave is next, dominating the waveform with its multiple reflections (2P, 4P, 6P, 8P etc.). The period between P-wave arrivals, t_T, denotes the time necessary for a stress wave to travel the distance, 2T, to the reflecting interface and back to the point of impact. This process is illustrated in Figure 3.3.

For ease of analysis and expediency, waveforms are transformed to the frequency domain using Fast Fourier Transform technique. The resulting amplitude spectrum is used to identify the dominant frequencies present in the waveform. Figure 3.3(C) is the spectrum corresponding to the waveform in Figure 3.3(B). The single dominant peak in the spectrum corresponds to the frequency of P-wave arrivals at the top surface of the plate. The frequency (f_T) at which the peak occurs is obtained by taking the inverse of the time between P-wave arrivals (t_T).

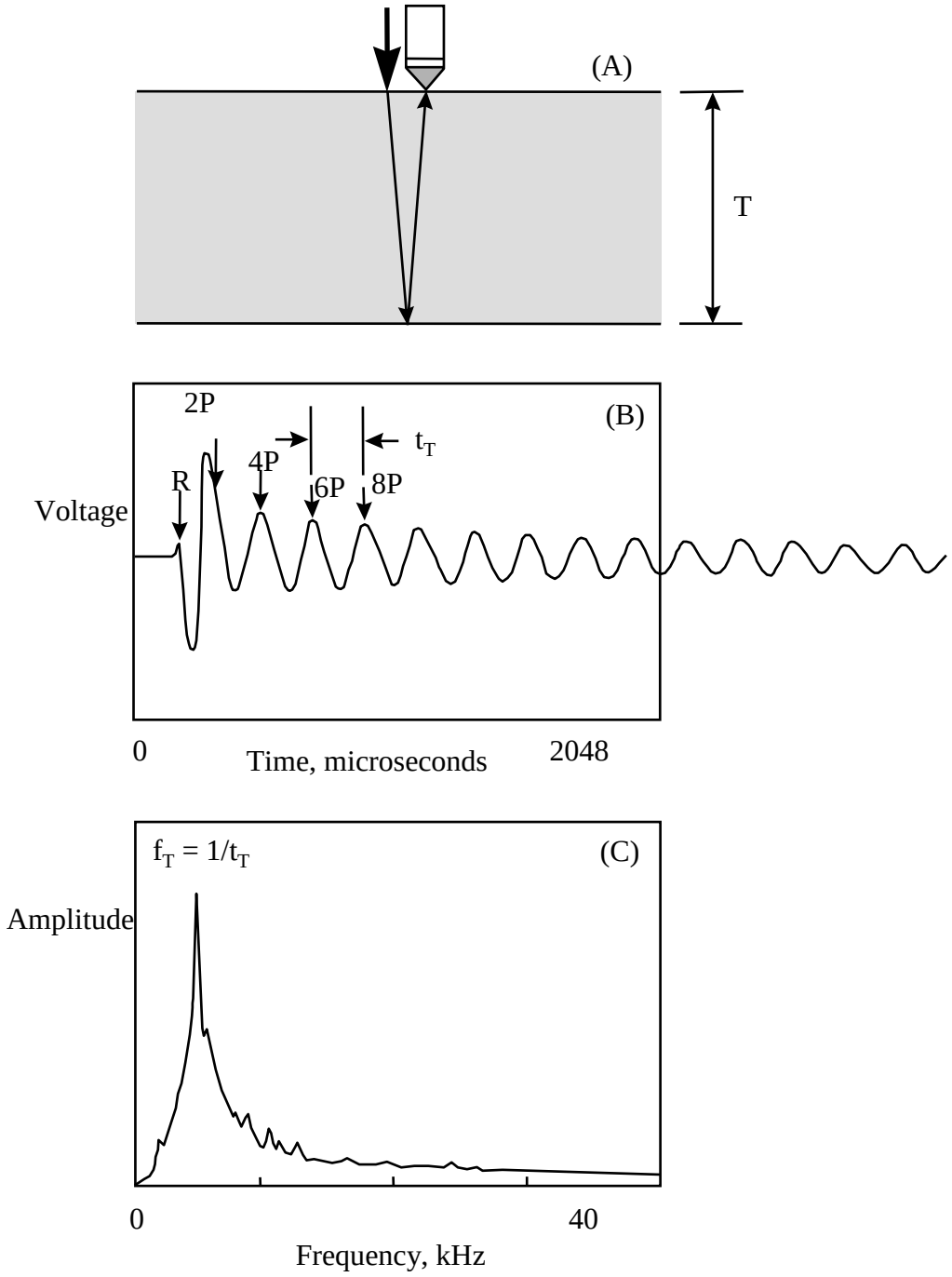

Figure 3.3 - Impact -echo test carried out on a solid concrete plate (A).
(B) waveform, and (C) spectrum (Adapted from Sansalone and Streett, 1997)

The waveform is clearly periodic. The period, t, is equal to the travel path, 2T, divided by the P-wave speed. Since frequency is the inverse of the period a standard set of equations becomes apparent:

$t = 2T / C_p$ or $T = C_p / 2f_p$ or $f_p = C_p / 2T$ (3-1)

where: C_p is the P- wave speed

f_p is the frequency of reflected waves

t is the period of reflected waves

T is the thickness of the medium (concrete plate)

Research on transient wave propagation has shown that a correction factor is needed to account for the geometry of the tested member. In the case of a plate, the shape factor is 0.96. And so the equation becomes:

$$f_p = 0.96\, C_p / 2T \quad (3\text{-}2)$$

P- wave speed is related to the concrete's density, aggregate type, moisture content as well as other factors. The P-wave speed can be determined in terms of the modulus of elasticity, E, and the Poisson's Ratio, ν, of the concrete in question. The P- wave speed is determined using the following equation: (Sansalone, 1986)

$$Cp = \sqrt{\frac{E \cdot (1-\nu)}{\rho \cdot (1+\nu) \cdot (1-2\nu)}} \quad (3\text{-}3)$$

During field testing, the P- wave speed is determined at a location where the concrete is sound and the thickness is known.

The amplitude response is altered by the presence of a flaw within the concrete. The effect of a flaw is illustrated by Figure 3.3(A) where the arrows schematically show the primary paths taken by the P- wave as it propagates into the

plate and is reflected and diffracted by the flaw and reflected by the bottom boundary. The waveform shown in Figure 3.4(B) illustrates the deflections caused by the multiple reflections of P-waves from both discontinuities. The frequency of the arrival of the P-waves increases due to the shorter travel path to the flaw in the concrete. Both sets of periodic displacements resulting from reflections from the flaw and from the bottom boundary are superimposed in the waveform shown. In the amplitude spectrum shown in Figure 3.4(C) the second (higher) frequency corresponds to the reflections from the flaw in the medium. The first (lower) frequency results from reflections from the bottom boundary of the medium. The depth of the flaw can be determined using Equations 1.

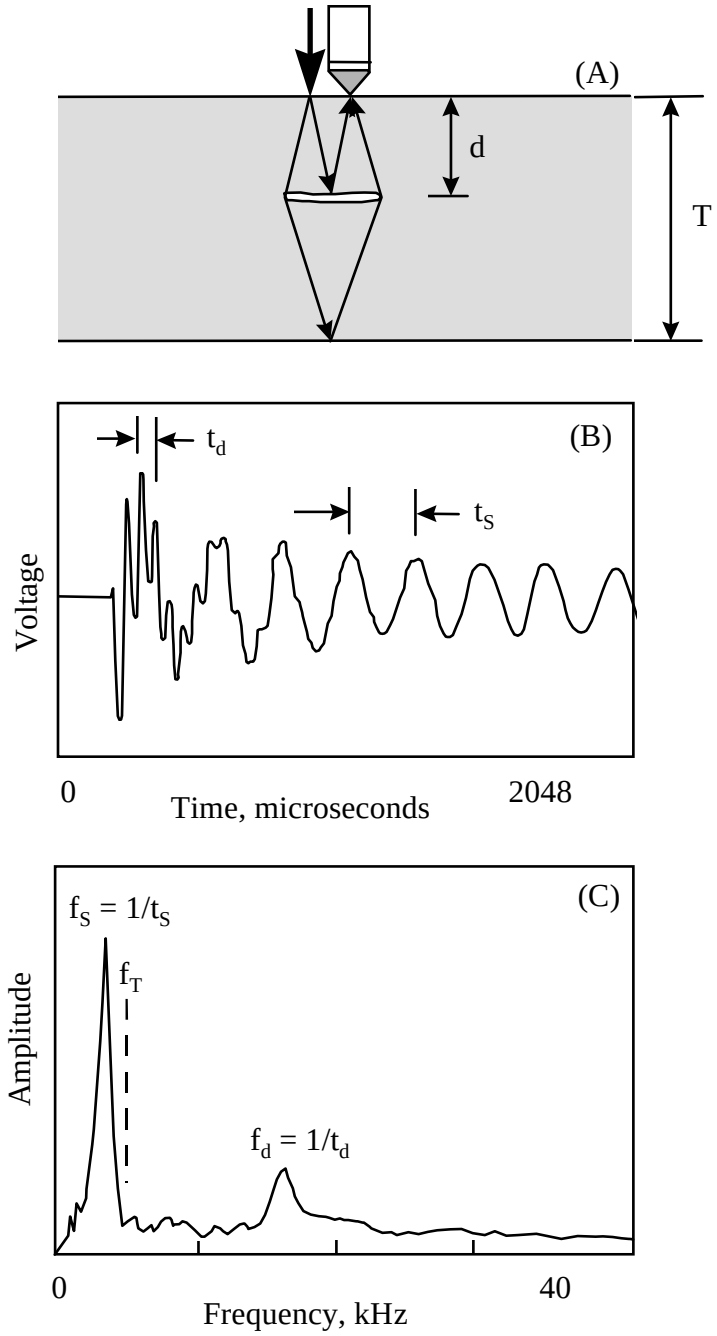

Figure 3.4 - Impact -echo test on a concrete plate containing a flaw. (A) (B) waveform, and (C) spectrum (Adapted from Sansalone and Streett, 1997)

3.6.1 Attenuation of Stress Waves

Attenuation is the result of scattering and absorption of the wave energy. As the spherical stress wave propagates through a material, the energy in the wave decreases the further the wave travels. This decrease in wave energy is due to attenuation and divergence. In a solid such as concrete, the scattering is the result of wave reflection, refraction, diffraction and mode conversion at each interface between dissimilar materials and especially at crack boundaries (Sansalone and Carino, 1986). Absorption is the direct conversion of stress wave energy into heat through friction caused by particle interaction. Divergence refers to the spreading of a spherical wavefront as it propagates through concrete.

The amplitude or intensity of the stress wave can be shown to be inversely proportional to the distance from its source. The relationship is described by the following equation:

$$I = I_0 / r \qquad (3\text{-}4)$$

Where: I_0 is the initial intensity of the stress waves

I is the stress wave intensity at r

R is the distance from the point of impact.

Since r is equal to the product of C_p and t, equation 3-3 can be written as:

$$I_2 = I_0 / C_p{*}t \qquad (3\text{-}5)$$

It can be seen that the decrease in energy over time is dependent on the P- wave speed in the material in question. The two previous equations describe the loss in intensity over time due to the divergence of the wavefront. In addition, when P- waves are incident upon the boundaries of the medium, a partial conversion of said P- waves

into S- waves occurs. This results in further losses in intensity. Clearly the more reflections, the more mode conversions that occur, and hence greater losses in wave intensity. For typical configurations, the mode conversion that occurs reduces the intensity of the reflected P-wave by approximately 3%. The theory described here is discussed in detail by Krautkramer and Krautkramer, 1990. That work is summarized in the following graph:

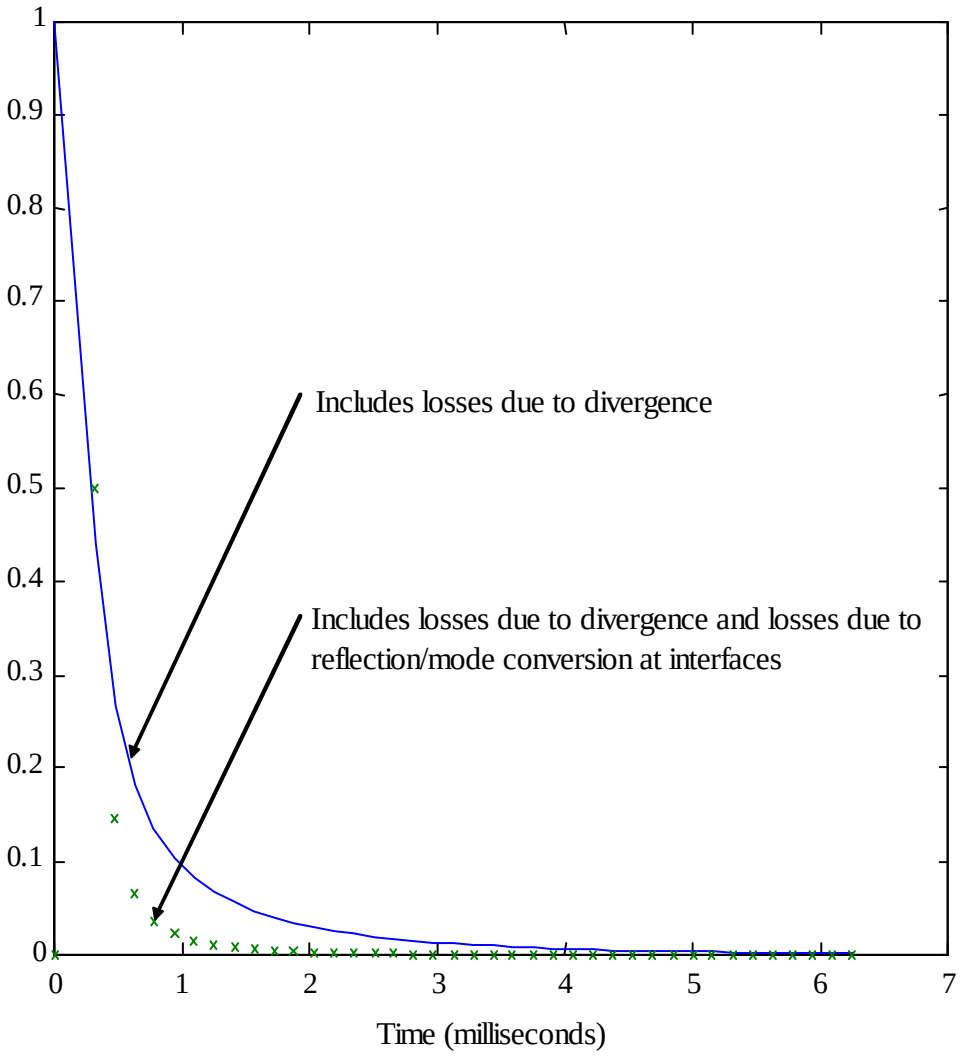

Figure 3.5 - Comparison of Stress Wave Intensity Losses

3.6.2 Losses in Real Materials

Krautkramer and Krautkramer have proposed that an exponential decay function be used to more accurately describe the losses that occur in real materials. In real materials, adsorption and scattering due to internal discontinuities occur in addition to attenuation, divergence and mode conversion. The form of the equation they propose is shown below:

$$I = I_0 \exp^{(-\alpha t)} \qquad (3\text{-}6)$$

Where: α - represents the decay constant

t – time

The advantages of using this equation are:

1. The decay constant provides a convenient measure of the rate that the intensity (pressure) in a P-wave decreases.
2. Losses due to divergence, scattering, and mode conversions can all be lumped together in the decay constant.
3. Use of a least squares curve fitting technique can be used to calculate the decay constant for real data. (P-wave arrivals in impact-echo waveforms)

The calculated decay constant is a convenient measure of the losses occurring as a P-wave propagates through a material. The use of this equation is described in Figure 3.6.

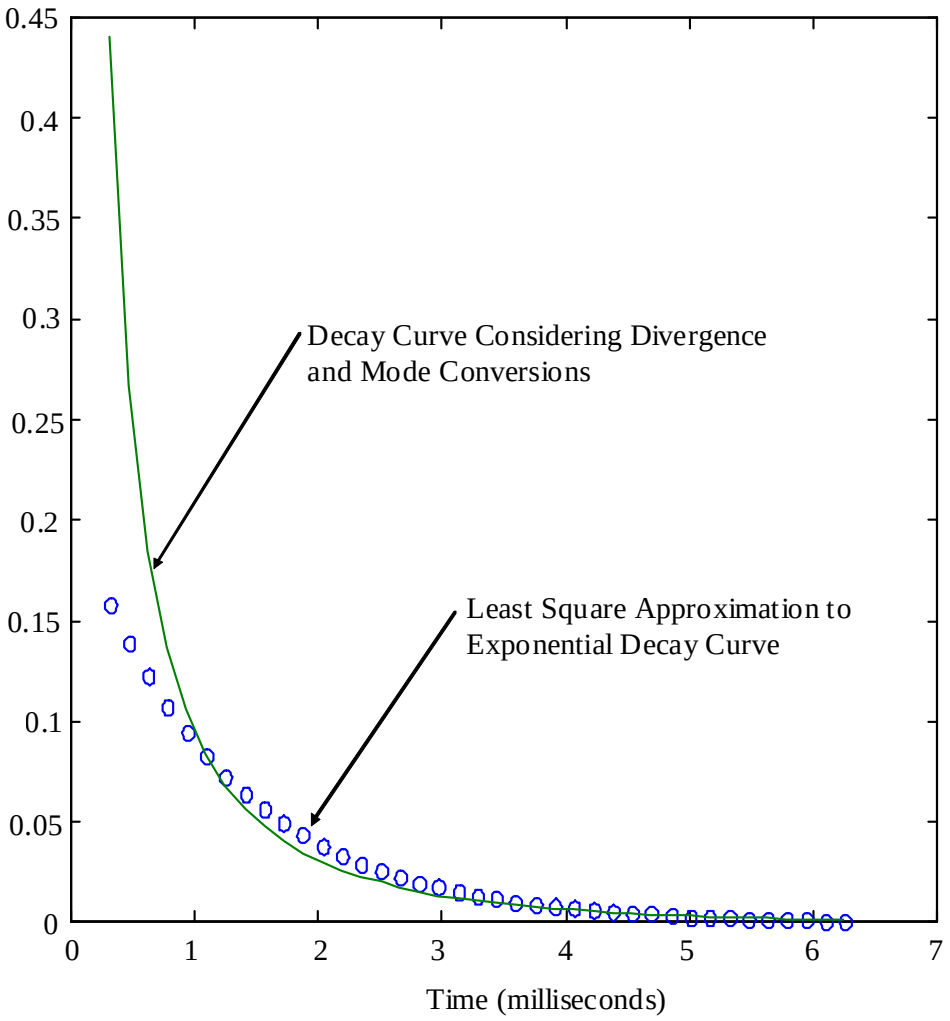

Figure 3.6 - Comparison of theoretical stress wave intensity curve and least squares curve fitting to decay curve.

3.6.3 Effects of Distributed Damage on Stress Wave Propagation

When stress waves propagate through concrete, they will be scattered at all crack boundaries and air voids. In good quality concrete, the amount of scattering that occurs due to microcracks and entrapped air voids has a negligible effect on the lower frequency stress waves used in impact-echo testing. (Sansalone and Carino, 1986) However, as the amount of cracking, caused by distributed damage mechanisms increases, the amount of scattering will increase.

Previous research on has shown that all cracks, having a crack opening larger than about 0.025 mm (0.001 in) will begin to scatter stress waves. (Cheng and Sansalone, 1995) As more cracks develop and open beyond 0.025 mm, they will transmit less energy across the crack and instead cause an increased amount of stress wave scattering. This will result in a more rapid decrease in stress wave intensity with time than is caused by divergence (beam spreading) alone. When cracks reach 0.08 mm (0.003 in) in width they become distinct cracks, and no energy is transmitted across the crack. (Sansalone and Streett, 1997)

3.6.4 Filtering of Waveforms

Impact on thin concrete plates excites flexural modes of vibration. These modes are apparent in the time domain as large amplitude, low frequency displacements superimposed upon the higher frequency displacement pattern caused by multiple reflections of the P-wave between the plate surfaces. In the frequency domain, peaks corresponding to the low frequency flexural vibrations appear at frequencies much lower than the thickness frequency and typically less than 5 kHz. As it is the decay in the amplitude of displacements caused by multiple P-wave

arrivals that is of interest, it is necessary to remove the displacements caused by the flexural vibrations.

Also, due to distributed damage there are several frequencies and the fluctuation of amplitude is large because there is beating of several frequencies and decay cannot be measured by using the raw signal. To measure the decay, the signal has to be band pass filtered around the frequencies presented in the spectrum and so the decay time can be measured to any frequency separately. This processing can be automated in MatLab. (Matlab, Signal Processing Toolbox, 1996)

3.7 Summary

To be sure, non-destructive evaluation of concrete is a serious and challenging problem. Improvements and new approaches are needed to meet this challenge, as existing ultrasonic and stress wave techniques are not yet adequate. All of the techniques discussed above require substantial theoretical and experimental development to meet the difficulties posed by this issue.

Chapter 4: Sample Preparation, Materials and Test Methods

4.1 Introduction

The procedures followed in order to prepare the concrete specimens for testing are outlined herein. The specifications of the materials and the subsequent test procedures are also explained. The preparation of the concrete specimens used in this study was done with the kind permission of the Civil and Environmental Engineering Lab of the University of Maryland at College Park and at the National Ready Mix Concrete Association Laboratory in Greenbelt, Maryland at their respective facilities.

Literature review and previous research done by Ceesay, 2007 concluded that adding potassium carbonate to the concrete mixture can accelerate its deterioration due to DEF. Two batches of concrete were prepared; the first was used as a control batch (Control), while the second was made with an additional 1.5% for a total of 2.06% of potassium carbonate per weight of cement (High Potassium). Both batches were subjected to a deteriorating method; either the UMD Modified Duggan Cycle, or Freeze-Thaw cycles. The degree of damage in the specimens was assessed by expansion tests, weight change measurements, compressive strength tests, Scanning Electron Microscopy (SEM), and impact-echo testing, the results of which would be used for further analysis.

4.2 Sample Preparation

4.2.1 Concrete Mix Design

Concrete specimens were prepared according to the ASTM C 192-06 standard for making and curing concrete specimens in the laboratory. An air-entrainment void system was not introduced to the concrete mixture since this would reduce the effect of secondary ettringite formation (Day, 1992) and reduce the amount of deterioration. The concrete mix was proportioned using the Absolute Volume Method and prepared with water to cement ratio of 0.5. Two batches were prepared. The first batch acted as the control batch and was made with no varying parameters. The second batch contained an additional 1.5% for a total of 2.06% of potassium carbonate by weight of cement. Potassium carbonate was added to second batch because, as stated before, the addition of potassium has proved to increase ettringite growth and expansion (Ceesay et al, 2007). The high potassium batch contained approximately 338.42 grams of potassium carbonate (KCO). Both batches were proportioned and mixed in the same manner. The mixing information of each batch is summarized in Table 4.1.

Table 4.1 – Concrete Mix Design

Constituent	**Weight**
Water	*24.89 lb*
Cement	*49.74 lb*
Coarse Aggregate	*111.6 lb*
Fine Aggregate	*81.62 lb*

The cement used was Portland Type III cement obtained from Greenwald Industrial Products of Hyattsville, Maryland. This type of cement was chosen because it has been proven to increase expansion and deterioration (Ceesay, 2007). An x-ray fluorescence (XRF) spectroscopy performed on a small sample of the cement done by CTL Group in Skokie, Illinois, revealed that the cement already contained 0.56% of potassium (K_2O) by weight. The complete report of the spectroscopy is included in Figure 4.1. The potassium already in the cement was not taken into account or subtracted from the 1.5% potassium carbonate per weight of cement added. Therefore, the High Potassium batch contained a total of 2.06% of potassium per weight of cement. The potassium used was anhydrous granular reagent grade potassium carbonate (KCO) obtained from Chemical & Scientific Advance in an online purchase. It was dissolved into the mix water of the concrete used for the High Potassium batch. The aggregates used were obtained from the LAFARGE quarry in Frederick, Maryland. The coarse aggregate consisted of 1-inch maximum diameter limestone aggregate. The technical information for the coarse aggregate is shown in Table 4.2. The fine aggregate was Frederick Stone Sand that conforms to ASTM C33-99a. The technical information for the fine aggregate is shown in Table 4.3. According to the Maryland State Highway Administration, the potential Alkali reactivity of the sand using ASTM C1260 is 0.9% and is considered intermediate reactive.

Analyte	Weight %
SiO_2	18.44
Al_2O_3	4.86
Fe_2O_3	3.36
CaO	58.46
MgO	3.87
SO_3	2.73
Na_2O	0.13
K_2O	0.56
TiO_2	0.30
P_2O_5	0.11
Mn_2O_3	0.31
SrO	0.06
Cr_2O_3	0.03
ZnO	0.09
L.O.I. (950°C)	6.58
Total	99.90
Alkalies as Na_2O	0.50

Calculated Compounds per ASTM C 150-05.

C3S	53
C2S	13
C3A	7
C4AF	10

Figure 4.1 – XRF Spectroscopy of Portland Type III Cement

Table 4.2 – Technical Information for Coarse Aggregate

LAFARGE Frederick Quarry ASTM # 57 Stone Technical Information Sheet			
Rock Type:	Carbonate		Calcitic Limestone
Color:	Light to dark gray		
Average Gradation	Dry Analysis		Wet Analysis
ASTM C136	% Passing		% Passing
1 (in)	0		100
3/4 (in)	7.3		93.5
1/2 (in)	48.6		39.1
3/8 (in)	26		15.3
# 4	15.1		3.7
# 8	1.9		1.1
Pan	1.1		1.1
	Bulk	SSD	Apparent
Specific Gravity (AASHTO T85)	2.712	2.75	2.74
Absorption (ASTM C127)	0.3%		
200 Wash (ASTM C 117)	1.5%		
Polish Value (MSMT 411)	7		
British Pendulum Number (ASTM D 411)	26		
Alkali Silica Reactivity (MSMT 212 / ASTM C1260)	0.09% expansion		
L.A Abrasion (AASHTO T96 / ASTM C131)	26% wear		
Sodium Sulfate Soundness (AASHTO T104)	0.1 % loss		
Unit weight, dry rodded (AASHTO T19)	95.7#/CF		
MOHs Hardness	4.0		
Sand equivalency (AASHTO T176)	94%		
Fractured faces (PMT 621)	100%		

Table 4.3 – Technical Information for Fine Aggregate

LAFARGE	**Frederick Quarry, Maryland Manufactured ASTM C33 Stone Sand Technical Information Sheet**	
Rock Type:	Carbonate	Calcitic Limestone
Color:	Light to dark gray	
Average Gradation	Analysis	
ASTM C136	% Passing	
3/8 (in)	100	
#4	98.3	
#8	86.6	
#16	53.9	
#30	29.4	
#50	16.9	
#100	6.2	
#200	3.4	
Specific Gravity (SG)	2.69	
Absorption	1.0%	
Alkali reactivity of aggregate (ASTM C1260)	0.09% expansion	
Soundness	1.2% Loss	
Unit weight, dry rodded	109#/CF	
Los Angeles Abrasion	22.0% Loss	
Deleterious Substances - 200 Wash	3.6% Dust of Fracture	

4.2.2 Casting Procedure

Concrete specimens were prepared using steel prism molds and PVC cylinder molds in accordance with ASTM C192. The prisms prepared were 3” wide by 3” high by 11.25” long, and the cylinders were 4” in diameter and 8” long as seen in Figure 4.2. The steel prism molds had to be assembled with steel gage studs, for expansion measurements, using a rod so that 10 inches of space was available between them in accordance to ASTM C490 as shown by Figure 4.3. The prisms were used for expansion tests, weight change measurements and impact-echo testing, while the cylinders were used for compressive strength tests.

Figure 4.2: Steel Prism Molds and Cylinder Molds

Figure 4.3 - Steel Gage Studs in Prisms and 10” Rod Spacer

Motor oil was spread inside the molds with a sponge to help the de-molding process. The materials were proportioned in buckets using a mechanical scale and the potassium carbonate was measured on a digital metric scale and dissolved in the water used for the high potassium batch. A rotating mixer with a capacity of 3.0 cubic feet was used to mix the concrete. After the concrete mix was prepared, it was poured into the cylinder molds in two layers, rodding each layer 25 times and tapping the cylinders against the floor after each layer. The prisms were also tapped against the floor as the mixture was poured. Once this was complete, the specimens were struck off to obtain a finished smooth surface and either covered with aluminum foil (prisms) or with a lid (cylinders) to prevent drying and shrinkage. A total of 28

concrete cylinders were prepared (14 for each batch) and 23 concrete prisms (12 for the Control batch and 11 for the High Potassium batch).

4.2.3 Curing Method and storage Condition

All 28 concrete cylinders and 17 of the concrete prisms (9 from the Control batch and 8 from the High Potassium batch) were steam cured directly after casting for four hours at 85 °C in a conventional oven. The concrete prisms (total of 6) which were not steam cured were used for Freeze-Thaw cycles and were room temperature cured. After curing, all the specimens were taken out of their molds and stored. Based on the results found by Ceesay et al (2007), it was concluded that limewater was the ideal storage condition to accelerate deterioration in the specimens through ettringite growth. The specimens were stored by fully submerging them in plastic containers with limewater, as seen by Figure 4.4, at the Civil and Environmental Engineering Lab at College Park for approximately 18 days before subjecting them to either the UMD Modified Duggan Cycle or the Freeze-Thaw cycles. The limewater was created by dissolving hydrated lime, obtained from a local plant store, in regular tap water. Once the Duggan Cycle was completed, the specimens were then returned to the limewater containers where they stayed for the remaining testing period.

Figure 4.4 – Duggan Cycle Concrete Prisms Stored in Limewater

4.3 Methods for Accelerating Concrete Deterioration

4.3.1 UMD Modified Duggan Heat Cycle

A total of 17 concrete prisms and 28 concrete cylinders were subjected to the UMD Modified Duggan heating cycle. This cycle has been proven to accelerate deterioration in concrete by initiating cracking and ettringite formation (Ceesay et al, 2007) and takes nine days to complete. The specimens were subjected to this heating regime approximately 18 days after casting. Although in previous studies, the Duggan Cycle is initiated seven days after casting, the decision to wait 18 days was based on the conclusion made by Ramadan (2000) which found that extended periods of water storage can accelerate crack initiation time and maximize the rate of expansion. The

Duggan Cycle was carried out in the following manner. The specimens were placed in an oven at 82 °C for the first 24 hours. In the second day, the specimens were taken out of the oven and allowed to cool down for one hour and a half before storing them in water for another 24 hours. This process was repeated on the third and fourth day. On the fifth day, the specimens were placed in the oven at 82 °C for the next 72 hours. Once this heating period was over, the specimens were allowed to cool down for the last 48 hours. The initial measurements of expansion, weight change, and impact echo testing were taken after the completion of this cycle and subsequent measurements were taken every three to five days.

4.3.2 Freeze Thaw Cycles

The Freeze-Thaw cycles were carried in accordance with ASTM C 666 standards. A total of 6 room temperature cured concrete prisms were used for freeze-thaw testing. Freeze Thaw testing on the concrete prisms was performed in a Rapid Freeze-Thaw Cabinet apparatus, see Figure 4.5. In this test six concrete prisms were used, three from each batch, and each cycle consisted of lowering the temperature from 4.4 °C to -18 °C and raising it back up to 4.4 °C. This apparatus was not programmable and therefore was manually stopped after every three cycles for the first 30 cycles and after five cycles thereafter until the Q-factor values could no longer be obtained or until the specimens failed. The average amount of time to complete one cycle was approximately 5.4 hours. However, the actual amount of time varied since it depended on the condition of the specimens. As the prisms deteriorated, the cycles became shorter.

Figure 4.5 - Rapid Freeze-Thaw Cabinet

4.4 Condition Evaluation of Concrete Specimens

4.4.1 Expansion Tests

Expansion measurements were taken in accordance with ASTM C 157 Standard Test Method for Length Change of Hardened Mortar and Concrete with a digital comparator accurate to + 0.0001 inches see Figure 4.6. The initial measurements were taken after the completion of the UMD Modified Duggan Cycle and before any Freeze-Thaw cycles were done. Subsequent readings were taken every three to five days (Duggan specimens), or after a specific number of Freeze-Thaw cycles (Freeze-Thaw specimens). The expansion measurements were made relative to a 10" long bar after the specimens were taken out of the water and the excess water was removed with a towel. The equation used to calculate expansion percentage was:

$$\Delta L = \frac{L_x - L_i}{G} \times 100\% \qquad (4\text{-}1)$$

Where,

ΔL - length change of the specimen at any age, %

L_x - comparator reading of specimen at *x* age minus comparator reading of reference bar at *x* age, inches

L_i - initial comparator reading of specimen minus comparator reading of reference bar at that same time, inches

G - nominal gage length, 10 inches

Figure 4.6 – Length Comparator Used for Expansion Tests

4.4.2 Weight Measurements

Weight change measurements were done after the expansion measurements. The initial measurements were taken after the completion of the UMD Modified Duggan Cycle and before any Freeze-Thaw cycles were done. A digital weighing scale was used, see Figure 4.7. The specimens were taken out of the water, dried off with a towel, and weighted. The equation for weight change was:

$$\Delta W = \frac{W_x - W_i}{W_i} \times 100\% \qquad (4\text{-}2)$$

Where,

ΔW - Weight change of the specimen at any age, %

W_x – Weight of specimen at age x.

W_i - Initial weight of specimen

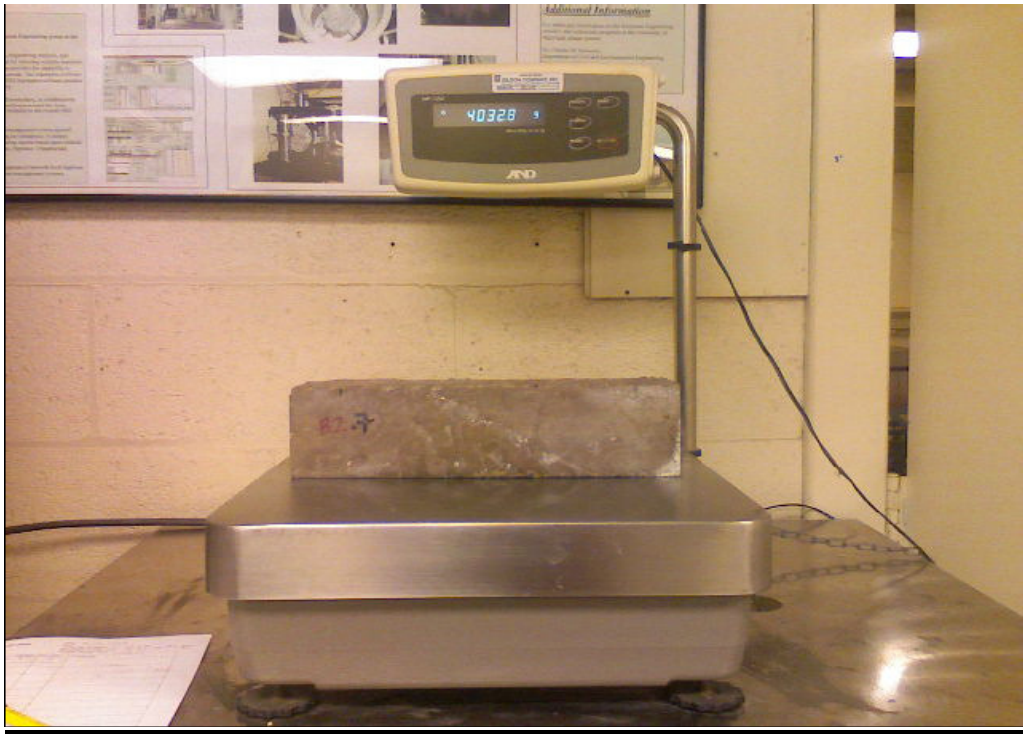

Figure 4.7 - Scale Used for Weight Measurements

4.4.3 Impact Echo Testing

Impact-echo testing was done every time weight and expansion measurements were taken. The specimens were tested using the standard method as set out in ASTM C215. The impact-echo apparatus used consisted of a Fourier Analyzer, an impact hammer, an accelerometer and power supply, a specimen support base, and a computer with Virtual Bench software, see Figure 4.8. The hammer was equipped with a tip of sufficient hardness and appropriate shape so as not to damage the concrete when used to impact it. It also contained an electronic load cell and a power supply capable of producing an output voltage that is proportional to the magnitude of the impact with the specimen. The accelerometer used was approximately 3/8 of an inch in diameter with a flat base and was attached to the specimens during testing using vacuum grease. The specimen support base is made up of two parallel piano wires of 0.0244-inches (0.62 mm) in diameter that allow the specimen to vibrate freely and minimize the amount of vibration energy absorbed from the specimen itself. The wires were set up to support the specimen at a specific distance from each end of the specimen. Virtual Bench DSA software was used to control the equipment and to record and store the data. OriginPro v.8 software was used to analyze the data.

The procedure used with this impact-echo device was different than that used by commercial products in the field. Testing a specimen consisted of centering it on the supporting wires in such a way as to have equal ends extending beyond the wire. The location of the wires was marked on all the specimens to keep the set up of each and their alignment consistent throughout the testing period. The accelerometer was attached to the top surface of the specimen as close to one end as possible using

vacuum grease. Securing the accelerometer on the specimen was important in order to prevent irregularities in the response curve. After setting the specimen in place, a vertical impact was applied centered on the top surface and on the opposite end to where the accelerometer was attached. The impact was applied as near the end of the specimen as possible. The responses from the impact hammer and the accelerometer were recorded using Virtual Bench software. At least three impacts on the specimens were applied before recording a final response, stopping vibrations between impacts, to observe a consistent response and a smooth shape. It was important to stop the vibrations between impacts because these can cause irregularities in the data. It was expected that as the specimens deteriorated, the response curve would become less smooth due to internal cracking.

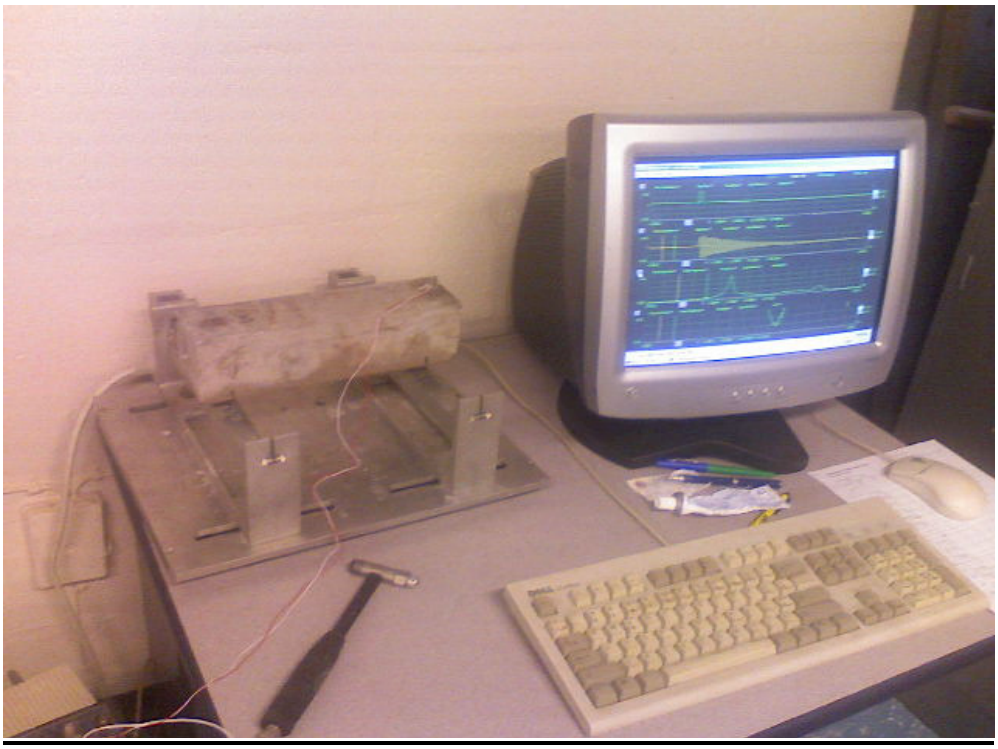

Figure 4.8 – Impact Echo Apparatus

4.4.4 Compression Strength Testing

Compression strength tests were performed in accordance with ASTM C39 standards on 24 concrete cylinders (12 from each batch) which were subjected to the Duggan Cycle. A machine with a 400,000 lbs capacity was used, as shown in Figure 4.9. The specimens were removed from the limewater, dried off with a paper towel, and measured (diameter measurements) before testing them at a load rate of approximately 25,000 lb/min. These tests were done at 7, 30, 90, 120, and 150 days (+ 2 day) after the completion of the Duggan Cycle. The compressive strength reported is the average compressive strength.

Figure 4.9 – Compression Strength Testing Machine

4.4.5 Scanning Electron Microscopy

In SEM a beam of electrons with an accelerated voltage of 10-20 kV is trained at the concrete sample. As a result, three signals are produced; secondary electrons (SE), backscattered electrons (BE), and X-ray. The SE are used to obtain the morphology of the microstructure of the samples while BE are used to reflect the differences in atomic number. Energy dispersive X-ray analysis (EDAX) is used to obtain the elemental composition of a point on the image produced. Each element is identified by its position of its peak and a quantitative analysis by weight of elements is calculated by a computer. This process must take place in a laboratory. Figure 4.10 shows the Scanning Electron Microscope that was used for this research.

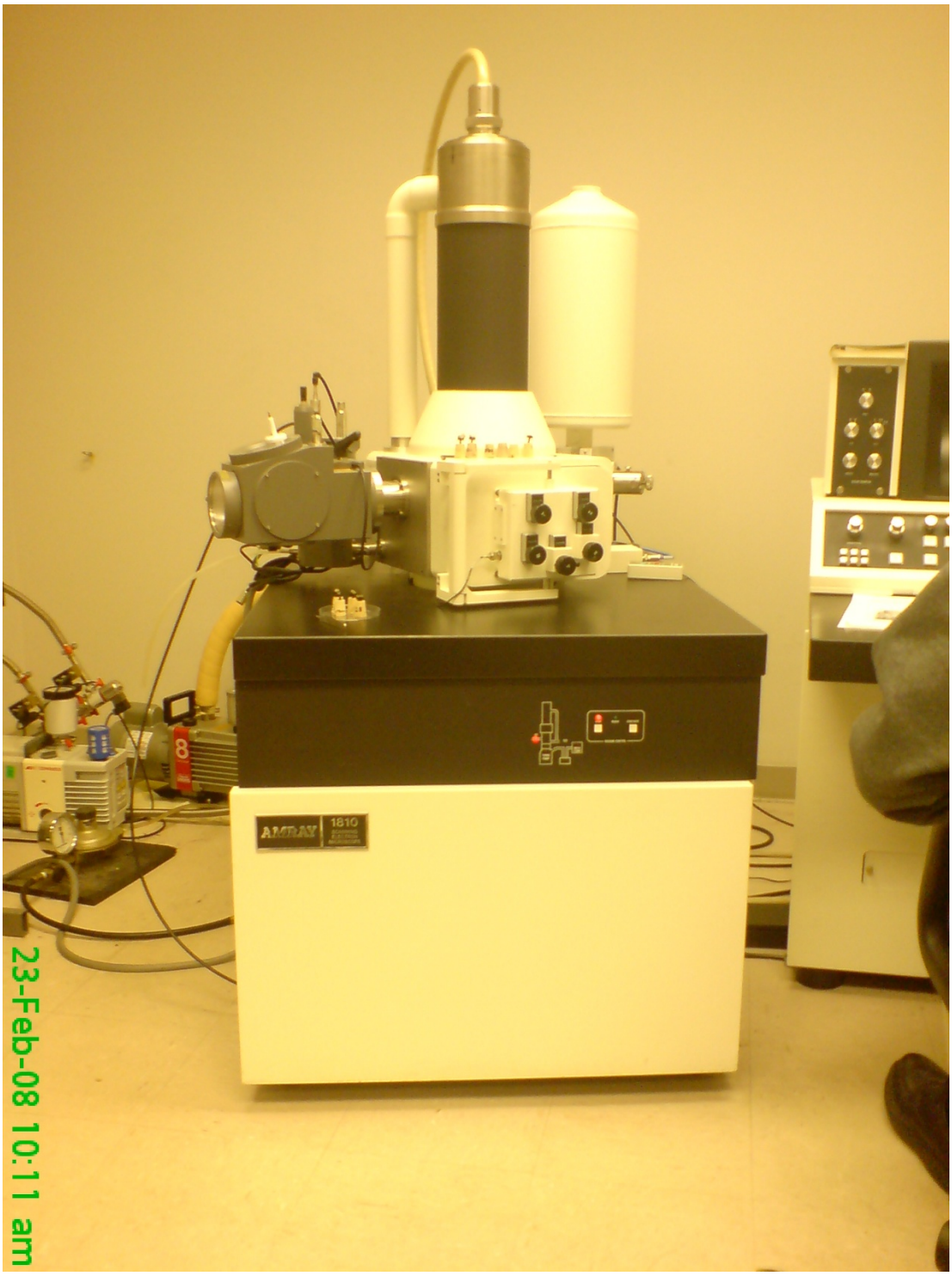

Figure 4.10 – Scanning Electron Microscope

Chapter 5: Concrete Samples Subjected to the Duggan Cycle

5.1 Introduction

The importance of accurately reproducing distributed damage due to DEF and ASR in the laboratory in order to properly investigate these mechanisms cannot be overstated. Numerous research projects have investigated various methods throughout the years. These attempts are chronicled by Shimada, 2005 and Famy et al., 2001. The Duggan cycle was used to reveal damage in the shortest amount of time and is intended to accelerate DEF and the associated expansion. Through literature review and previous research experience, factors such as exposure conditions and concrete treatment were optimised to facilitate the acceleration of DEF and its associated expansion.

The concrete samples prepared for laboratory testing were produced using standard techniques for the production of small quantities of concrete. Proportioning of the concrete was done using volumetric methods. Both the mix designs and the concrete curing regimes were altered from standard practice to accelerate the formation of distributed damage in the concrete specimens. All concrete specimens (prisms) are 29.21 x 7.62 x 7.62 cm (11 ½ x 3 x 3 inches). This specimen size is in accordance with ASTM standards. Each of the components of the concrete mix was chosen specifically to accelerate the formation of distributed damage primarily by means of ettringite formation.

Two batches of concrete mixes were used in the experimental program. The first batch, (Control), was created as the control specimens with no additional

potassium carbonate added. The second batch, (High Potassium), was made with an additional 1.5% potassium carbonate by weight added to the mix water. Potassium carbonate was added to increase the alkali content of the concrete specimens. Anhydrous granular reagent grade (K_2CO_3) was used. Potassium carbonate was chosen because the result of the chemical reaction in the concrete mix is the same as that which occurs with the normal reaction of potassium, as potassium sulfate, which is contained in Portland cement. Ordinary tap water and a water cement ratio of 0.5 were used for all batches. Frederick Sand (manufactured sand) was used in all the batch mixes and, according to the Maryland State Highway Administration (MDSHA), the ASR result is 0.09%. The MDHSA classified the Frederick Sand to be of medium reactivity. Limestone ASTM # 57 stone was used for the coarse aggregate for the entire study. All specimens were steam cured and then stored under water for six days. Subsequently each specimen was subjected to the Duggan cycle. Expansion, weight change and Impact Echo tests were continuously performed on these specimens throughout the duration of the research.

In addition to the concrete prisms that were prepared, concrete cylinders were also prepared. These cylinders were produced using the same materials and within the same guidelines described above and therefore also fall into the categories of Control and High Potassium. Compressive strength tests were performed after 28days and then at various intervals throughout the duration of the research. Three (3) concrete cylinders from each exposure condition were tested, and the average result used.

In order to directly determine the presence of ettringite, samples of the specimens taken from the compressive tests were examined using a scanning electron

microscope. In each case the cylinders were broken up into pieces by the compressive tests and polished. Several samples were prepared for each specimen. In addition to the images provided by the scanning electron microscope, and energy dispersive X-ray analysis (EDAX) was performed on each sample to determine the exact composition of suspected deposits of ettringite. Ettringite is seen as needle like crystals in the SEM images.

The objectives were to monitor the deterioration of the concrete specimens in a comparative and quantitative way. The creation of a control batch and a high potassium batch of specimens allowed for comparative monitoring. The use of expansion, weight change, compressive strength and fundamental frequency measurements allowed for the quantitative monitoring of the deterioration of specimens subjected to the Duggan cycle.

5.2 Influence of Curing Methods and Concrete Treatments

The influence the exposure condition has on the form and size of the ettringite found in mortar or concrete specimens is significant. Ceesay, 2006 and Azzam, 2001 investigated several exposure conditions and highlighted the most severe. Exposure conditions with abundant moisture are ideal for expansion associated with delayed ettringite formation. Ettringite formation requires a sufficient supply of water.

Immediately after casting, the specimens, while in steel molds and covered with aluminum foil, are placed in a water bath in an oven, the temperature of which is raised to 85°C for 2 hours. The heat of the oven is then maintained at 85°C for 4 hours, after which the specimens are allowed to cool overnight. This constitutes the

steam curing procedure which simulates precast concrete in which much of the early cases of DEF were found. Most cases of distributed damage (DEF in particular) have been associated with the use of heat treatment such as this.

Duggan heat and Freeze-Thaw cycles (discussed in the subsequent chapter) were used to create microcracks in order to accelerate the expansion of the concrete specimens. The specimens were placed in an exposure condition of limewater (pH maintained at 12.5) after the microcrack-inducing treatments. Gage studs were installed at the ends of the concrete prisms to facilitate length-change measurements.

5.3 Expansion Results

The Duggan test was seen as the best method to achieve accelerated expansion because it produces quantitative data in less than a month. Expansion measurements were done in accordance with ASTM C490. Expansion is measured as the change in displacement between two points on opposite ends of the test specimen. It should be noted that this measurement implies that the expansion would be linear and/or uniform throughout the specimen, which of course is not the case. Due to micro-cracking caused by DEF, there is actually a volumetric expansion in association with the differential movement of individual pieces of the material as the micro-cracks form and propagate. However, for our intents and purposes this measurement was found to be suitable.

5.3.1 Expansion of Concrete Prisms

The initial length measurements were taken after two (2) days of cooling after the Duggan heat cycle and before storage to the respective exposure conditions. Expansion readings were then collected at specific intervals. The expansion value after 21 days of storage was 0.0054% and 0.0083% respectively for control and high potassium specimens.

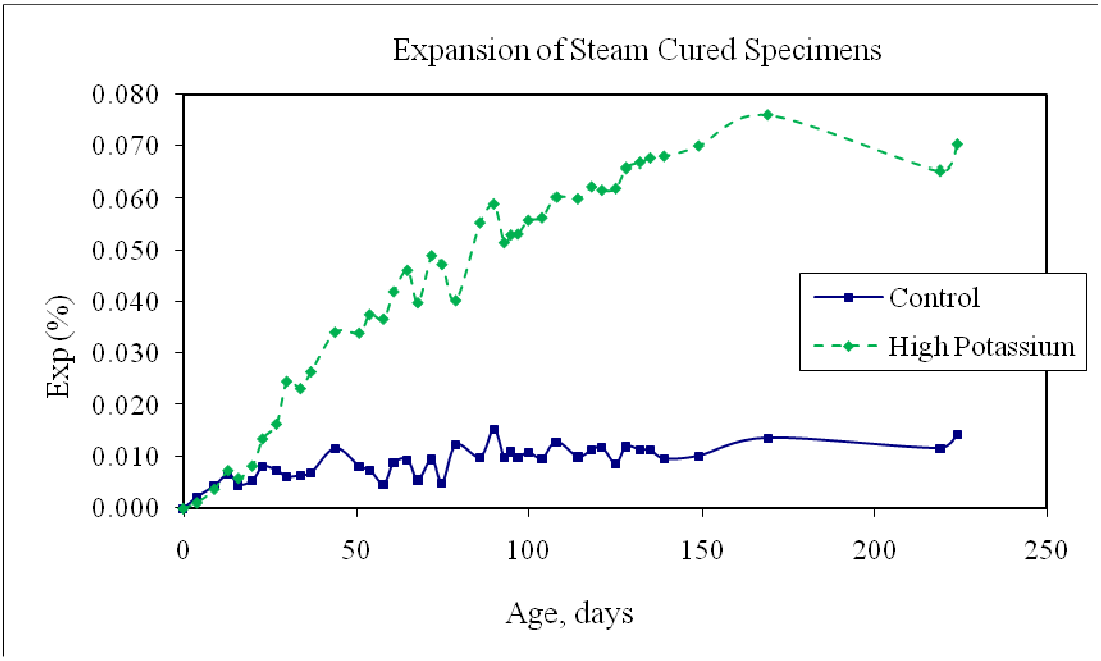

Figure 5.1: Expansion of Steam-Cured Concrete Prisms Subjected to Duggan Cycle

The overall expansion of the high potassium specimens far exceeded the expansion of the control specimens. After 150 days the expansion values were 0.0102% and 0.0700% for control and high potassium specimens respectively. The point of divergence between the two expansion curves occurs at about 22 days, where the control curve continues its gradual expansion and the high potassium curve distinctly increases its rate of expansion in comparison to the control specimens.

Figure 5.1 shows the expansion history of both sets of specimens whilst Figures 5.2 and 5.3 show the individual expansion histories of each set of specimens.

Linear regression analyses were performed on both sets of data. Each set of data was easily separated into two parts and a regression analysis was performed on each. The R^2 term gives some indication about the goodness of fit of the data to the regression model (line). For instance, and R^2 value of 1 indicates that the data fits the regression line perfectly. Figures 5.2and 5.3 show this data and Table 5.1 summarizes the regression results.

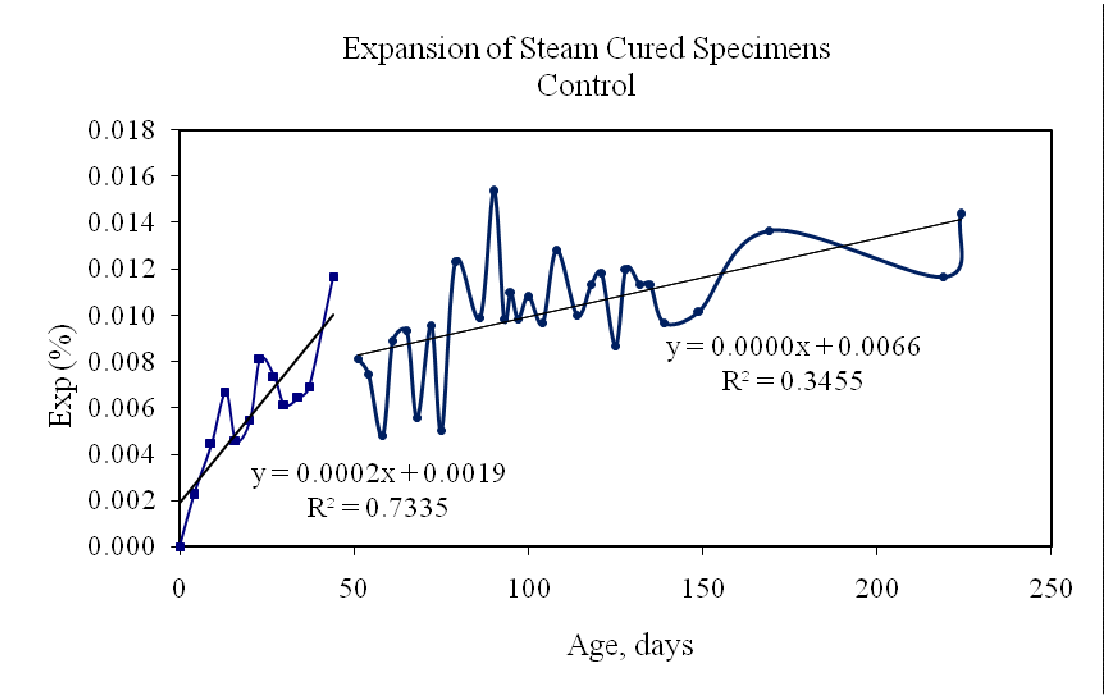

Figure 5.2: Expansion of Control Concrete Prisms Subjected to Duggan Cycle

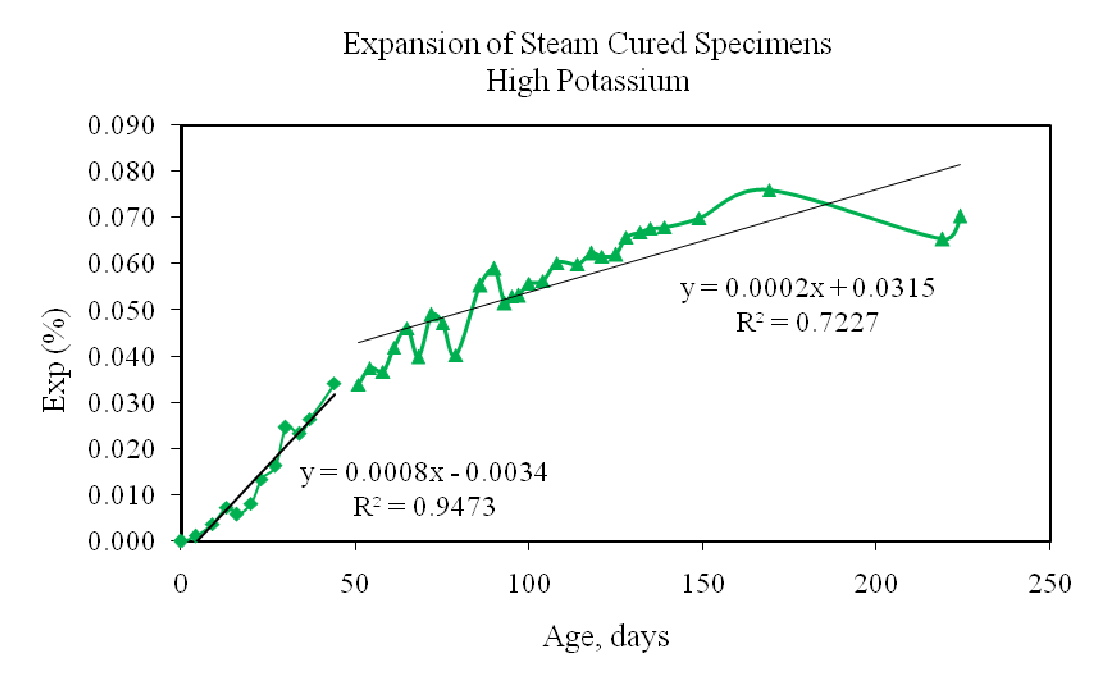

Figure 5.3: Expansion of High Potassium Concrete Prisms Subjected to Duggan Cycle

Table 5.1 Equations for Expansion vs. Age of Concrete Specimens Subjected to Duggan Cycle

Specimen	**Max. Expansion**	**Curve 1**		**Curve 2**	
		Equation	R^2	*Equation*	R^2
Control	0.015%	y=2E-04x+0.0019	0.734	y=3E-05x+0.0066	0.346
High Potassium	0.076%	y=8E-04x-0.0034	0.947	y=2E-04x+0.0315	0.723

5.4Weight Change Results

The pattern of weight change is quite similar for both control and high potassium specimens. Figure 5.4 shows the comparison of weight change for control and high potassium specimens. Each point is the averaged result of 10 or more specimens for each batch mix (control or high potassium). Weight measurements were recorded on each test day after 30 minutes had elapsed since removing them from the limewater. This gave sufficient time for excess water to evaporate as well as assure the consistency of the measuring technique.

The overall weight change and the rate of weight change were consistently similar for both control and high potassium batches. After 34 days the percentage weight changes were 0.51% and 0.49% respectively for control and high potassium batches. The maximum weight changes were equally comparable at 0.678% and 0.697% respectively.

Figures 5.5 and 5.6 show the individual weight change histories. These Figures also show the Linear fitting analysis that was done for each batch. Table 5.2 summarizes the linear fit equations and the maximum weight change for each batch.

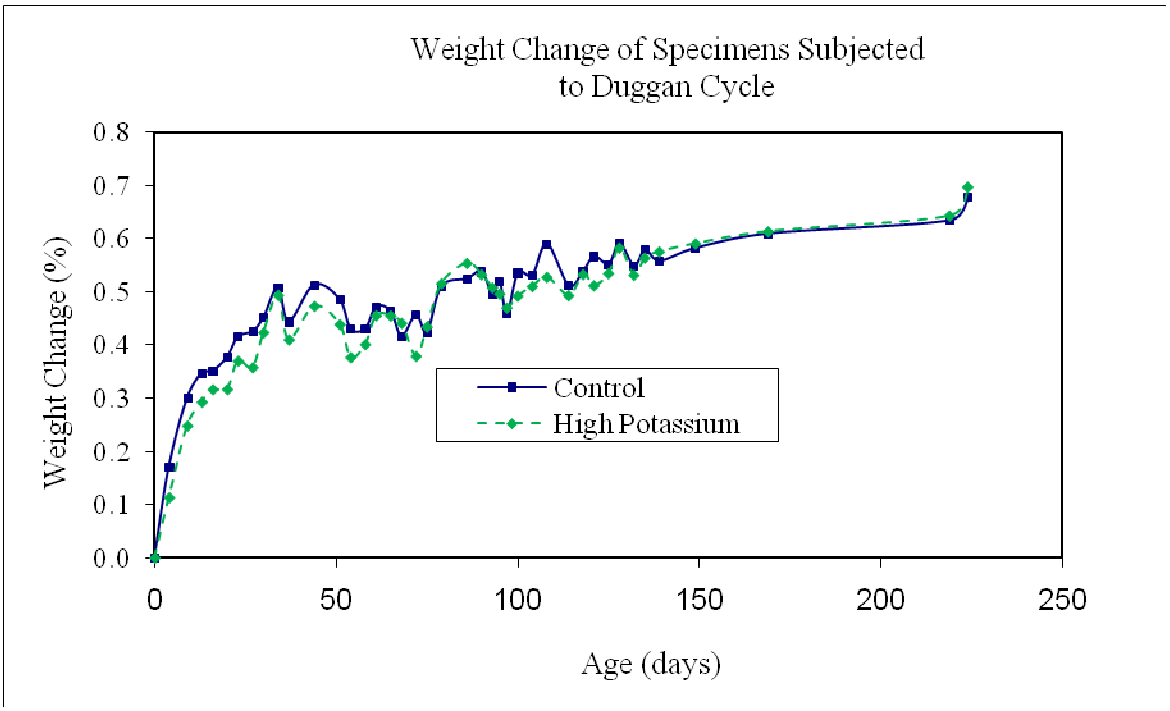

Figure 5.4: Weight Change of Steam-Cured Concrete Prisms Subjected to Duggan Cycle

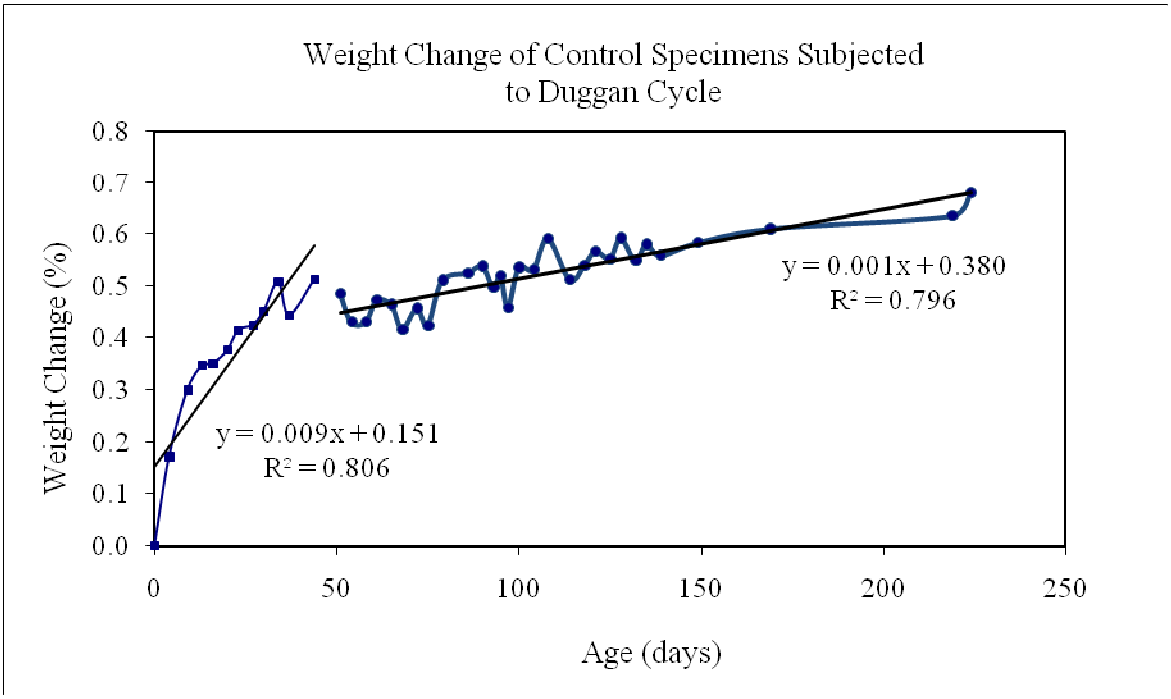

Figure 5.5: Weight Change of Control Concrete Prisms Subjected to Duggan Cycle

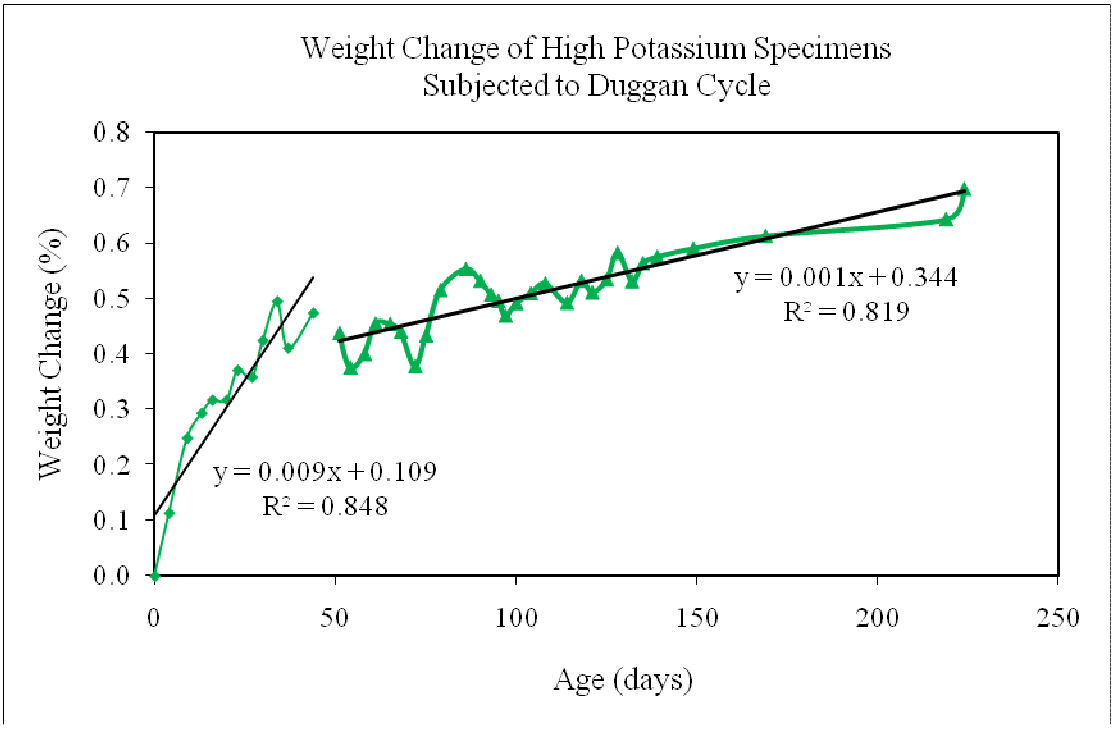

Figure 5.6: Weight Change of High Potassium Concrete Prisms Subjected to Duggan Cycle

Table 5.2 Equations for Weight Change vs. Age of Concrete Specimens Subjected to Duggan Cycle

Specimen	**Max. Wgt Change**	**Curve 1**		**Curve 2**	
		Equation	R^2	*Equation*	R^2
Control	0.678%	y=9.7E-03x+0.151	0.806	y=1.3E-03x+0.381	0.796
High Potassium	0.697%	y=9.7E-07x+0.110	0.848	y=1.6E-03x+0.345	0.820

5.5 Expansion vs. Weight Change

Weight change and expansion results were analyzed simultaneously in order to investigate a possible correlation. Shimada (2005) had proposed that the weight change during the early stage was primarily due to the cement hydration process. After the onset of expansion there is a large weight increase which is attributed to the storage solution which has been imbibed to fill the structural defects.

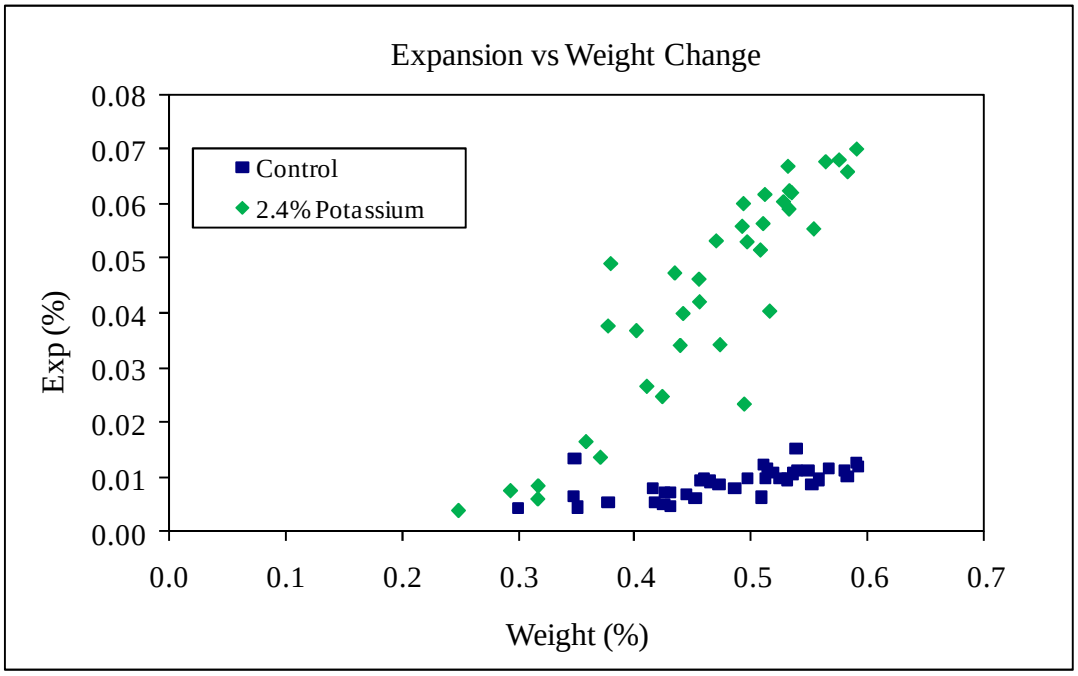

Figure 5.7: Expansion vs. Weight Change of Steam Cured Concrete Prisms Subjected to Duggan Cycle

Figure 5.7 shows the correlation between weight change and expansion for both the control and high potassium batches. It can be seen that only the high potassium specimens display significant increase in weight accompanied by expansion. Linear regression curves were applied to each individual set of data in

order to elucidate the relationships present. These are highlighted in Figures 5.8 and 5.9 and furthermore in Table 5.3.

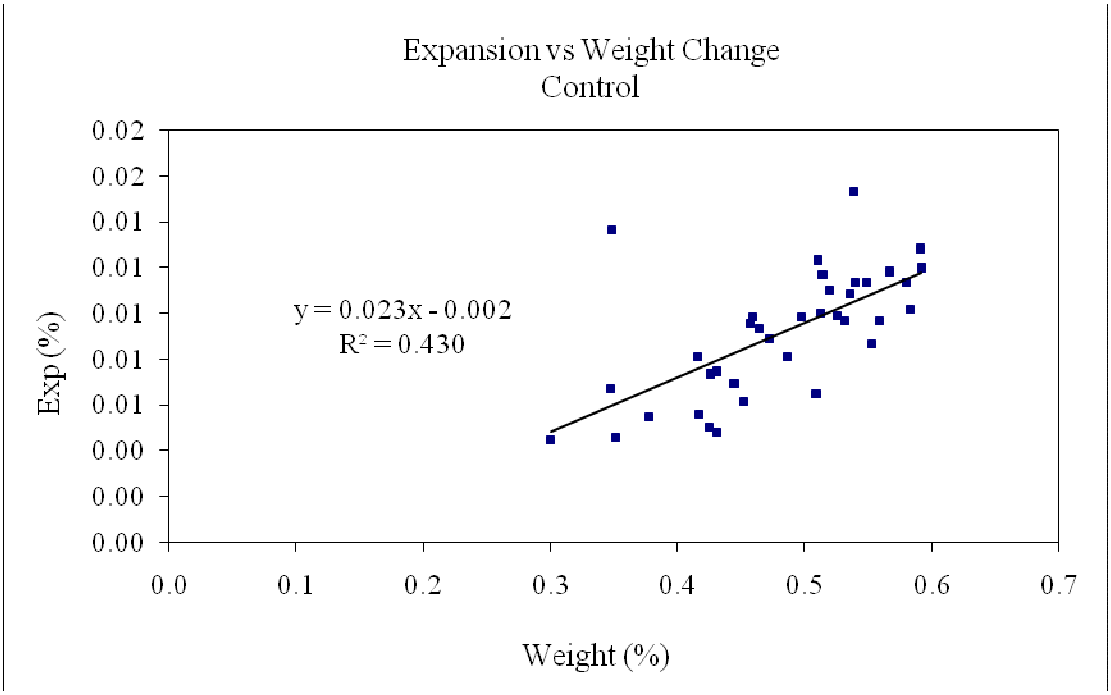

Figure 5.8: Expansion vs. Weight Change of Control Concrete Prisms Subjected to Duggan Cycle

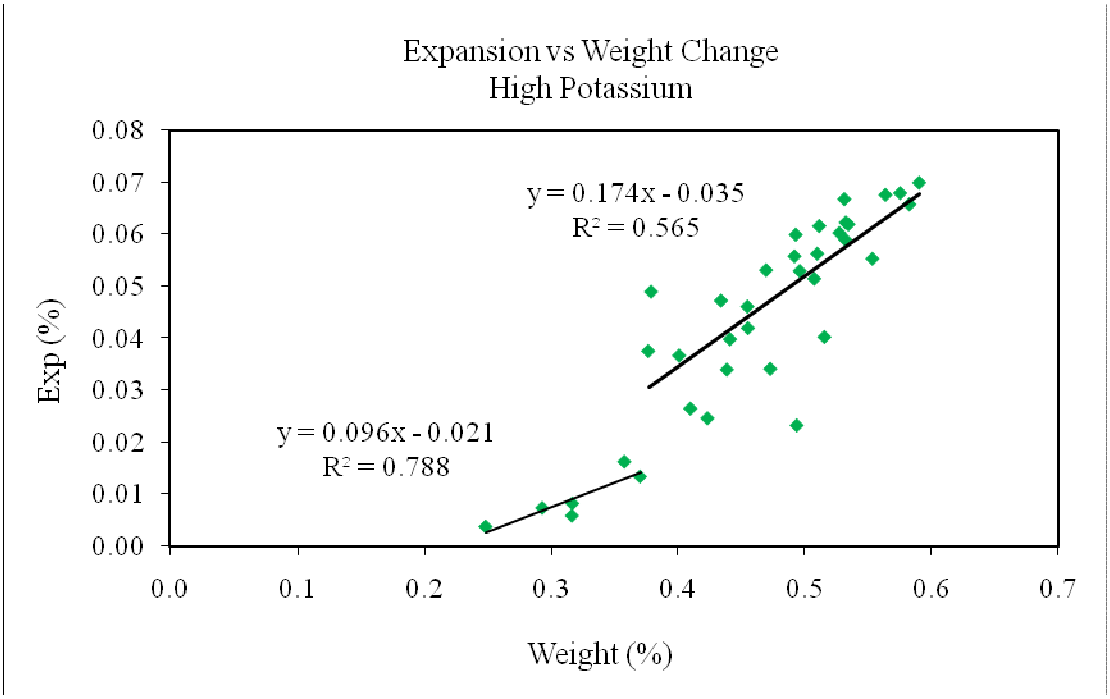

Figure 5.9: Expansion vs. Weight Change of High Potassium Concrete Prisms Subjected to Duggan Cycle

Table 5.3 Equations for Expansion vs. Weight Change of Concrete Specimens Subjected to Duggan Cycle

Specimen	**Curve 1**		**Curve 2**	
	Equation	R^2	*Equation*	R^2
Control	y=0.024x-0.002	0.431	-	-
High Potassium	y=0.096x-0.021	0.788	y=0.174x-0.035	0.565

5.6 Compressive Strength

The results of the compressive strength tests are shown in Figure 5.10. Compressive strength testing was done in accordance with ASTM C 39 – 05. The tested cylinders were approximately 4" in diameter and 8" long. The 28 day strength of the cylinders after being steam cured and subjected to the Duggan cycle were, on average, 1854 psi and 2001 psi respectively. After 150 days the compressive strengths were 5739 psi and 3115 psi respectively for the control and high potassium specimens. The high potassium specimens peaked in strength at around 90 days at 3748 psi and then began a steady decline. Table 5.4 summarizes the compressive strength of the specimens subjected to the Duggan cycle.

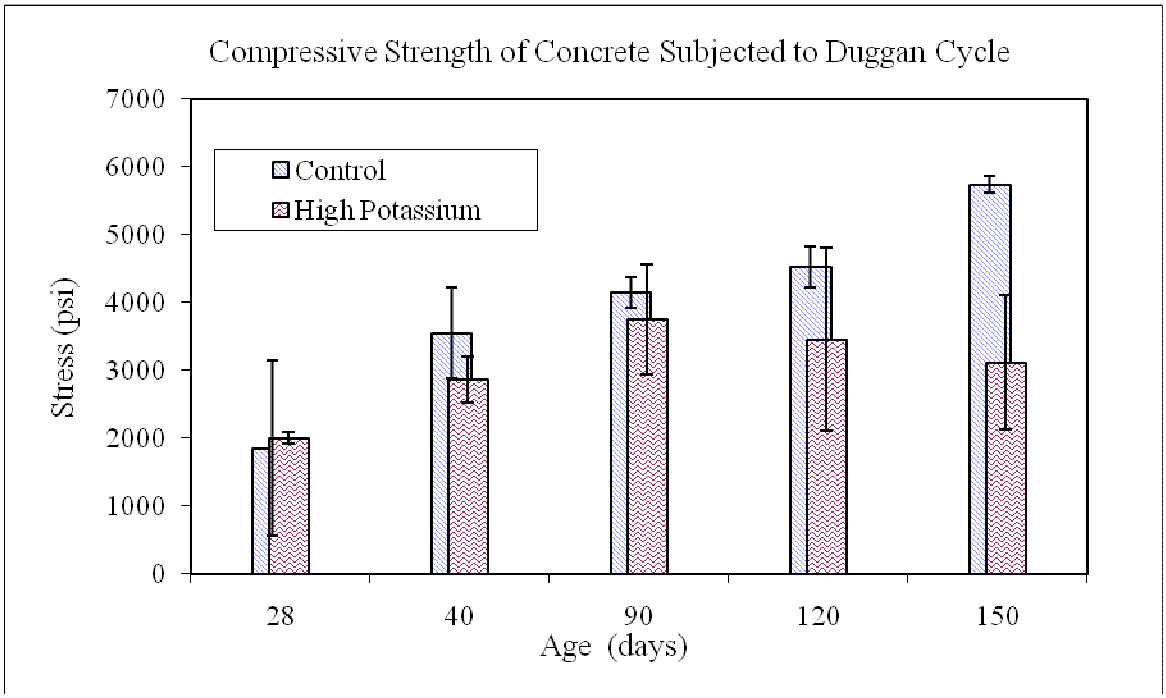

Figure 5.10: Compressive Strength Bar Chart of Concrete Prisms Subjected to Duggan Cycle

Table 5.4 Compressive Strength of Concrete Specimens Subjected to Duggan Cycle

Age	B1			Std Dev	B2			Std Dev
	1	2	3		1	2	3	
28	1855	3682	-	1291.9	2001	1879	-	86.3
40	4079	2806	3764	663.0	3011	2709	2343	334.5
90	3975	4063	4397	222.6	3781	3715	2342	812.4
120	4,370	4,873	4,330	302.5	3,233	3,689	1,166	1344.7
150	5,885	5,679	5,654	127.1	2,694	3,537	1,563	990.6

5.7 Fundamental Frequency

The test results for the fundamental transverse frequencies of the concrete prisms subjected to the Duggan cycle are shown in Figure 5.11. The tests were performed in accordance with ASTM C 215 – 02. Janssen and Snyder have proposed the use of this method for determining the amount of deterioration produced by accelerated durability tests. The resonant frequency of a concrete prism depends on its orientation. Square test prisms 3" x 3" x 11 ¼" were used. Figure 5.11 shows the results of the frequency testing. After a slight increase the results are relatively consistent throughout the duration of testing. The high potassium batch produces a consistently lower fundamental transverse frequency than the control batch.

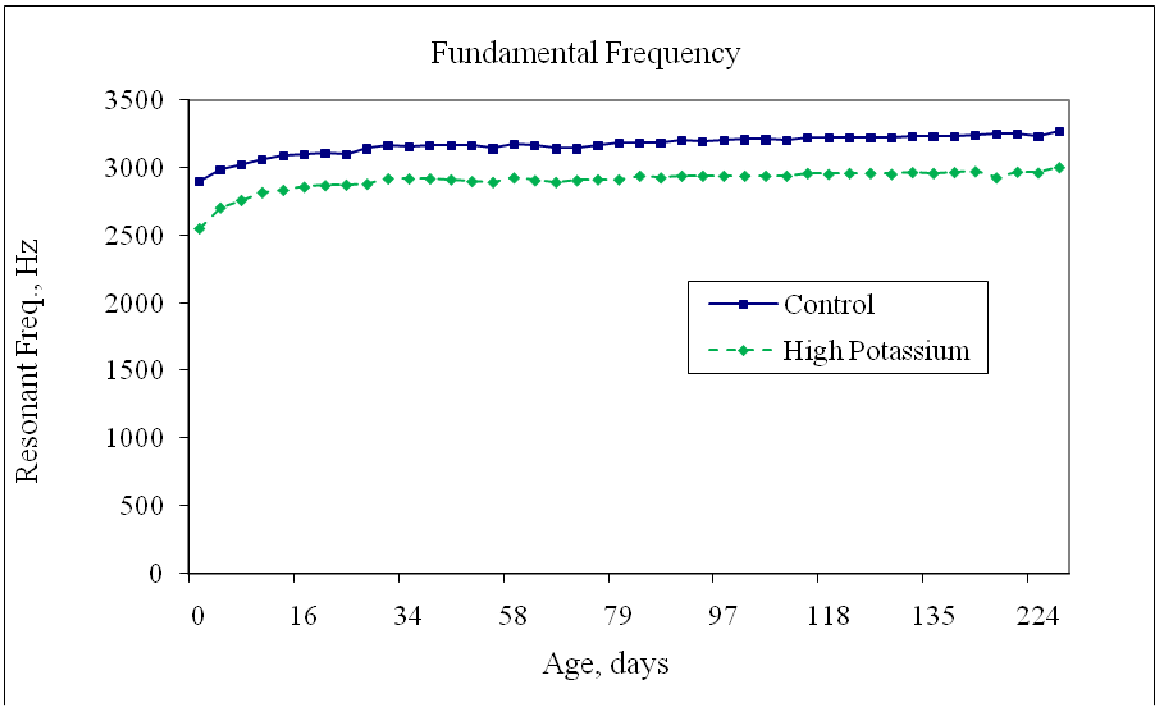

Figure 5.11: Fundamental Frequency of Steam-Cured Concrete Prisms Subjected to Duggan Cycle

5.8 SEM and EDAX Analysis

Scanning electron microscopy (SEM) in correlation with Energy dispersive x-ray analysis (EDAX) can be used to determine the presence of ettringite in concrete. Ettringite produces Ca, Al and Sulfur peaks on the EDAX with the rule of thumb being that a 2:1 S to Al weight ratio is the best bet for ettringite. Correction factors Z, A and F correct the peak heights to more accurate weight numbers. The correction factors being for Atomic number, Absorption and Flourescence.

Small relatively flat pieces of concrete were chosen from the interior and exterior of the prisms as test specimens for the SEM. They should contain aggregate as well as cement paste. The samples were mounted on corks (Figure 5.12) with special carbon glue. Samples are then dried in a vacuum oven for approx. 20 minutes. Then the samples are coated with carbon to enable better viewing (see Fig. 2). Carbon is used b/c it is the only element that will not show up on the EDAX analysis.

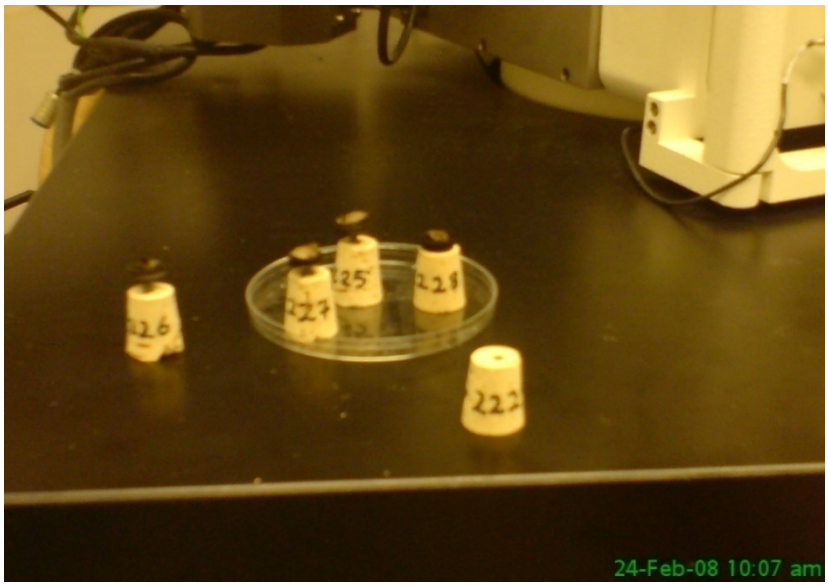

Figure 5.12: Samples prepared for SEM testing

5.8.1 Control Concrete Specimens @ 100 days

Upon examination of five different prepared SEM samples it was not possible to find an instance of ettringite crystals from these specimens. Both cement matrix and aggregate particles were free of ettringite needles. Figure 5.13 is a characteristic SEM image of the microstructure of these specimens.

Figure 5.13: SEM and EDAX Analysis of Control Concrete Prisms @ 100 days

5.8.2 High Potassium Concrete Specimens @ 100 days

At 100 days of storage in calcium hydroxide, SEM images showed numerous ettringite balls and needles throughout the samples. Ettringite needles were found in the cavities between the aggregate particles and the cement paste. Energy Dispersive Analysis X-ray (EDAX) verifies the elemental composition of the crystal formations by showing the distinct aluminum, sulfur, and calcium pattern in general. Figures

5.14 and 5.15 show the two morphologies of ettringite, the first being clusters or balls of ettringite and the second being the needle like shape of the crystals.

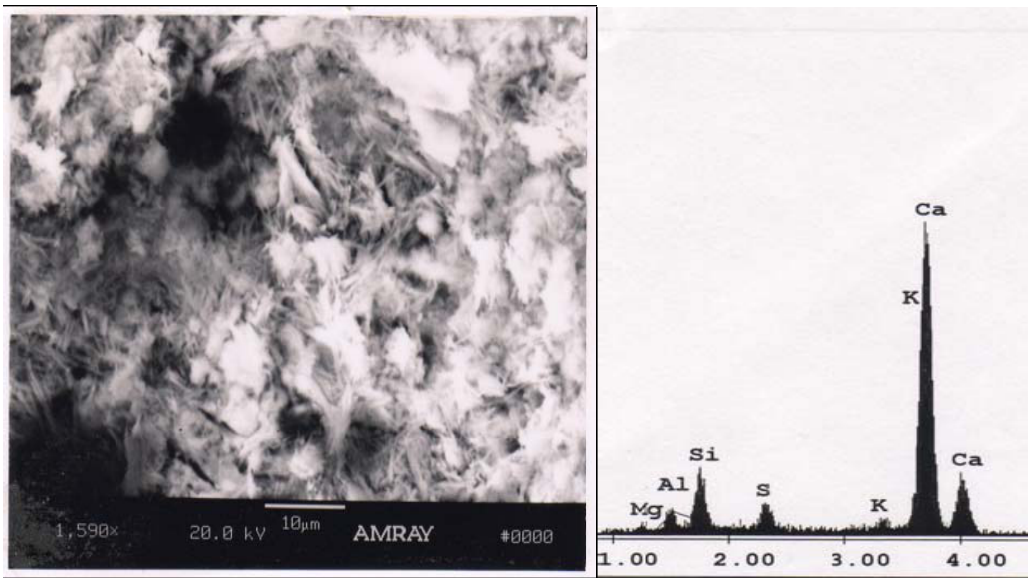

Figure 5.14: SEM and EDAX Analysis of High Potassium Concrete Prisms @ 100 days

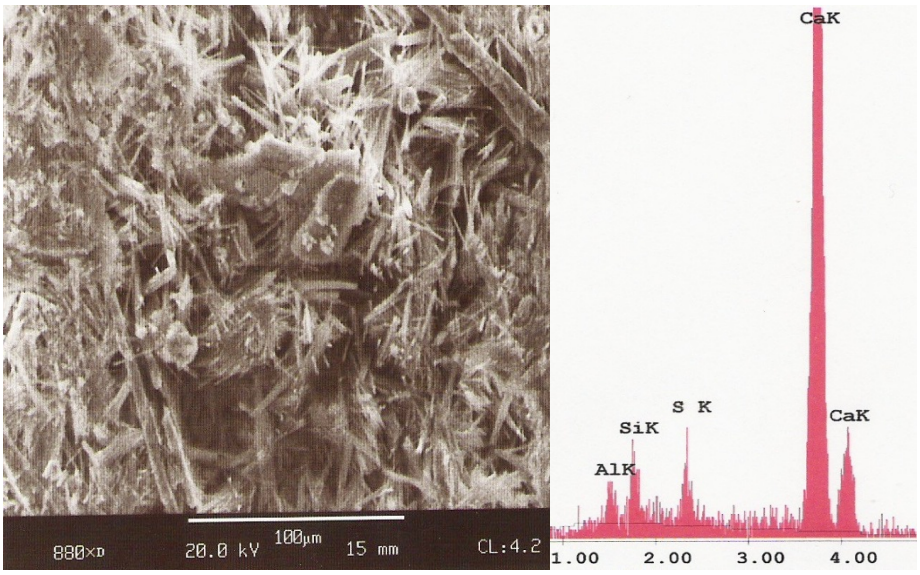

Figure 5.15: SEM and EDAX Analysis of High Potassium Concrete Prisms @ 100 days

5.8.3 Control Concrete Specimens @ 150 days

The samples prepared at this stage contained long ettringite crystals that filled anywhere from much less than 5% to not more than 20% of the voids. Ettringite crystal morphology was found but the EDAX analysis, a graph of intensity against x-ray energy could not verify the result. The high silicon (Si) peak presence in this analysis revealed the early presence of C-S-H gel, which is later converted to ettringite, as water became predominantly available.

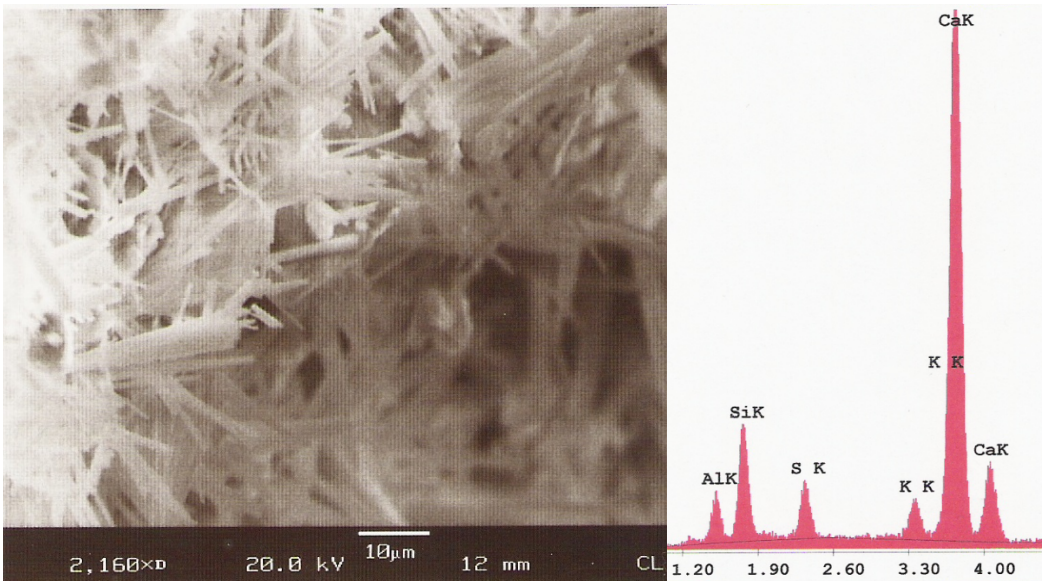

Figure 5.16: SEM and EDAX Analysis of Control Concrete Prisms @ 150 days

5.8.4 High Potassium Concrete Specimens @ 150 days

At this stage several beds of balls of ettringite were found throughout the samples that were tested. The EDAX analysis verified these observations by exhibiting the typical relationship between the elements needed for ettringite. The EDAX results revealed that the scanned deposits had the chemical composition of Al

= 3.00% wt., Si = 2.25% wt., S = 7.87% wt., and Ca = 83.21% wt. This is characteristic of ettringite and was mostly observed in air voids and at the aggregate boundaries.

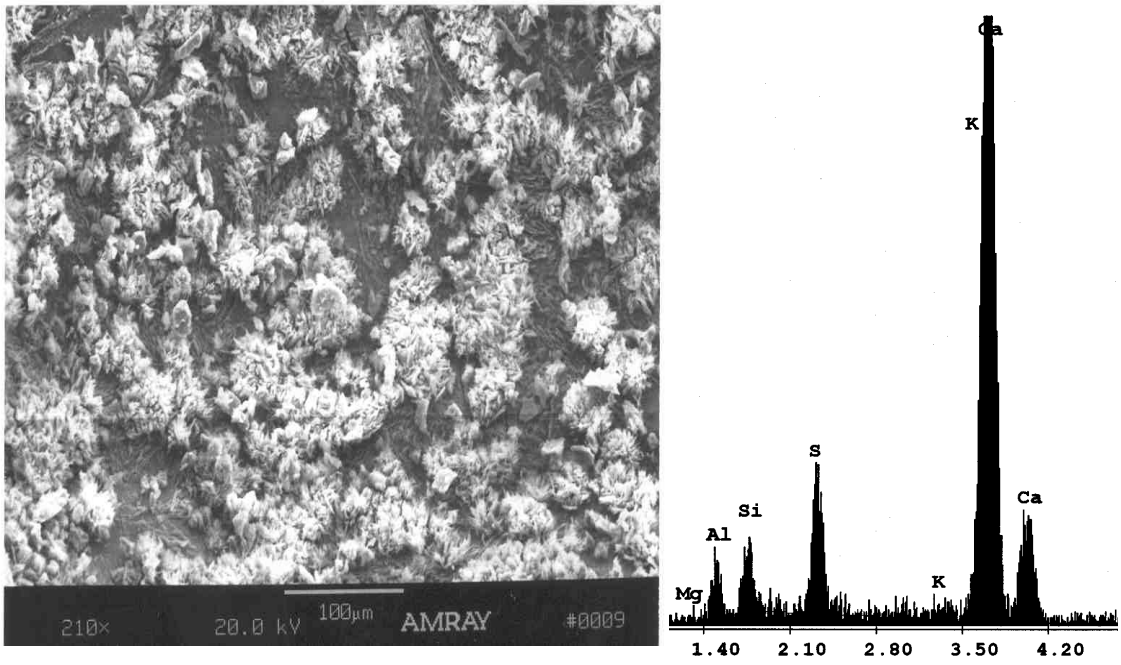

Figure 5.17: SEM and EDAX Analysis of High Potassium Concrete Prisms @ 150 days

5.8.5 Control Concrete Specimens @ 200 days

At this stage occasional voids were found with long ettringite crystals that filled anywhere from much less than 5% to not greater than 50% of the voids. An SEM image and the related EDAX graph are shown in Figure 5.18. The SEM image shows ettringite rims near a sand particle. Energy Dispersive Analysis X-ray (EDAX) verifies the elemental composition of the crystal formations by showing the distinct aluminum, sulfur, and calcium pattern in general.

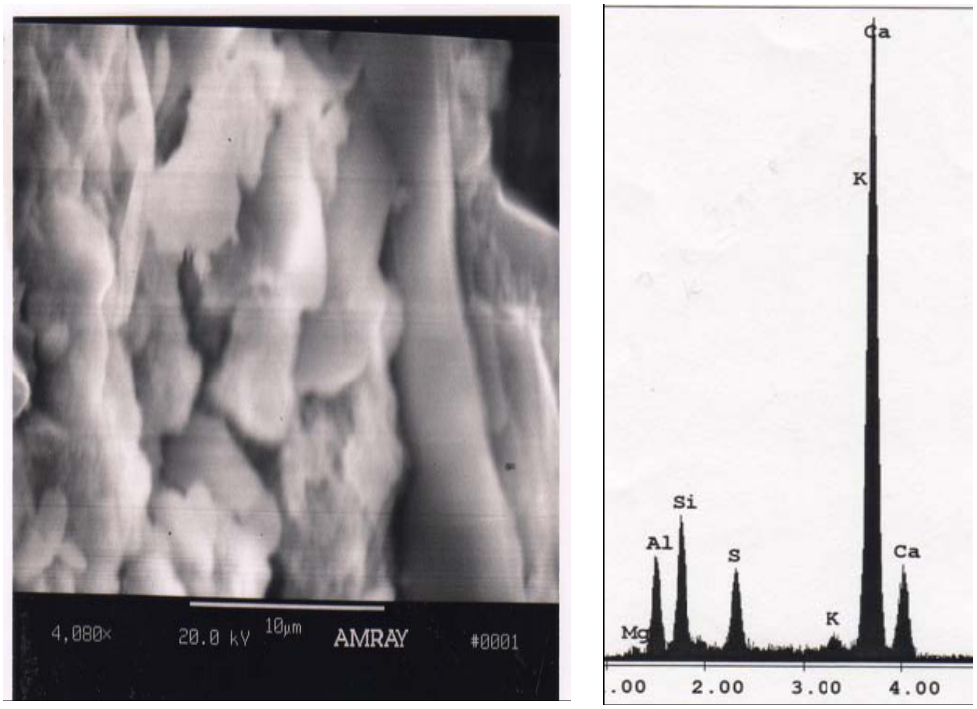

Figure 5.18: SEM and EDAX Analysis of Control Concrete Prisms @ 200 days

5.8.6 High Potassium Concrete Specimens @ 200 days

At this stage ettringite dominates the samples. Different samples show different relationships in their EDAX analysis. The EDAX results indicate that the material deposits have a chemical composition of Al = 3.05% wt., Si = 1.38% wt., S = 8.11% wt., and Ca = 85.55% wt., which is characteristic of ettringite. The chemical composition from the EDAX analysis varies because of experimental errors and isomorphous substitutions of elements. Elements may substitute for one another, for instance Al for Si.

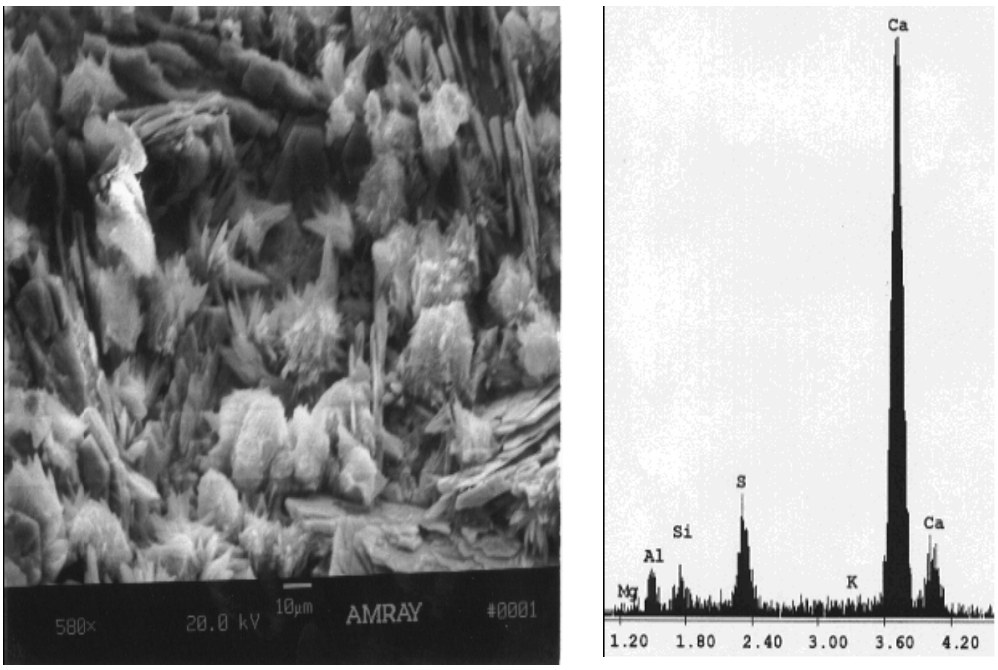

Figure 5.19: SEM and EDAX Analysis of High Potassium Concrete Prisms @ 200 days

5.9 Summary and Discussion

It is well understood that the presence of micro-cracking in cementitious systems weakens the paste matrix while providing space for the crystallization of ettringite. Micro-cracks were induced in the concrete samples in an effort to replicate distributed damage observed in the field due primarily to DEF as well as other mechanisms. Ekolu, Thomas and Hooton (2006) considered the Duggan test severe and observed that it might induce DEF. This corroborates well with the goal of this portion of the research which was to accelerate DEF and induce distributed damage that could later be monitored using non-destructive techniques.

Both the control and the high potassium concrete samples show moderate expansion up until 44 days after casting. At this stage there is a sharp increase in expansion of the high potassium sample compared to the control concrete samples. There is continuous debate in the literature between the supporters of the crystal pressure theory and supporters of the paste expansion theory as to whether DEF is a cause or consequence of expansion. The results depicted herein do not pretend to settle this debate but with the corroboration of the SEM images the results definitely highlight the relationship between expansion and DEF, that is, they go hand in hand.

Both sets of concrete samples exhibited similar weight change patterns. Weight change is perhaps best monitored using mortar bars that contain only the paste of concrete and not the aggregate. It is inferred that the aggregate comprises most of the mass of the concrete specimen and since it is inert the weight change and in particular the difference in weight change between the two batches will be minimal. This issue will also be manifested in the expansion vs. weight change plots. For the high potassium samples, the point of divergence in the expansion plots can be correlated to the gradient change in the expansion vs. weight change plots. Again this increase in expansion is associated with crack propagation in the concrete samples.

The compressive strengths of both batches of concrete samples showed a steady increase up to 90 days after casting. Coinciding with the first set of SEM images which show the high potassium batch to contain significant amounts of ettringite crystals, the compressive strength of the high potassium batch starts to decline. This decline continues through the remainder of the experiment. The relationship between the loss of strength and the expansion does not go unnoticed.

The differences in the rate of development of early strength and the time required to trigger the deleterious reaction is of importance in enabling the concrete to develop its early hydration largely uninterrupted and to mature before the effects of expansion take place. The increased expansion allows for the interconnection of micro-cracks and voids in the concrete which weakens the microstructure and reduces the compressive strength.

The resonant frequency results obtained were of crucial importance in lieu of what was ahead in the research. The resonant frequency of a concrete prism varies depending on the testing mode and the orientation of the prism. The resonant frequency in the longitudinal direction is typically higher than in the transverse direction. Tests performed during this research were in the transverse direction and in accordance with ASTM C215. The high potassium batch of concrete specimens produced a consistently lower fundamental frequency than its control counterpart. What is also noticeably absent is a correlation between the fundamental frequency and the sudden increase in expansion rate at around 44 days. Micro-cracks increase the damping of the concrete reducing the vibration amplitude and flattening the frequency response curve. Cracking and deterioration also cause the resonant frequency to decrease; because waves take longer to travel through concrete with many cracks and voids. Sansalone and Streett discuss this in detail.

Scanning electron microscopy (SEM) in collaboration with Energy dispersive x-ray analysis (EDAX) techniques were used to analyze the microstructure of the concrete. The SEM images can show small particles or components of deterioration and provide the elemental chemical analysis of what is observed. Obvious features

associated with DEF are cracks around aggregate particles which form part of the intricate network of cracks that assist DEF, whether by crystal pressure theory or by paste expansion theory. The continuous availability of water to cracked concrete creates ideal conditions for DEF. The morphology of ettringite changes over time from small spherical ettringite balls to needle-like crystals. These crystals eventually grow to form massive ettringite crystals. The storage condition of limewater obviously assisted the growth of DEF particles especially in the case of the high potassium batch of concrete. Calcium hydroxide (CH) crystals were found in the SEM examinations of concrete specimens and this might be from the un-reacted products produced during the hydration of Portland cement.

The SEM images did not reveal the presence of ASR in any of the samples investigated. This leads to the conclusion that DEF was the primary contributor to the deterioration of the concrete samples that was observed. Pavoine, Divet and Fenouillet (2006) suggest that the Duggan cycle has a two fold impact on concrete, both of which were recognized in this research:

i) Favoring local ettringite formation and,

ii) Increasing cracking in the concrete specimens.

The Duggan cycle proved extremely useful in accelerating the damage in the concrete specimens to enable concurrent testing using non-destructive techniques. Table 5.4 summarizes the test results for specimens subjected to the Duggan cycle.

Table 5.4 Summary of Test Results of Steam Cured Concrete Specimens Subjected to Duggan Cycle

Test		Control	High Potassium
Expansion (Max)		0.015%	0.076%
Weight Change (Max)		0.678%	0.697%
Resonant Frequency, Hz (Max)		3267	3003
Compressive Strength, psi	37 days	1854	2001
	58 days	3550	2860
	90 days	4146	3748
	120 days	4524	3461
	150 days	5739	3115
SEM Analysis	100 days	No ettringite	Ettringite balls
	150 days	Random ettringite.	Numerous ettrigite balls
	200 days	Ettringite crystals	Numerous ettringite balls

Chapter 6: Concrete Samples Subjected to Freeze Thaw Cycles

The main influence of Freeze-Thaw action on concrete is through the formation of Freeze-Thaw micro-cracks. This mechanical effect directly reduces the modulus of elasticity of concrete and is the basis for some Freeze-Thaw test methods. Stark and Ludwig have even suggested that Freeze-Thaw conditions might support the formation of ettringite at the expense of monosulphate within a cementitious system. Additionally, proponents of the crystal pressure theory of DEF suggest that the crystallization of ettringite in pre-formed micro-cracks generates the pressure that causes expansion. The goal of the Freeze-Thaw test portion of this research is congruent with the efforts of the Duggan Cycle test portion, namely, to introduce distributed damage to the concrete specimens for non-destructive testing and subsequent analysis.

The concrete samples prepared for laboratory testing were produced using standard techniques for the production of small quantities of concrete. Proportioning of the concrete was done using volumetric methods. Both the mix designs and the concrete curing regimes were altered from standard practice to accelerate the formation of distributed damage in the concrete specimens. All concrete specimens (prisms) are 29.21 x 7.62 x 7.62 cm (11 ½ x 3 x 3 inches). This specimen size is in accordance with ASTM standards. The concrete mix designs were identical to those prepared for the Duggan Cycle (Chapter 5). However, none of the Freeze-Thaw specimens were steam cured; they were cured at room temperature. With the

exception of compressive testing, the Freeze-Thaw specimens were subjected to the same distributed damage monitoring tests as laid out in Chapter 5.

The Freeze-Thaw testing was completed in a Rapid Freeze-Thaw Cabinet apparatus, see Figure 4.5. In this test six concrete prisms were used, three from each batch, and each cycle consisted of lowering the temperature from 4.4 °C to -18 °C and raising it back up to 4.4 °C. This apparatus was manually stopped after every three cycles for the first 30 cycles and after five cycles thereafter until the Q-factor values could no longer be obtained. The average amount of time to complete one cycle was approximately 5.4 hours. However, the actual amount of time varied since it depended on the condition of the specimens. As the prisms deteriorated, the cycles became shorter.

6.1 Freeze Thaw Cycles

The control samples were able to endure more cycles of Freeze-Thaw testing than the high potassium samples. Of the three control samples subject to testing, two were able to endure 110 cycles whilst one endured only 105 cycles. The testing was stopped on these control samples because they ceased to produce meaningful results. Two of the high potassium samples were able to endure 95 cycles while one endured 105 cycles. Of the two high potassium samples that endured 95 cycles one of them actually failed and is depicted in Figure 6.1. The other two ceased to produce meaningful results.

Figure 6.1: (a) Freeze Thaw Specimen during Expansion Tests with Length Comparator. (After 12 cycles, note concrete integrity)
(b) Failed Freeze Thaw Specimen after 95 cycles.

6.2 Expansion Results

The concrete samples subjected to Freeze-Thaw cycles exhibited higher expansion values than those subjected to the Duggan cycle. At the end of the Freeze-Thaw testing, about 100 days (110 cycles), the expansion values for the control and high potassium batches were 1.25% and 1.35% respectively. Samples subjected to steam curing and the Duggan cycle exhibited maximum expansion of 0.0153% and 0.0760% overall. The average maximum expansion achieved by the high potassium samples was only 8% higher than the average maximum expansion achieved by the control samples.

Figure 6.2 plots the results of the average expansion versus time of both sets of specimens. The graph clearly shows that the addition of potassium increased the average expansion. This increase in expansion is not as pronounced as for the samples subjected to the Duggan cycle even though the maximum expansion is greater.

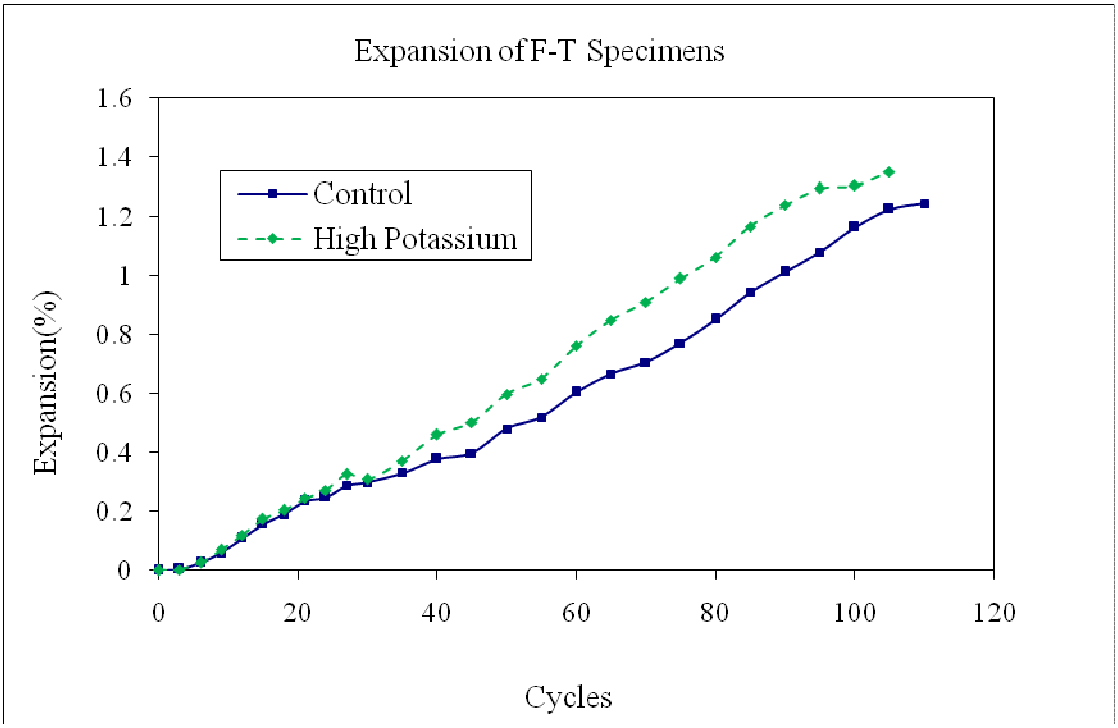

Figure 6.2: Expansion of Concrete Prisms Subjected to Freeze Thaw Cycles

6.3 Weight Change Results

The overall weight change exhibited by the samples subjected to Freeze-Thaw cycles was greater than the weight change exhibited by the samples subjected to the Duggan cycle. The maximum weight increase for Freeze-Thaw samples occurred after 80 cycles (81 days) for control samples and 75 cycles (78 days) for the high potassium samples. These weight change values were 1.852% and 1.696% respectively. The maximum weight increase for the samples subjected to the Duggan cycle 0.678% and 0.697% respectively.

The Freeze-Thaw samples experienced weight increase until around 80 cycles, after which both sets of samples began to experience a decline in weight change. The decline in weight change began at 75 cycles for the high potassium samples and also

declined faster for the remainder of the test. Figure 6.3 shows the plot of weight change versus the number of cycles for both sets of specimens.

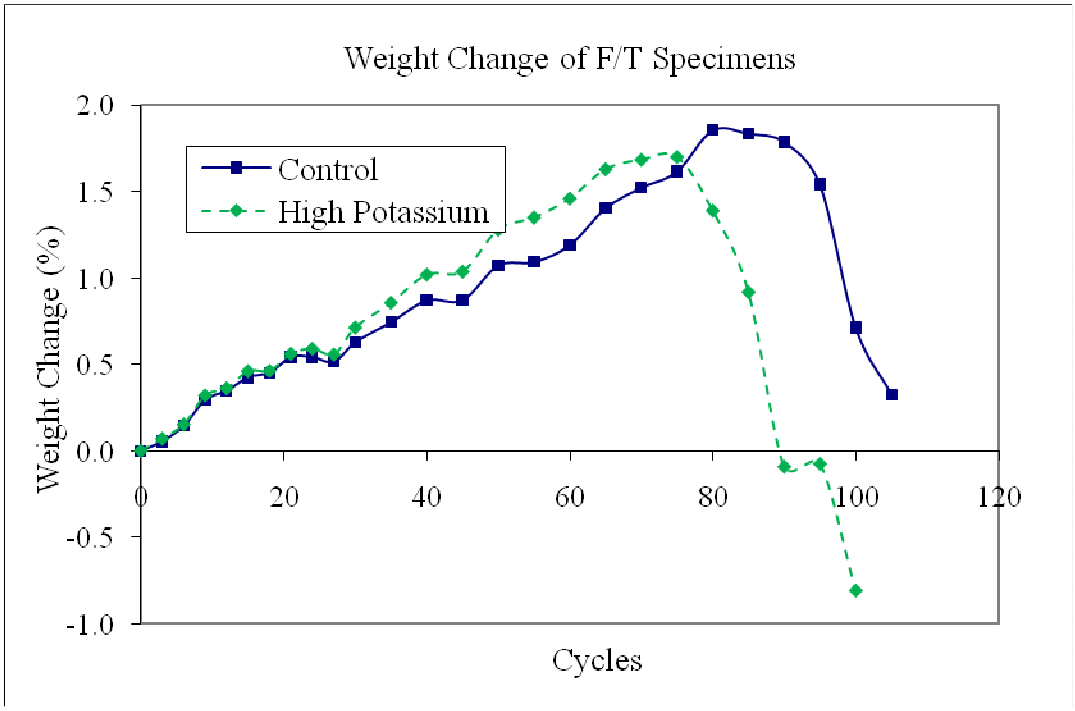

Figure 6.3: Weight Change of Concrete Prisms Subjected to Freeze Thaw Cycles

6.4 Expansion vs. Weight Change

Weight change and expansion results were analyzed simultaneously in order to investigate a possible correlation. The samples subjected to the Duggan cycle displayed a stronger disparity between batches (control and high potassium) than samples subjected to the Freeze-thaw cycles. The samples subjected to the Freeze-thaw cycles exhibited almost identical relationships between expansion and weight change as shown in Figure 6.4, whereas for the Duggan cycle there was a marked difference (see Figure 5.7).

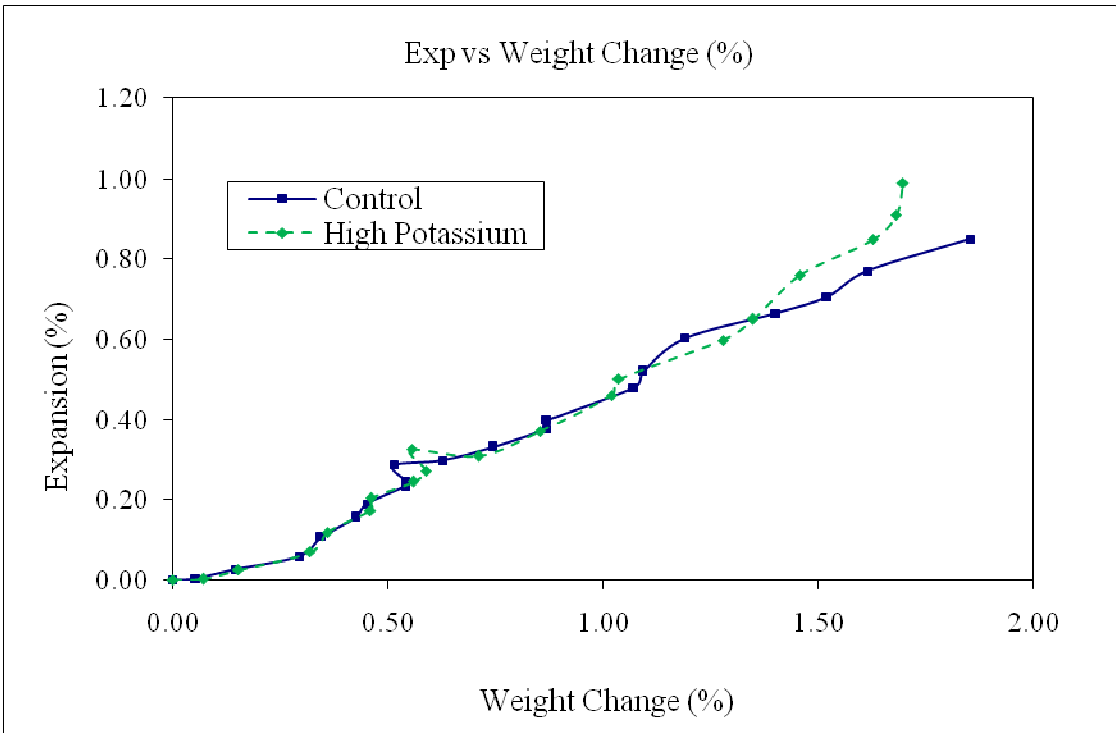

Figure 6.4: Expansion vs. Weight Change of Concrete Prisms Subjected to Freeze Thaw Cycles

6.5 Fundamental Frequency

The Freeze-Thaw tests were performed in accordance with ASTM 666 M-03. This standard recommends testing for the fundamental transverse frequency in order to determine the relative dynamic modulus. The method of determining the fundamental frequency for ASTM 666 and ASTM C 215 are the same. The tests were performed in accordance with ASTM C 215 – 02. As expected the fundamental frequency decreases through the duration of the test. With increasing Freeze-Thaw cycles the distributed damage increases, which causes damping that lowers the fundamental frequency. As depicted in Figure 6.5 the control samples, which are able to resist damage more, consistently record higher fundamental frequencies than the high potassium samples.

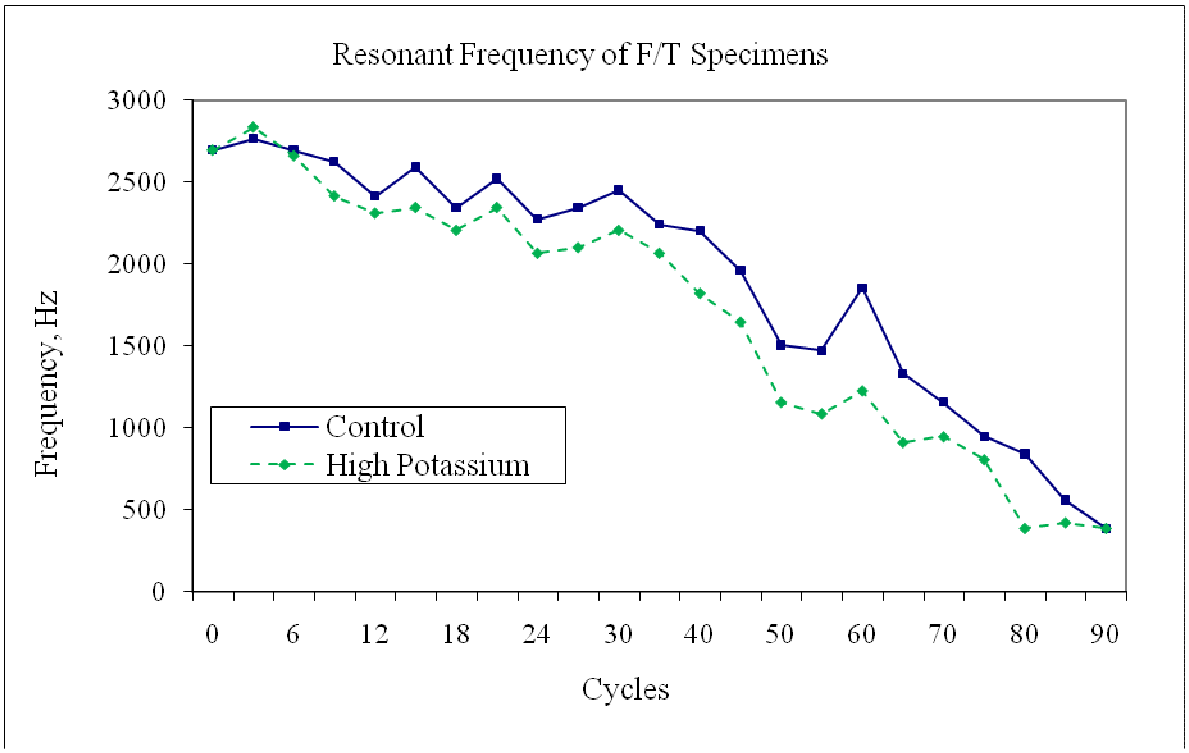

Figure 6.5: Fundamental Frequency of Concrete Prisms Subjected to Freeze Thaw Cycles

6.6 SEM and EDAX Analysis

Scanning electron microscopy (SEM) in correlation with Energy dispersive x-ray analysis (EDAX) was used to determine the presence of ettringite in Freeze-Thaw concrete samples. Testing using SEM and EDAX began at the end of the Freeze-Thaw cycle testing program. This program was completed at 96 days (110 cycles) and SEM tests were started at 100 days for both the Duggan specimens and the Freeze-Thaw specimens.

The stage of most importance for the Freeze-Thaw specimens is, directly after testing, at 100 days. For comparison only, the Freeze-Thaw specimens were also tested using the SEM and EDAX at 150 and 200 days. Consequently, after Freeze-Thaw testing, the specimens were stored in the same conditions as the Duggan

specimens; in limewater. Figures 6.6 through 6.12 show the SEM images and their related EDAX spectrums for both batches at 100, 150 and 200 days respectively. A general progression in the growth of ettringite crystals is perceived at these stages. This growth is considered to be due to the combination of distributed damage present and the storage solution which would promote the growth of ettringite.

6.6.1 Control Concrete Specimens

SEM tests were performed on the crumbling remains of the freeze-Thaw samples using the techniques described in Chapters 4. At 100 days it was difficult to find any DEF crystals in any of the control Freeze-thaw specimens that were investigated. In an hour of searching, using the 'across and down' technique, only one cluster of ettringite was found. This paucity of ettringite is inferred to be indicative of the entire sample. Figure 6.6 – 6.9 shows the ettrigite that was found and its associated EDAX spectrum.

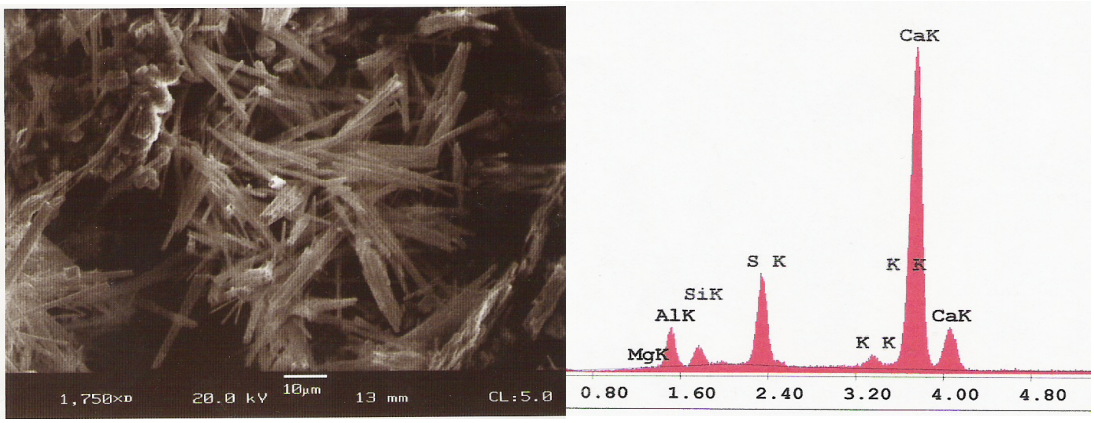

Figure 6.6: SEM and EDAX Analysis of Control Concrete Prisms @ 100 days

Figure 6.7: SEM Image of Control Concrete Prisms @ 150 days

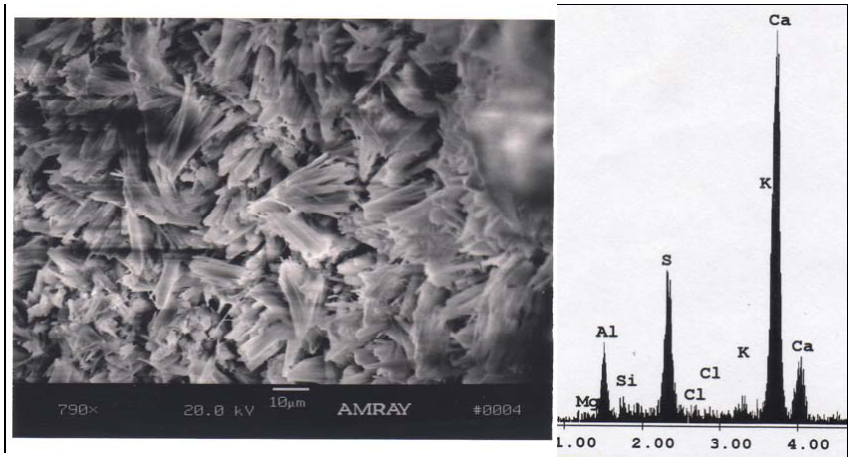

Figure 6.8: SEM and EDAX Analysis of Control Concrete Prisms @ 150 days

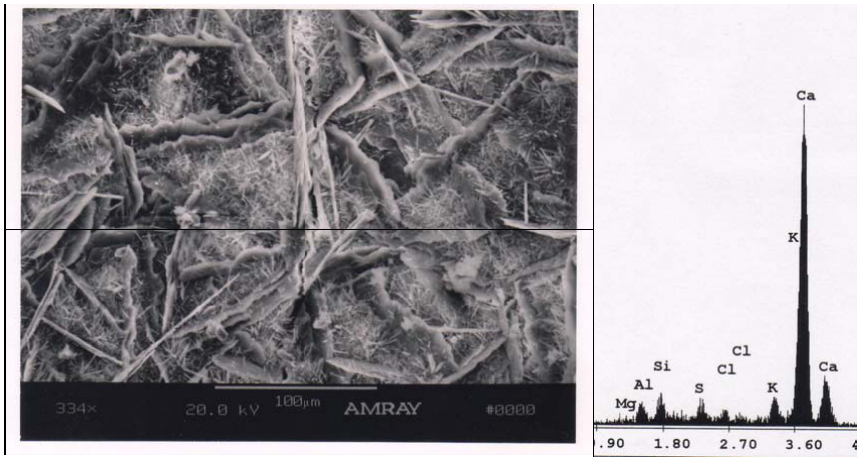

Figure 6.9: SEM and EDAX Analysis of Control Concrete

Prisms @ 200 days

6.6.2 High Potassium Concrete Specimens

Figure 6.10 – 6.12 shows SEM images and their associated EDAX analyses for the high potassium samples subjected to the Freeze-Thaw cycle. Visible in the image are Calcium Hydroxide crystals (the plate like elements) and ettringite crystals (the needle like elements). The EDAX analysis gives a good representation of the S to Al ratio indicative of ettringite.

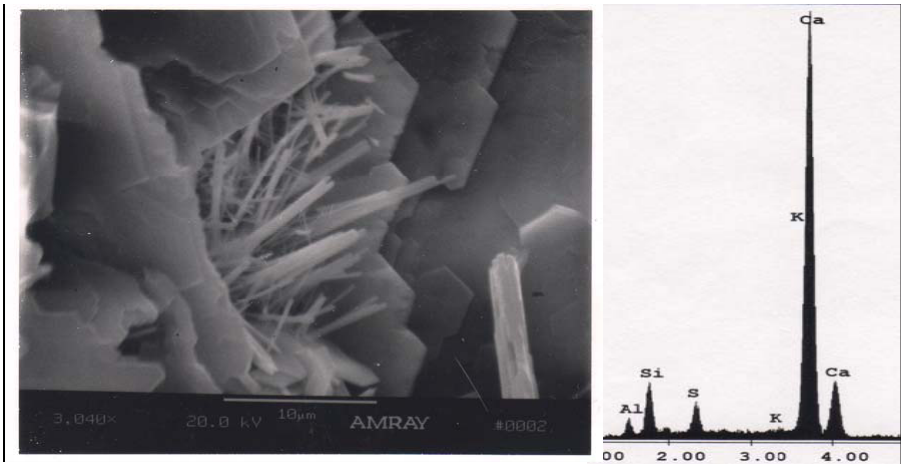

Figure 6.10: SEM and EDAX Analysis of High Potassium Concrete Prisms @ 100 days

Figure 6.11: SEM and EDAX Analysis of High Potassium Concrete Prisms @ 150 days

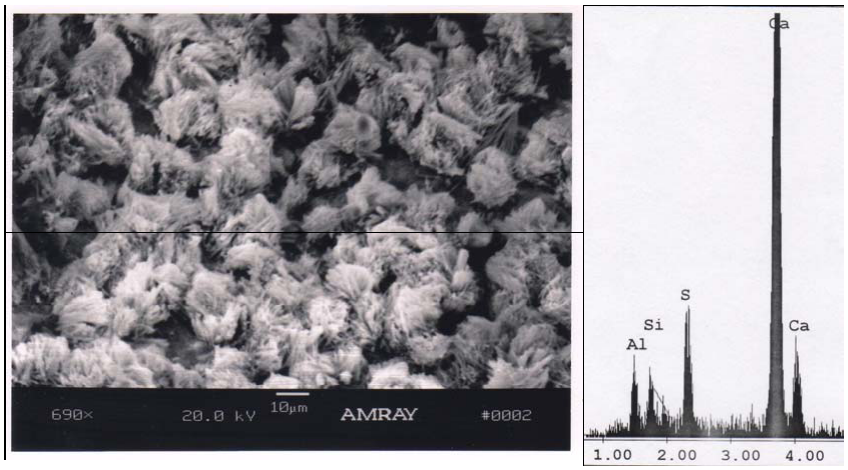

Figure 6.12: SEM and EDAX Analysis of High Potassium Concrete Prisms @ 200 days

6.7 Summary and Discussion

The specimens subjected to the Freeze-Thaw cycles experienced heavy deterioration. This is evident in Figure 6.1a which shows one of the specimens which has failed after 95 cycles. Ekolu, Thomas and Hooton (2006),have suggested that micro-cracking reduces the tensile strength of the paste and therefore its ability to resist expansion. The Freeze-Thaw cycles were used as a means of inducing distributed damage in the concrete specimens whose integrity was evaluated using non-destructive techniques. This distributed damage was also instrumental in promoting DEF.

The addition of potassium carbonate to the concrete mix has been moderately successful in increasing distributed damage as elucidated by the three tests (length change, weight change and fundamental frequency). The effect of the potassium carbonate was more pronounced in samples subjected to the Duggan cycle when compared to the control samples. This is probably due to the storage solution of limewater for the Duggan samples which facilitates the deleterious effect of potassium carbonate. Also, the Duggan samples had more time for the influence of potassium carbonate to become dominant. For the Freeze Thaw samples the dominant method of deterioration was the constant cycling between freezing and thawing. Compared to the Duggan specimens, the Freeze-Thaw samples produced higher overall expansion, weight gain and change in the fundamental frequency for both the control and high potassium samples. Table 6.1 summarizes the results of the Freeze-Thaw samples.

Table 6.1 Summary of Test Results for Concrete Specimens Subjected to Freeze-Thaw Cycles

Test		Control	High Potassium
Expansion (Max)		1.250%	1.350%
Weight Change (Max)		1.852%	1.696%
Resonant Frequency, Hz (Max)		3240	3227
SEM Analysis	100 days	Minor ettringite	Ettringite balls
	150 days	Random ettringite.	Numerous ettrigite balls
	200 days	Ettringite crystals	Numerous ettringite balls

Chapter 7: Impact Echo Signal Processing of Concrete Samples Subjected to the Duggan Cycle

7.1 Introduction

No reliable non-destructive testing (NDT) methods currently exist for early damage detection in concrete. Deterioration of concrete is usually accompanied by micro-cracking which can be caused by reactive aggregate, DEF and/or Freeze Thaw damage.

Damage in concrete first develops as micro-cracking when curing, due to shrinkage and the resulting stresses. If the concrete is heat cured then the possibility of DEF is increased which will lead to further micro-cracking and deterioration. The micro-cracks form at the weakest parts of the concrete; the boundaries between the aggregate and the paste matrix. This boundary is known as the interfacial transition zone (ITZ) and is weakest due to the disparities in properties between the aggregate and the paste such as modulus of elasticity, density and moisture content.

This chapter presents the results and analysis of the non-destructive (Impact Echo) portion of the tests performed on the concrete samples of Chapter 5. The significant damage related parameters were highlighted in this chapter with the intention to corroborate them with the results of the signal processing analysis techniques discussed herein.

7.2 Signal Processing Techniques

Conventional ultrasonic based methods such as the impact echo have been used to characterize damage in terms of changes to the attenuation factor or pulse velocity. ASTM has a standard test for pulse velocity of longitudinal stress waves through concrete (ASTM C597) and it has been used to determine the extent of distributed damage in concrete. Sanasalone and Kesner (2004) have also suggested that since successive echoes arrive from the reflector (whether the boundary surface or a crack) at a fixed distance, the process can be ideally represented as a decaying standing wave. The benefits and drawbacks of these methods were discussed in Chapter 3. Both these methods perform their signal processing in the time domain.

Due to the availability of non-destructive test instruments using digital processing, signal processing can be done in the frequency domain. Through Fast Fourier Transform techniques (FFT), the time domain waveforms can be transformed into the frequency domain response spectrum. The information in the response spectrum incorporates the specimen geometry, density and elastic modulus making it easier to compare damage among different specimens.

7.2.1 The Quality Factor

Distributed damage causes the scattering of the impact echo stress waves. In a solid such as concrete, the scattering is the result of wave reflection, refraction, diffraction and mode conversion at each interface between dissimilar materials and especially at crack boundaries (Sansalone and Carino, 1986). This scattering is a form of attenuation or damping and is associated with the dynamic response of the structure. This damping limits the response at resonance and affects the rate at which

the vibrations decay. The quality factor (Q-factor) is a measurement of this attenuation.

There are two common methods used to characterize damping in concrete. The first method is the log decrement method or viscous damping, which quantifies the decrease in amplitude of successive P-waves.

$$\text{Log decrement, } \delta = \ln\left(\frac{h_1}{h_2}\right) \qquad (7\text{-}1)$$

Malhotra and Carino (2004) have reviewed the damping properties of concrete. For analysis purposes, a quality factor (Q) is frequently used instead of viscous damping. While viscous damping increases with deterioration, the quality factor decreases and is easier to monitor quantitatively. The Q-factor is a measure of the spectral width of the peak frequency of the stress wave. The Q-factor is defined as the full-width at half maximum (FWHM) of the peak at the fundamental or resonant frequency:

$$Q = \frac{\omega_o}{\omega_2 - \omega_1} \qquad (7\text{-}2)$$

where ω_1 and ω_2 are the frequencies on either side of ω_o for the points on the curve where $U(\omega) = U_o/2$, and U_o is the peak height. In the case of ideal linear dynamics, $Q = \omega_o/2\alpha$. Thus the Q factor is the decay constant scaled by the resonant frequency. Since ω_o incorporates the specimen geometry, density and elastic modulus, this normalization makes it possible to compare damage among different specimens. Another physical interpretation of Q is based on the fact that the period of

the resonant frequency, T, equals $2\pi/\omega_o$ and the characteristic relaxation time, τ, of the exponential decay is $1/\alpha$.

Hence:

$$Q = \frac{\pi\tau}{T} \qquad (7\text{-}3)$$

This indicates that Q is a measure of how much decay occurs during the time of a single cycle of the resonant frequency.

7.2.2 Lorentzian Analysis

In order to avoid the shortcomings of the Q-factor approach, McMorris et al. (2007) have proposed signal processing methods in the frequency domain that explicitly quantify the nonlinearity. This is based on the fact that the Fourier transform of the decaying standing wave equation is a Lorentzian function defined by:

$$U(\omega) = \frac{U_o \Gamma^2}{4(\omega - \omega_o)^2 + \Gamma^2} \qquad (7\text{-}4)$$

where $U(\omega)$ is the Fourier transform of $u(t)$, ω_o is the resonant frequency, the peak height $U_o = U(\omega_o)$, and Γ is the full width at half maximum (FWHM). As shown in Figure 7.1, this function has a single peak centered at ω_o. Its shape can be characterized by just two parameters: U_o and Γ.

It can be shown that $Q = \omega_o/\Gamma$, and this implies that $\Gamma = 2\alpha$. However, this is strictly true only in the case where the Fourier-transformed signal is a Lorentzian function. As discussed above, as the distributed damage becomes more severe, the shape of the peak in the frequency spectrum departs from the Lorentzian.

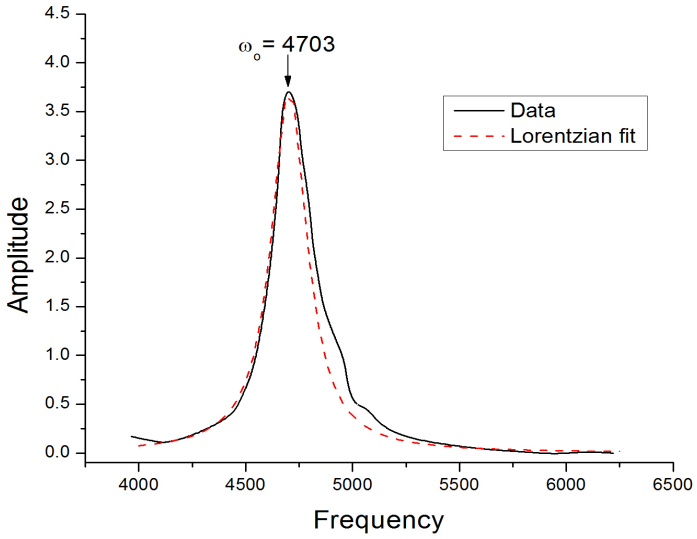

Figure 7.1: Typical spectrum of impact-response of sound concrete prism

Since the Lorentzian function represents the Fourier transform of the ideal linear dynamics response, one measure of nonlinearity would be the difference between the observed spectrum and the Lorentzian function for undamaged concrete. The damaged concrete peak can be overlaid with the Lorentzian derived from the control specimen by scaling it vertically to match the peak height observed for the damaged specimen. This identifies a significant difference between the two curves. Monitoring the areas under each curve provides useful information which manifests this measure of non-linearity. The Lorentzian area ratio is the ratio of the area under the Lorentzian fit to the data to the area under the data.

7.2.3 Harmonic Analysis

The other nonlinear approach is derived from a Taylor expansion in the elastic modulus of the standard differential equation for stress wave motion which leads to;

$$\frac{\partial^2 u}{\partial t^2} = c_o^2 \left[1 - 2\beta_2 \frac{\partial u}{\partial x} + \ldots \right] \frac{\partial^2 u}{\partial x^2} \qquad (7\text{-}5)$$

where c_o is a constant and β_2 is known as the second-order nonlinear coefficient. This approach can be extended to yield higher order nonlinear coefficients.

The amplitude of the second order harmonic can be related to the fundamental by:

$$A_2 = \left(\frac{\beta_2}{4} \right) k^2 A_1^2 x \qquad (7\text{-}6)$$

where A_2 is the amplitude of the second harmonic, A_1 is the amplitude of the fundamental frequency, k is the wave number and x is the propagation distance. Similarly the third harmonic is given by:

$$A_3 = \left(\frac{\beta_3}{6} \right) k^2 A_1^3 x \qquad (7\text{-}7)$$

In general, the harmonic ratio $A_2/(A_1)^2$ is sensitive to micro-structural changes and micro-cracking in the interfacial transition zone while the third harmonic ratio, $A_3/(A_1)^3$ is more sensitive to micro-cracking. These are not mutually exclusive, however, since both deterioration mechanisms contribute to both harmonic ratios.

7.3 Impact Echo Tests

Transient stress waves are generated by short duration, elastic impact on a concrete surface. The stress wave generated propagates into the test medium along spherical wave-fronts as compression (P-) and shear (S-) waves. The P- and S- waves are reflected by internal discontinuities and external boundaries. The reflected waves returning to the surface of impact generate displacements that can be measured by a receiving transducer placed near the point of impact. For ease of analysis and expediency, waveforms are transformed to the frequency domain using Fast Fourier Transform technique. The resulting amplitude spectrum is used to identify the dominant frequencies present in the waveform. Wave reflections from the boundary or existing flaws give rise to transient resonance that can be identified in the spectrum.

The impact echo tests were performed in accordance with ASTM C 215-02. For each specimen tested on each test date the specimen was impacted with the hammer at least three times and the data recorded. The waveforms and response spectrums in Figs. 7.2 and 7.3 are typical of the data obtained. Interesting points to note are (i) the number of P-wave peaks have decreased over time (ii) the response peak is broader and a harmonic peak can be seen in Fig 7.3b.

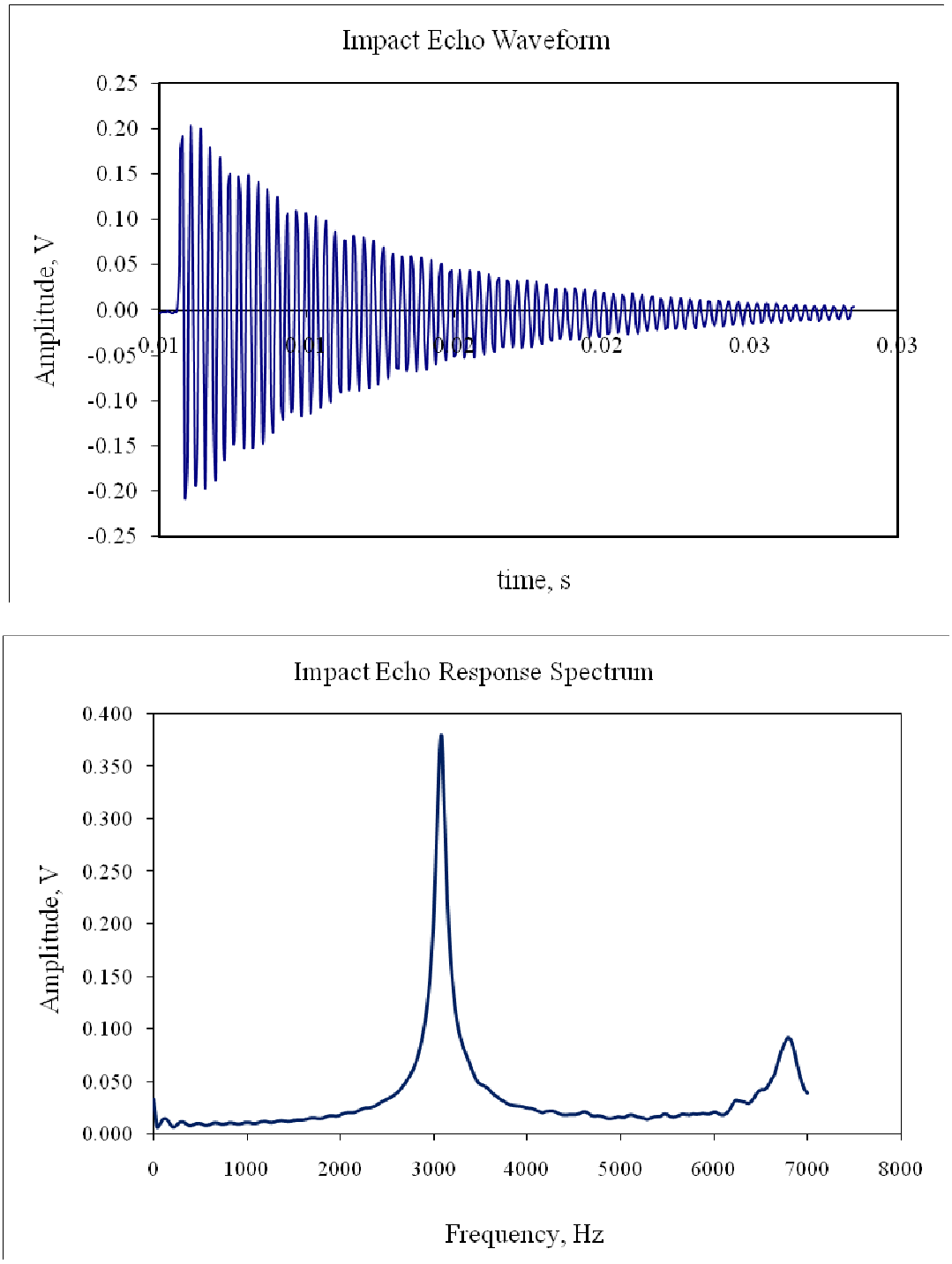

Figure 7.2: Waveform and Spectrum of a Duggan Specimen @ 23 days

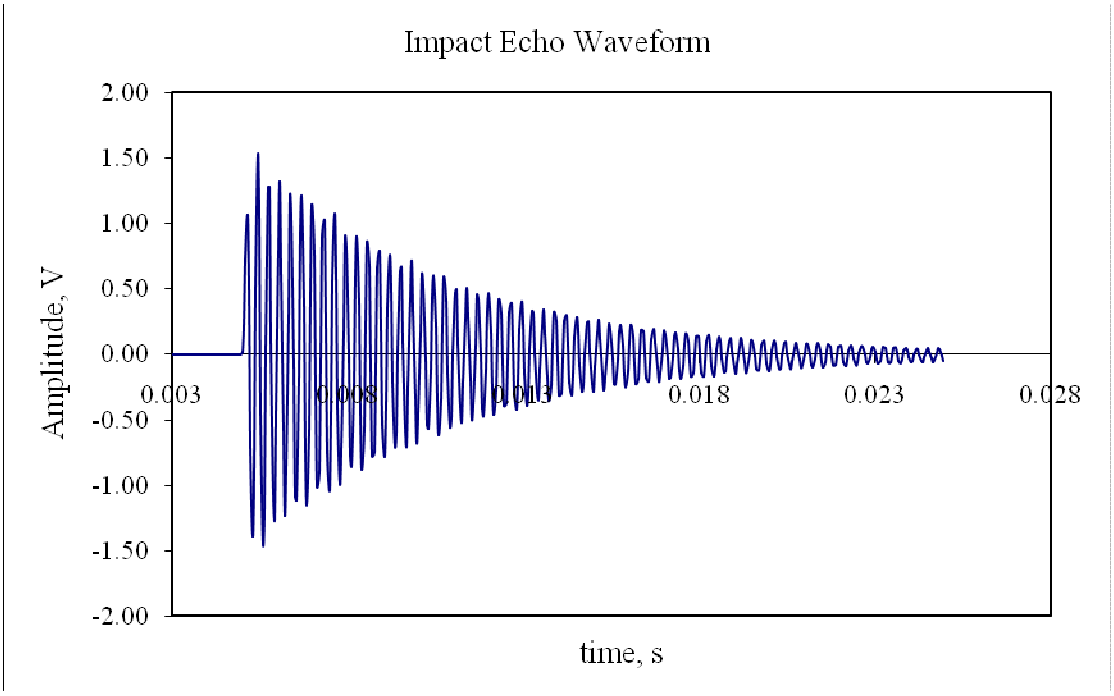

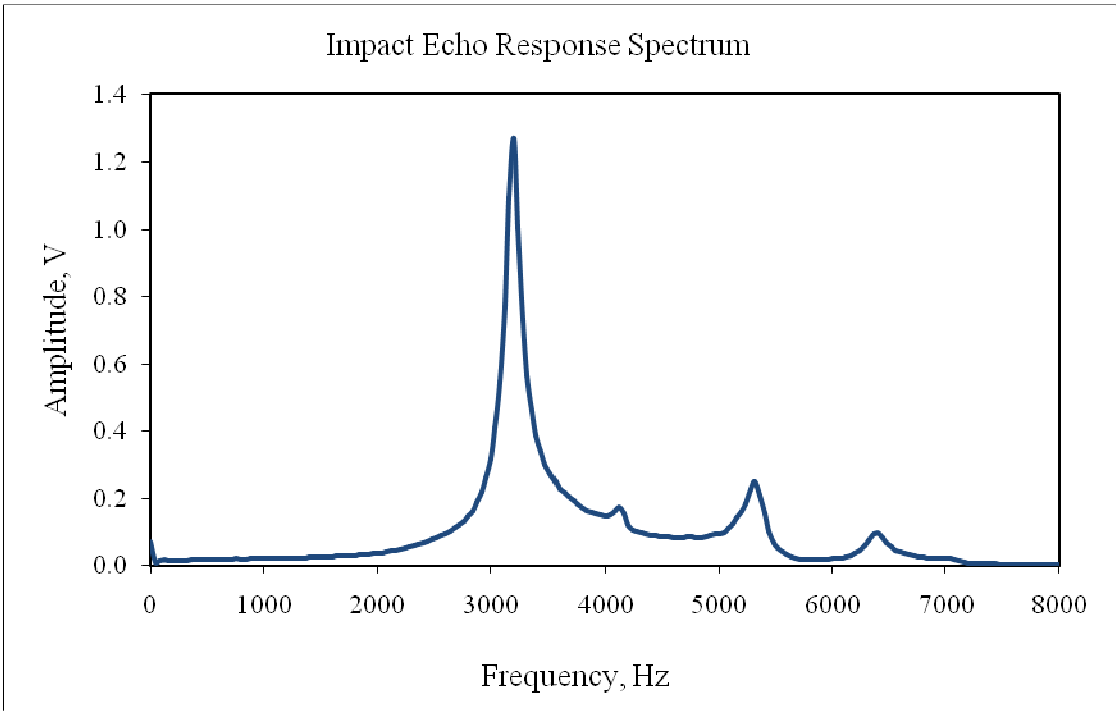

Figure 7.3: Waveform and Spectrum of a Duggan Specimen @ 138 days

7.4 The Q-Factor

The Q-factors from the specimens subjected to the Duggan Cycle were acquired through impact-echo testing, which was performed along with expansion and weight change measurements every three to five days after the completion of the heating regime. Figure 7.4 shows the variation of the Q-factor over time. It is clear to see that there is a gradual increase in Q-factor over time for the control batch of concrete specimens. This increase is expected, as the Q-factor is also used as a non-destructive method of determining concrete strength (Tesfamariam, Sadri and Thomas, 2006). For the high potassium batch the average Q-factor over time, as delineated by the linear regression fit, remains basically unchanged. A decrease in Q-factor over time was expected based on the degradation of the specimens observed in Chapter 5.

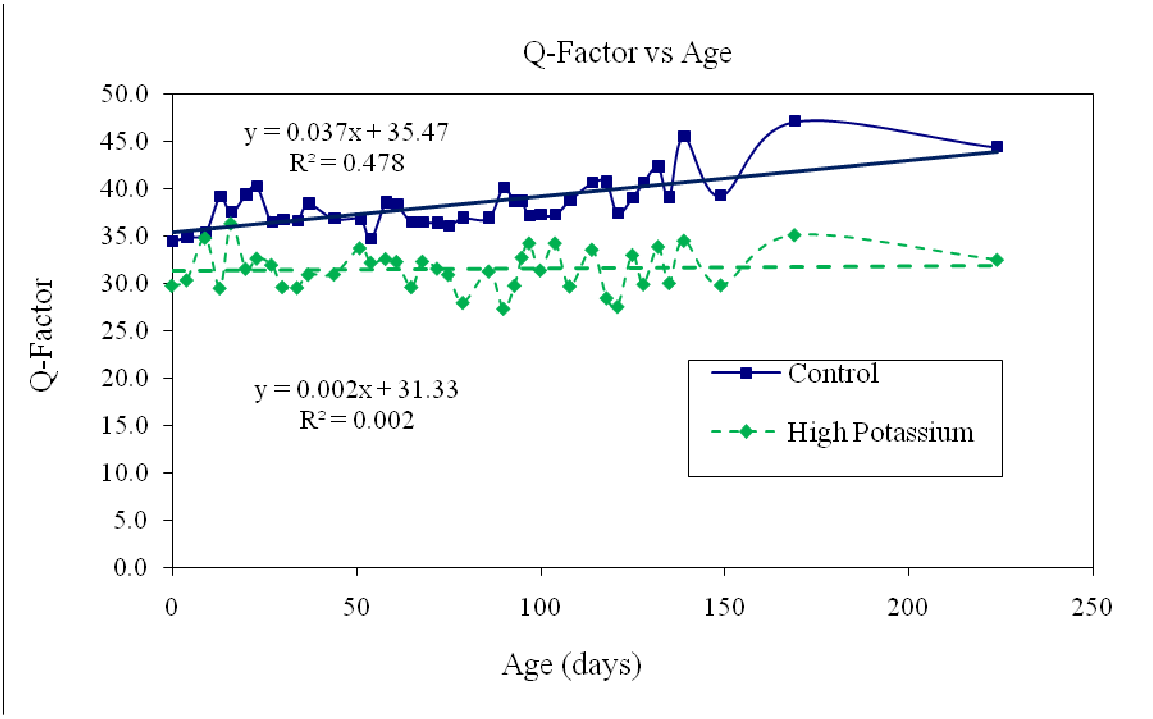

Figure 7.4: The Q-factor of Duggan Specimens over time

The standard deviation, a measure of the data spread about the mean, of the Control specimens was found to be 1.0933, while the standard deviation of the high potassium specimens was 1.0546. This confirmed that the Q-factors obtained from both batches did not vary much over the duration of the research study.

7.4.1 The Q-Factor related to Expansion

Expansion is the primary test used in previous chapters to evaluate the condition of the concrete. In Chapter 5 the control specimens experienced moderate expansion whilst the high potassium samples experienced more severe expansion. Consequently the frequency domain analysis of the impact echo tests should correlate this data. Figures 7.5 through 7.7 show the relationship between the Q-factor and expansion of the Duggan specimens.

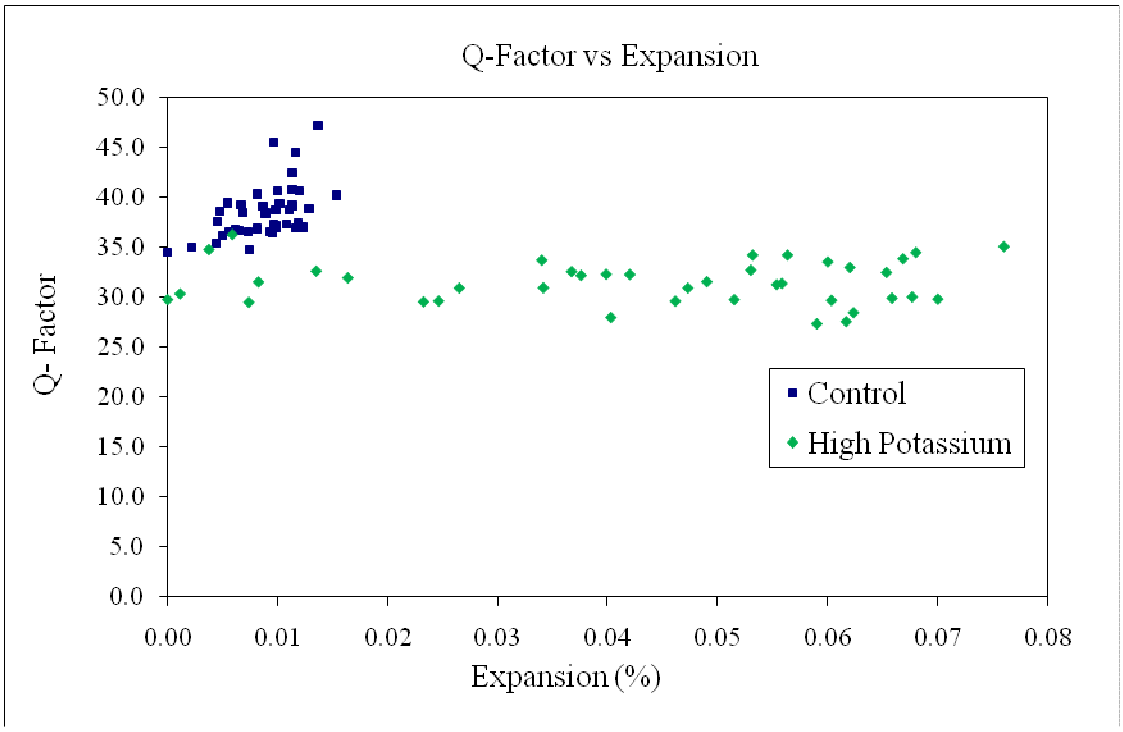

Figure 7.5: The Q-factor of Duggan Specimens over time

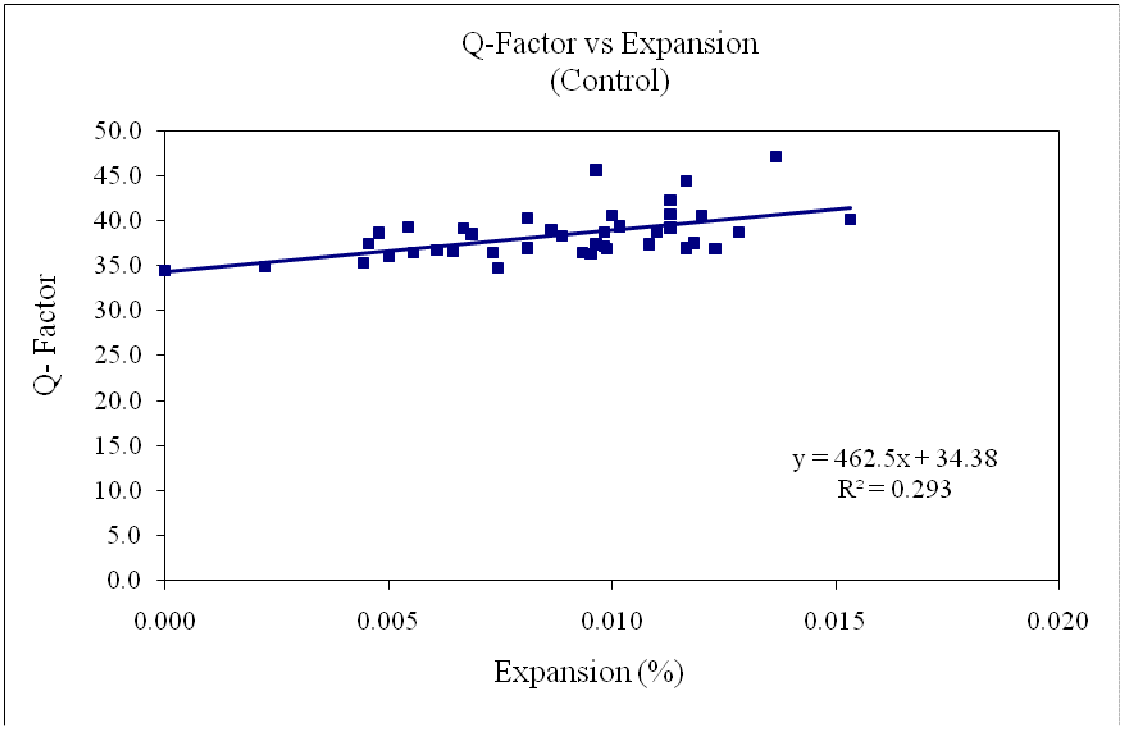

Figure 7.6: The Q-factor vs. Expansion for Control Specimens

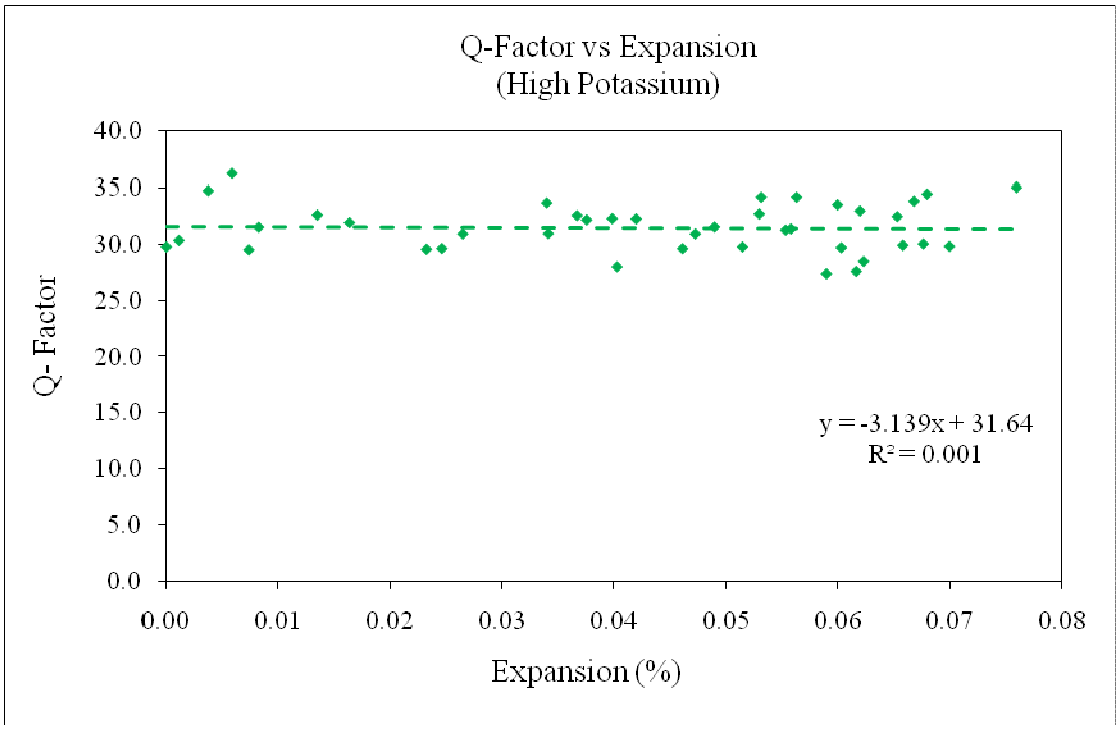

Figure 7.7: The Q-factor vs. Expansion for High Potassium Specimens

The relationship of the Q-factor with expansion is as expected. For the control batch there is an increase in Q-factor with only minor expansion. For the high potassium batch there is a slight decrease in Q-factor associated with more severe expansion. This is represented by the negative gradient of the linear fit. However the correlation of the linear fit to the data is weak as indicated by the small R^2 value.

El-Korchi et al (1989) suggest that one way the value of Q can increase is through the creation of a more dense material through increased or continued hydration of cement. El-Korchi et al (1989) concluded that continued cement hydration would decrease void space and hence decrease the damping and internal friction which would minimize the energy loss associated with the transfer of P-waves resulting in large Q-factor values. Thus, the increase in Q-factors found in this

study could be due to the storage condition since the specimens were stored in limewater before subjecting them to the Duggan Cycle and throughout the entire period of the research study.

7.5 Non-Linear Analysis – Lorenztian Mismatch Analysis

In implementing this analysis, it was found necessary to add several steps. The software for the system actually calculates the power spectrum, which is the square of the real part of the Fourier transform. Therefore, the function used for the model is actually the Lorentzian squared. In order to preserve the correct shape of the curve when it is scaled vertically to the peak height of the data, it is also necessary to scale the width by the same factor. Therefore the scaled width Γ_d is given by:

$$\Gamma_d = \frac{U_d}{U_o}\Gamma_o \qquad (7\text{-}8)$$

where Γ_o is the width for the Lorentzian model of the undamaged concrete, U_o is the peak height for the undamaged concrete, and U_d is the peak height for the damaged concrete. Finally, it was necessary to subtract a baseline to eliminate background noise. As a result most Lorentzian fits do not start at the baseline of y = 0, but slightly above it.

In all the plots of the Lorenztian mismatch analysis, the area under the data is shaded while the area under the Lorentzian fit is blank/white.

7.5.1 Control Samples

The Lorentzian mismatch analysis was acquired through impact-echo testing, which was performed along with expansion and weight change measurements every

three to five days after the completion of the heating regime. As a result there is a frequency spectrum and Lorezntian fit for each specimen for each day the specimens were tested. Figures 7.8 and 7.9 show typical Lorentzian analysis plots of sound concrete and damaged concrete specimens. Figure 7.10 plots the variation of the Lorentzian area ratios over the duration of the testing. The steady increase noted represents the increase in strength and integrity of the specimens. Recall that the Q-factors for the control samples increased over time which corroborates well with Figure 7.10 which demonstrates that the control samples are better approximating the Lorentzian ideal.

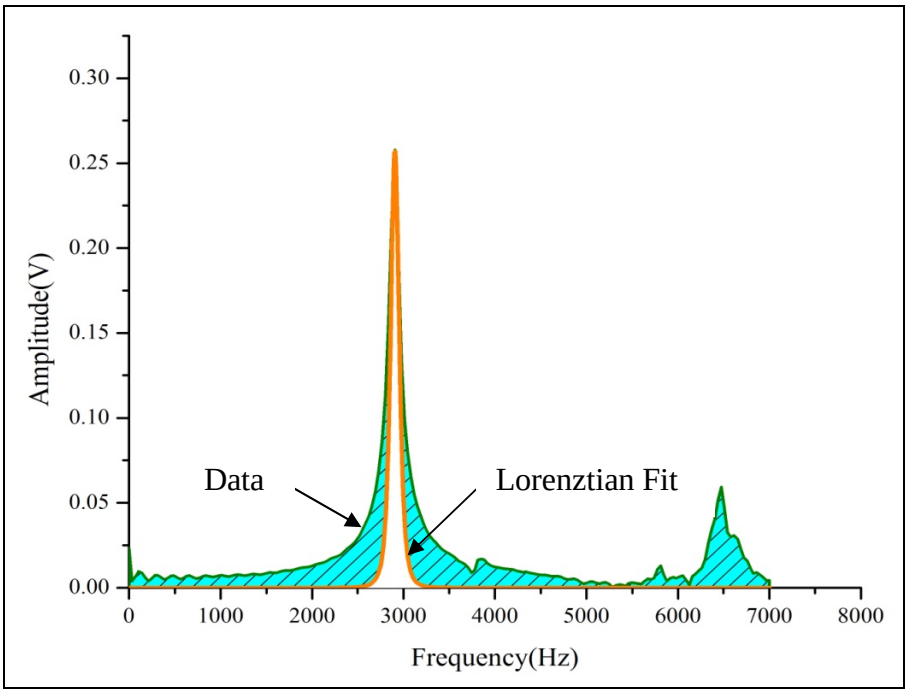

Figure 7.8: Lorentzian Analysis of Undamaged Control Concrete Specimen

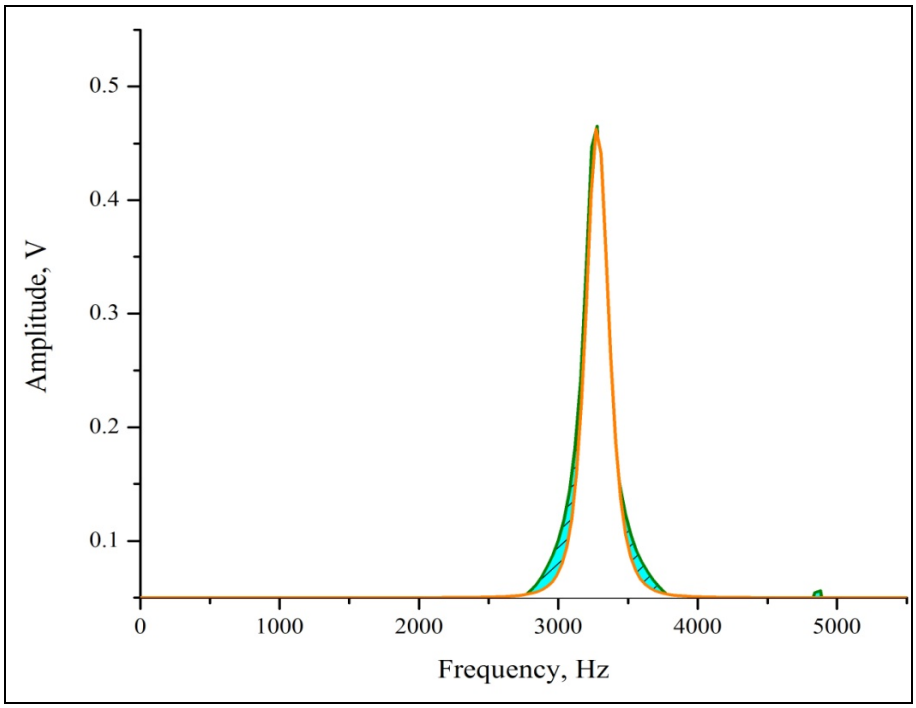

Figure 7.9: Lorentzian Analysis of a Control Specimen @ 139 days.

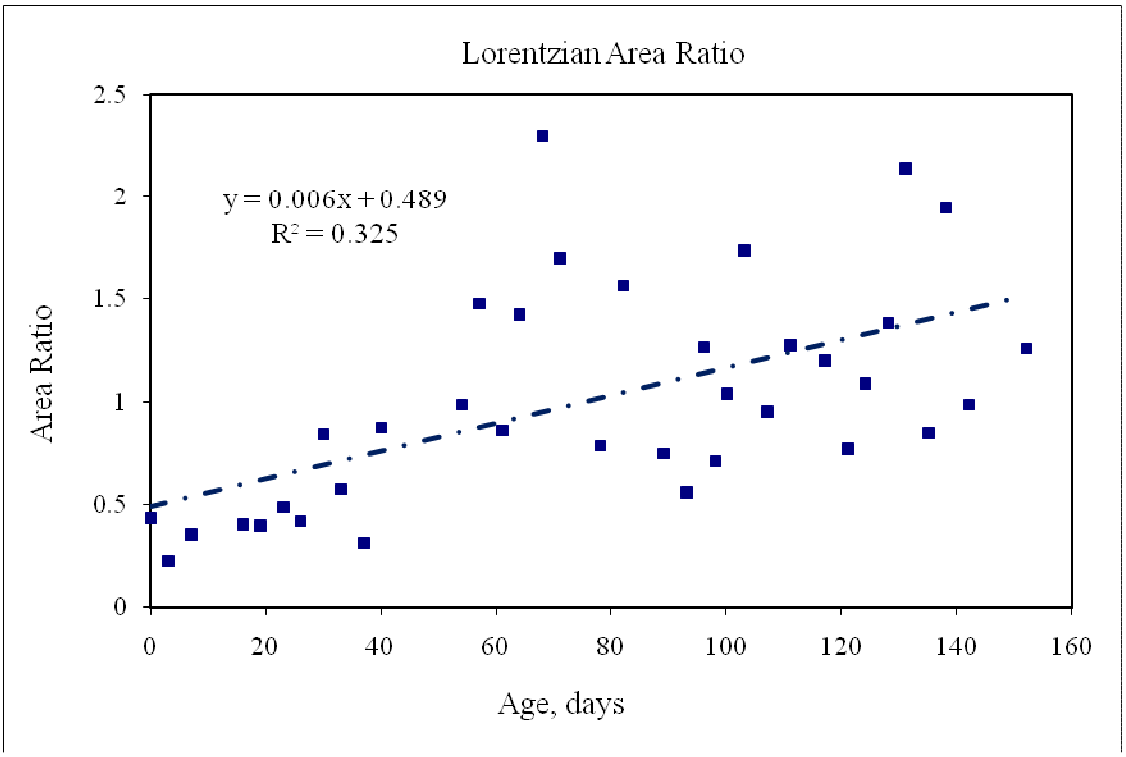

Figure 7.10: The Lorentzian Area Ratios over time for Control Specimens

7.5.2 High Potassium Samples

Figures 7.11 and 7.12 show typical Lorentzian analysis plots of sound concrete and damaged concrete specimens. Figure 7.13 plots the variation of the Lorentzian area ratios over the duration of the testing for the high potassium specimens. The Lorentzian fit in this case is based on the sound concrete specimen of a high potassium sample just after the Duggan cycle. The damaged or heavily expanded specimens seem to produce sharper response spectrums than their Lorentzian fits would suggest. This trend is complimentary to what is observed with the Q-factor, whereby the Q-factor increases with increased expansion.

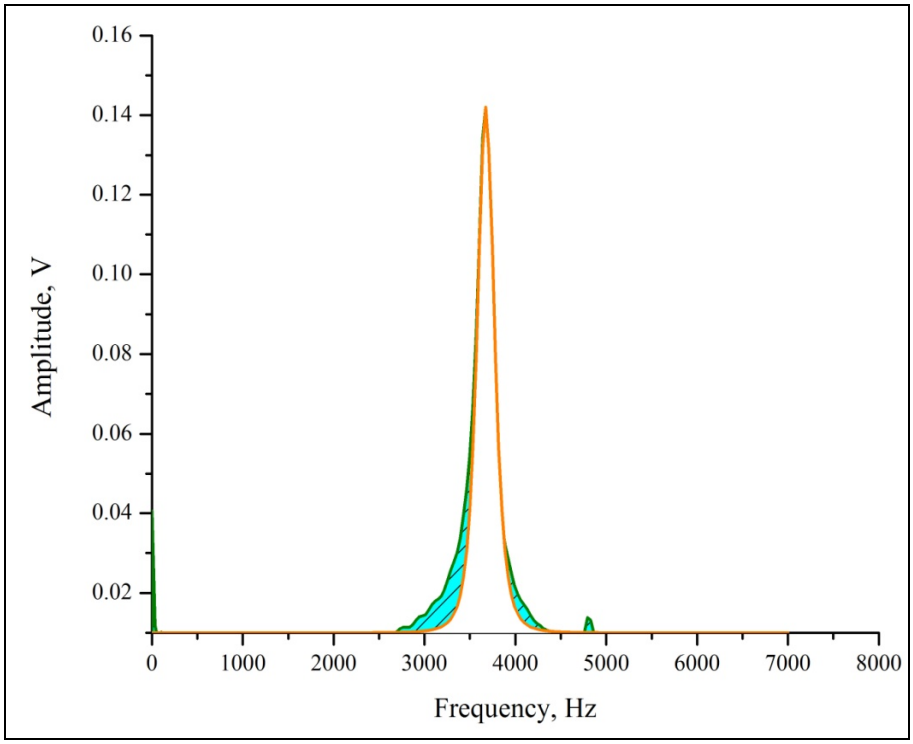

Figure 7.11: Lorentzian Analysis of Undamaged, High Potassium Concrete Specimen

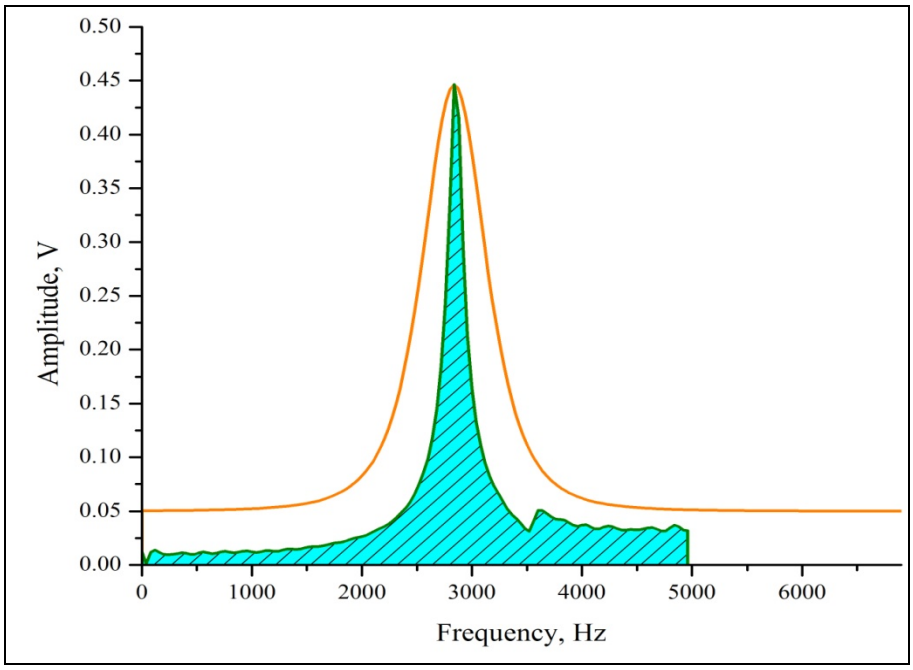

Figure 7.12: Lorentzian Analysis of High Potassium Concrete Specimen @ 132days

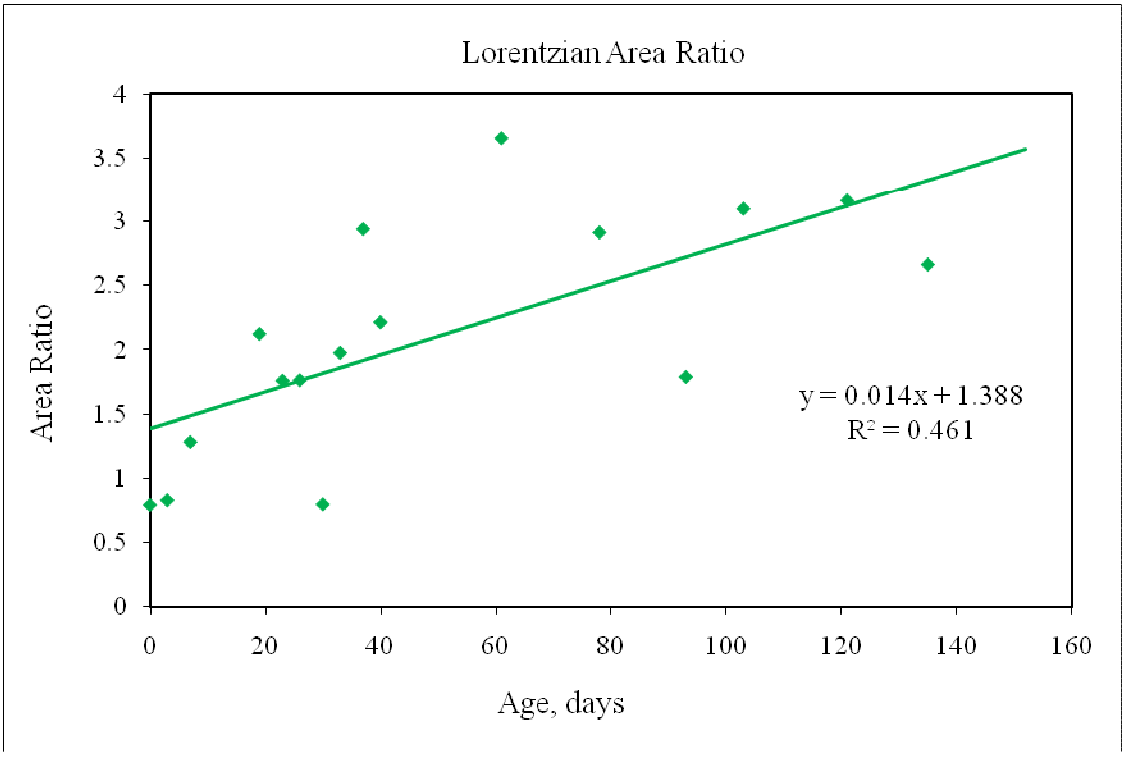

Figure 7.13: The Lorentzian Area Ratios over time for High Potassium Specimens

7.5.3 High Potassium vs. Control Samples

The Lorentzian mismatch analysis was also performed by matching the Lorentzian fit of the control concrete specimens to the response spectra of the high potassium specimens. This provides a better comparison which eliminates the possibility of any early damage caused by the combination of the heating regimen and the high potassium. Figures 7.14 and 7.15 represent the mismatch analysis at different stages. Figure 7.16 shows the resulting trend of the area ratios between the Lorentz fit and the damaged response spectra. The area ratios generally increase over time. This is contrary to what is expected because the damage should create a more distorted spectrum which should have less congruent fit with the Lorentzian as damage increases.

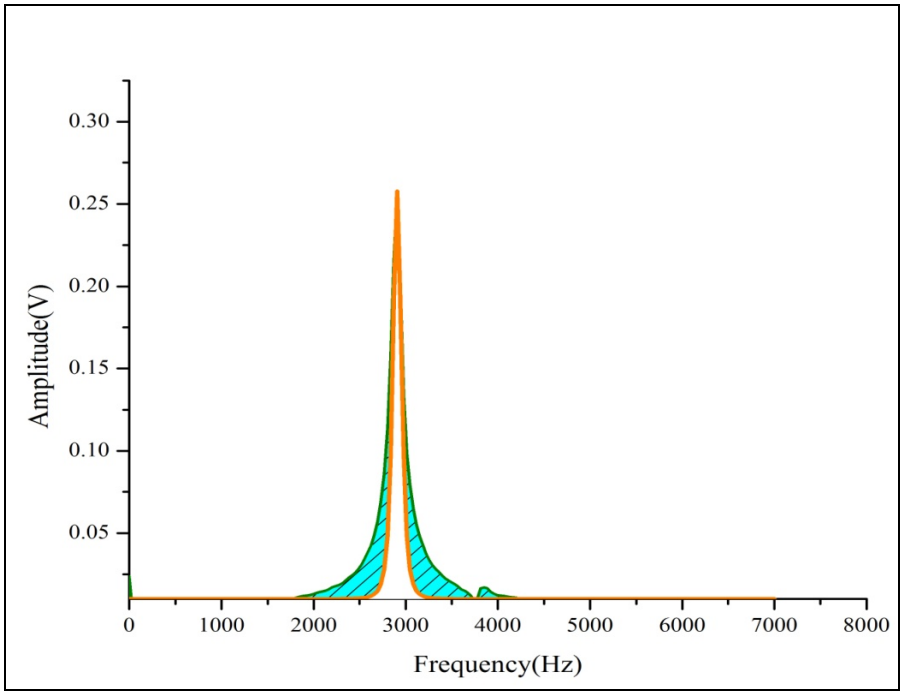

Figure 7.14: Lorentzian Fit of Control Concrete specimen against High Potassium Specimen Response Spectra for Undamaged specimen.

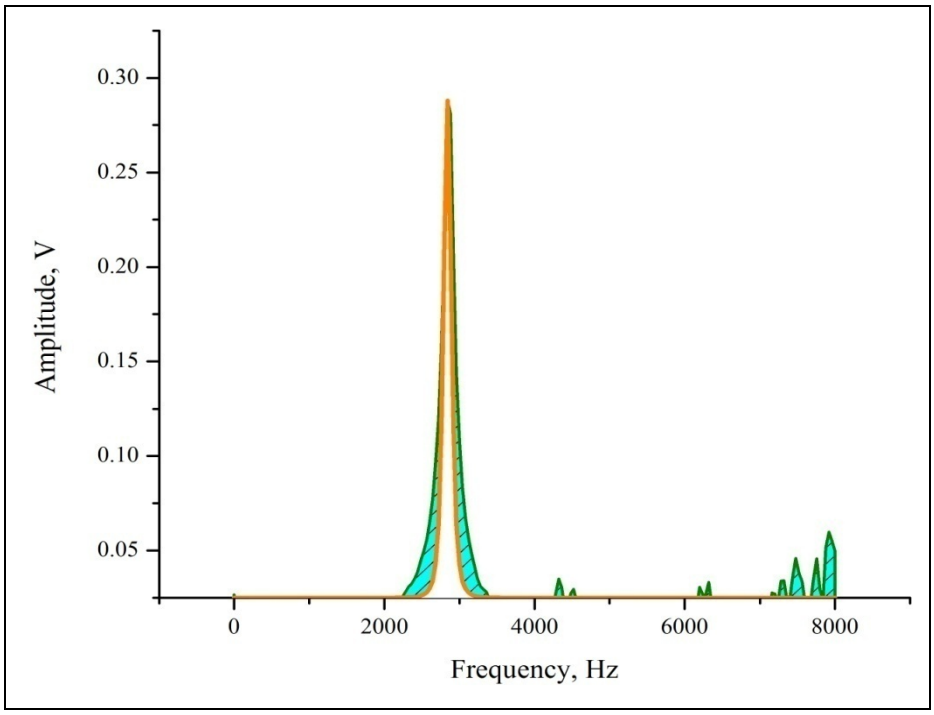

Figure 7.15: Lorentzian Fit of Control Undamaged Concrete specimen against High Potassium Specimen Response Spectra @ 139 days

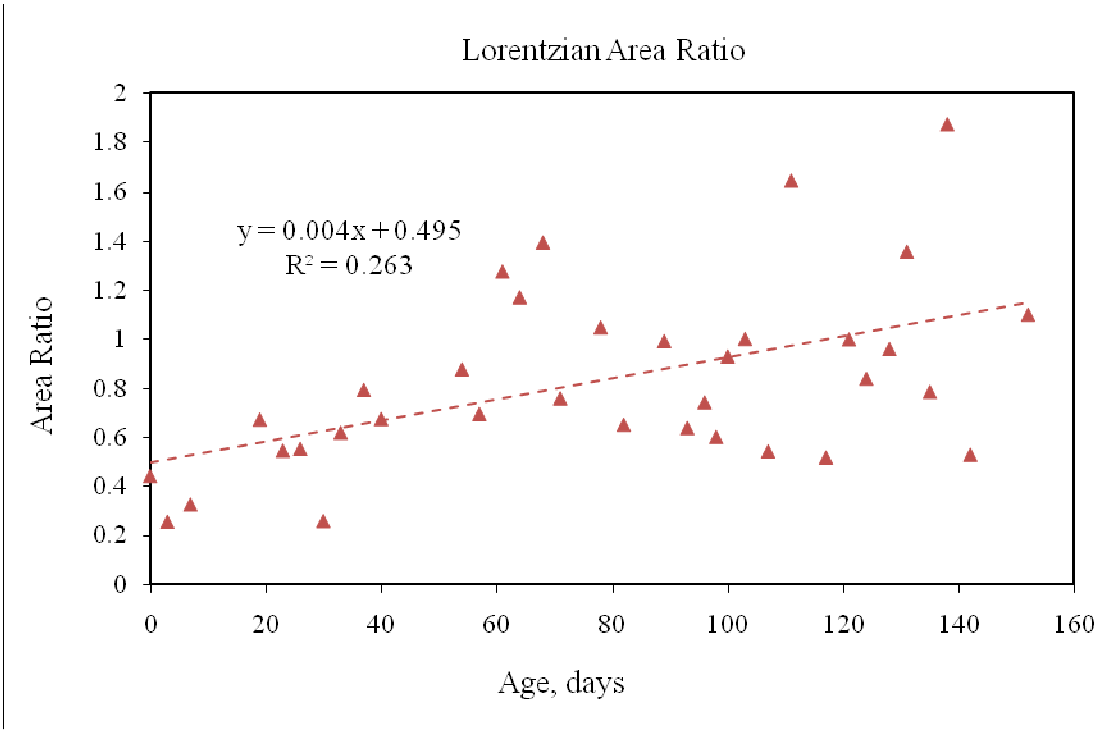

Figure 7.16: The Lorentzian Area Ratios over time for Control Undamaged Concrete specimen against High Potassium Specimen

7.6 Non-Linear Analysis – Harmonic Ratios

Micro-cracking, especially in the interfacial transition zone, is responsible, in theory, for acoustic non-linearity in concrete. As the amount of micro-cracking increases, more of the fundamental frequency is expected to be transformed into higher order harmonics.

The amplitudes of the first and second harmonics were recorded from the response spectrum of each specimen. Figure 7.17 shows a typical example of a response spectrum. In many cases the 2nd harmonic was not easily discernible. In some cases the 2nd harmonic was even less dominant than some mixed modes. The amplitudes were used to calculate the 2nd harmonic ratio as discussed in 7.2.3.

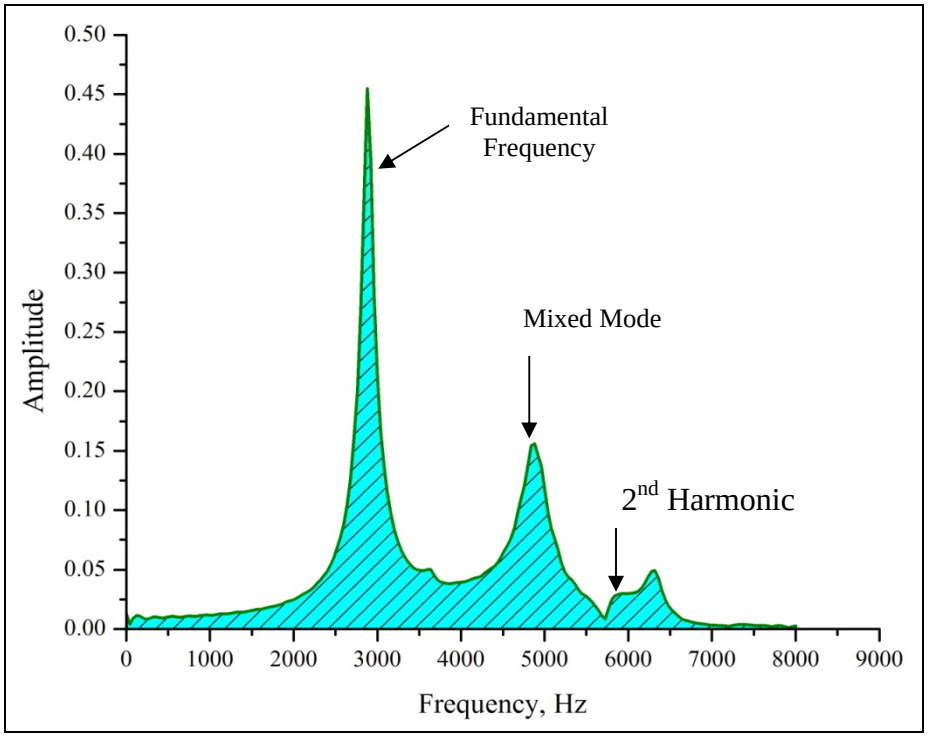

Figure 7.17: Harmonics in Response Spectrum

Figure 7.18 does not reveal a consistent trend in the variance of the harmonic ratio. In most cases this is because the 2nd harmonic is of negligible magnitude. Attenuation is a major factor influencing the magnitude of the second harmonic ratio, and though these samples display significant expansion, they were not severely cracked at the end of testing. Additionally, the 2nd harmonics proved difficult to detect without the use of special filters. On the contrary the Freeze-Thaw specimens were significantly cracked and produced more meaningful results.

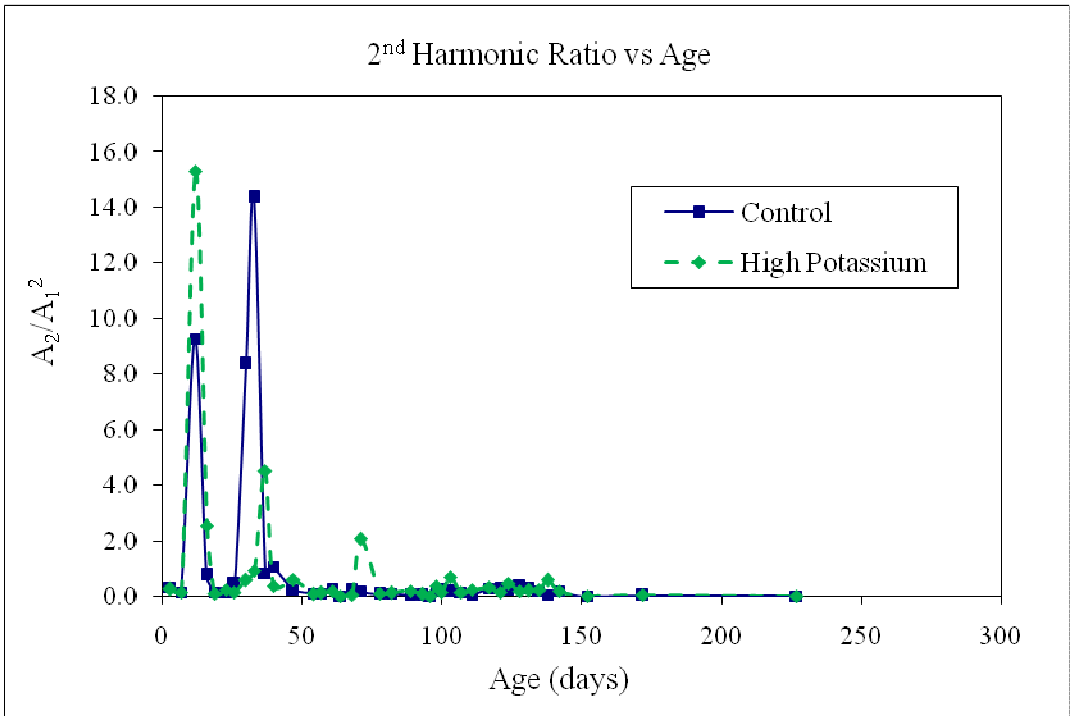

Figure 7.18: Change in 2nd Order Harmonics with time.

7.7 Summary and Discussion

It is clear from Chapter 5 that the addition of potassium carbonate to the concrete mix significantly aided the deterioration of the concrete samples. This deterioration was primarily manifested as expansion of the concrete specimens. Correlation of expansion with non-destructive test parameters proved inconsistent, though the basis of these methods remains sound.

The Q-factor results obtained from the impact echo testing clearly highlighted the deterioration caused by the increased potassium in the concrete mix. While the control samples gained strength and their Q-factors increased, the high potassium samples showed only a very slight increase. El-Korchi et al (1989) suggest that one way the value of Q can increase is through the creation of a more dense material through increased or continued hydration of cement. El-Korchi et al (1989) concluded that continued cement hydration would decrease void space and hence decrease the damping and internal friction which would minimize the energy loss associated with the transfer of P-waves resulting in large Q-factor values. Thus, the increase in Q-factors found in this study could be due to the storage condition since the specimens were stored in limewater before subjecting them to the Duggan Cycle and throughout the entire period of the research study.

As the damage becomes more severe, nonlinear effects develop. The peak in the frequency spectrum then displays a distorted shape which produces inconsistent Q-factor calculations. In an attempt to quantify the non-linearity and the distorted shape of the response spectra, a Lorentzian analysis was performed to determine the

ratios of the areas of undamaged, undistorted spectra to the areas of the distorted spectra. The results of this analysis are summarized in Figure 7.19.

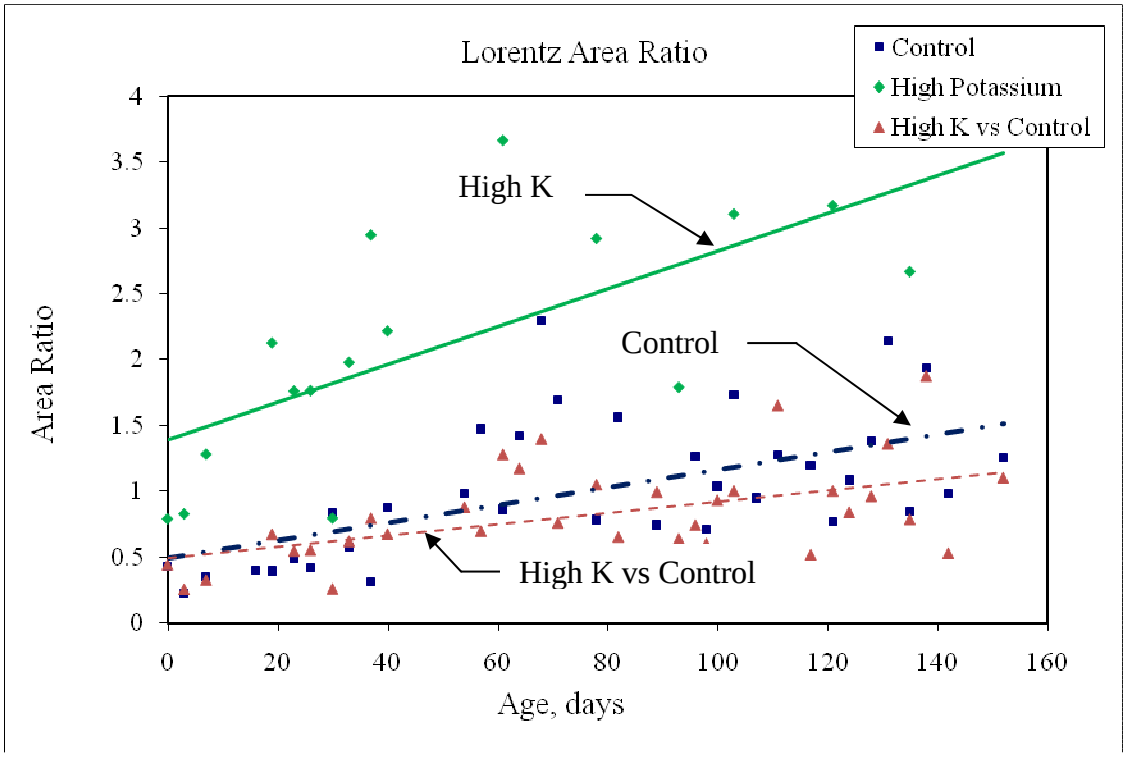

Figure 7.19: The Lorentzian Area Ratios over time for all Concrete Batches

Attenuation has been found to be a major factor influencing the second and third harmonic ratios. Since the fundamental frequency term is squared in the second harmonic ratio and cubed for the third harmonic ratio then it has a major effect on these terms as damage progresses. However, only in a few cases were the third harmonics visible in the response spectra and generally are not visible without special filters.

As micro-cracking increases a larger portion of the fundamental wave is expected to be converted into higher order harmonics. Stauffer et al (2005), suggest that casting direction has a significant influence on the second harmonic where

harmonic growth is substantially greater when the wave was propagating in the casting direction rather than against it. This is thought to be due in part to condensation on the bottom side of the aggregate and the formation of bleed water on the top surface. Both mechanisms weaken the paste at that location and lead to micro-cracking which influences the non-linear behavior of the material.

Chapter 8: Impact Echo Signal Processing of Concrete Samples Subjected to the Freeze Thaw Cycles

8.1 Introduction

The concrete samples prepared for this part of the research were subjected to Freeze Thaw cycles primarily to induce distributed damage in the form of micro-cracking. Based on the test results of Chapter 6 and the photographic evidence, sufficient distributed damage was induced for the proposed signal analysis techniques to yield meaningful results.

The ASTM standard for Freeze Thaw testing utilizes the transverse fundamental frequency and the Relative Dynamic Modulus (RDM). In this case it is necessary to test the samples for 300 cycles or until failure. This is because the RDM is not sensitive to low levels of damage. As a result this testing standard cannot be used to predict the failure of concrete subjected to Freeze Thaw cycles. While sinusoidal excitation (ASTM C 215) is the standard method for measuring resonance frequency, impulse excitation has been approved by ASTM as an alternate. Important advantages of the impulse method are that it is rapid, quite reproducible, and also produces information on the damping characteristics of the vibrational modes with no additional testing.

Frost resistance of concrete made with durable aggregate is determined by the air-void system's ability to prevent development of destructive pressures due to freezing and associated movement of moisture in the concrete pores. The specific requirements of the air-void system depend on the amount and mobility of the water

in the pores. Research in materials science by Coppola and Bradt (1973) has suggested that viscous damping is more sensitive to thermal damage than elastic modulus. For analysis purposes, a quality factor (Q) is frequently used instead of viscous damping. While viscous damping increases with deterioration, the quality factor decreases and is easier to monitor quantitatively.

8.2 Impact Echo Tests

The impact echo tests were performed in accordance with ASTM C 215-02 as required by the ASTM standard for Freeze Thaw testing. Figure 8.1 shows the impact echo waveform and spectrum for a high potassium sample before being subjected to the Freeze Thaw process. The waveform has several P-wave peaks and a discernible decay constant. The spectrum is a single relatively sharp peak with a resonant frequency of 2695 Hz. Figure 8.2 shows the impact echo waveform and spectrum for a high potassium sample at 80 cycles. The waveform has only a few peaks which are insufficient to truly determine a decay constant. The spectrum now has several secondary peaks and the resonant frequency has shifted to 720 Hz.

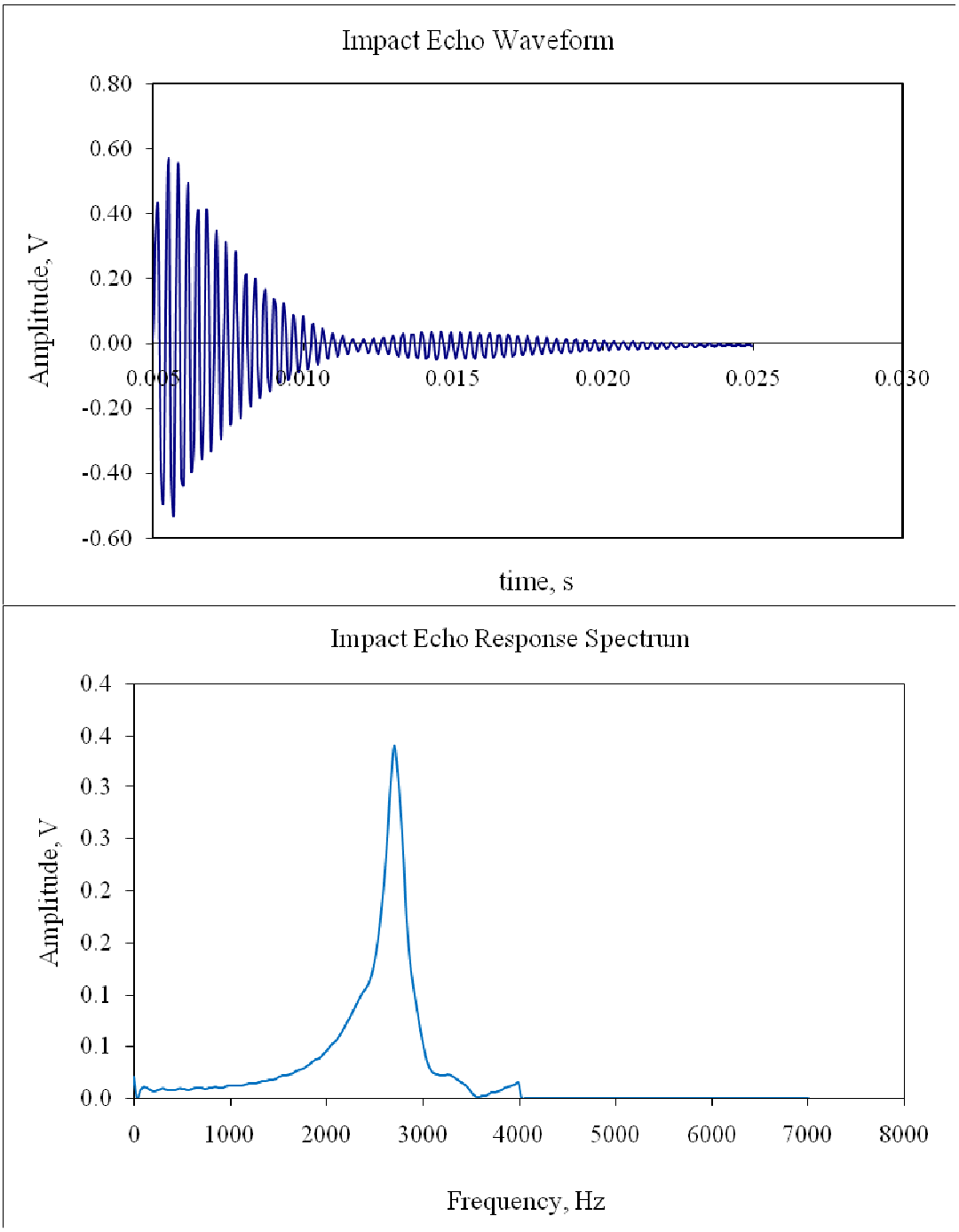

Figure 8.1: Waveform and Spectrum of a High Potassium F/T @ Zero Cycles

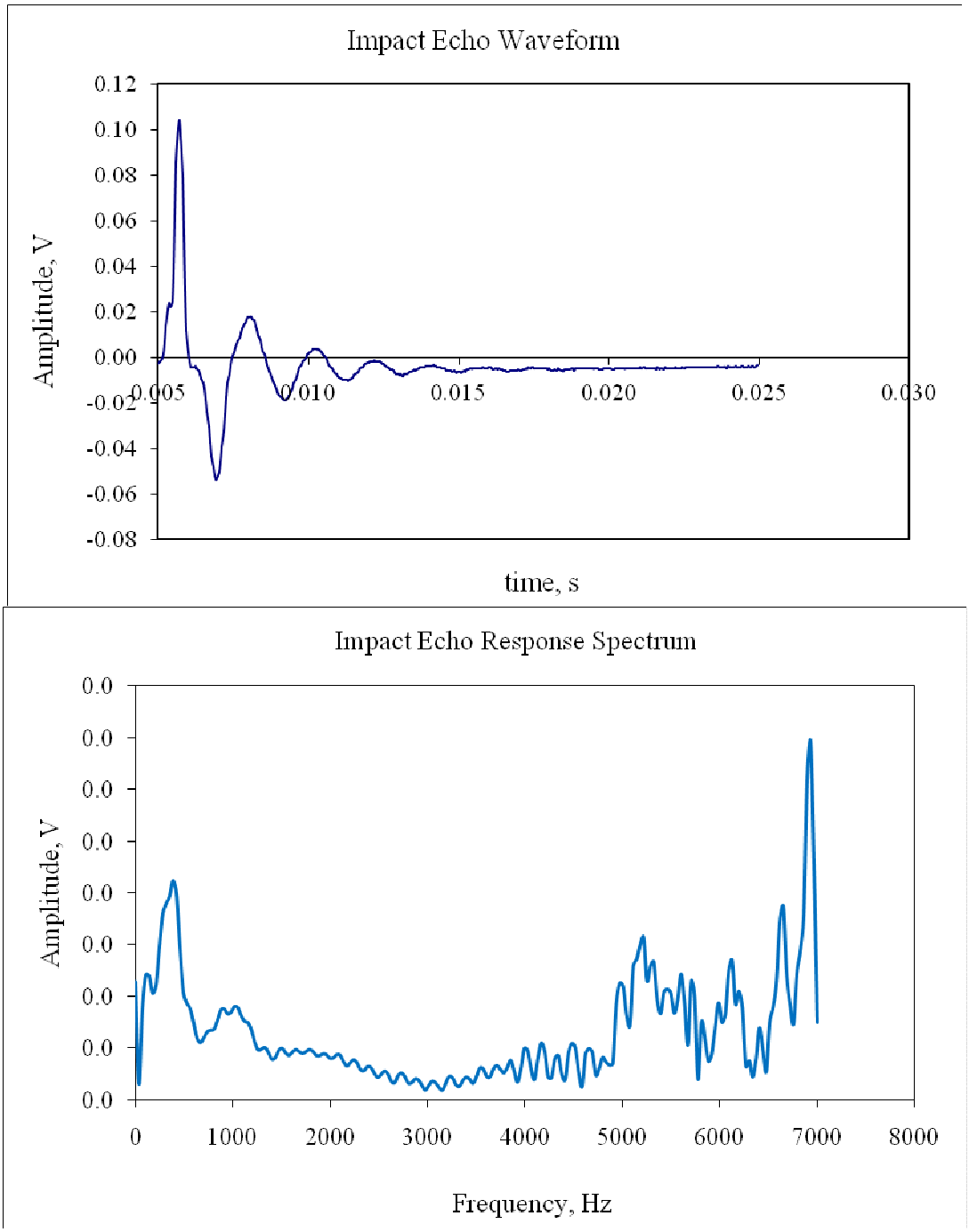

Figure 8.2: Waveform and Spectrum of a High Potassium F/T @ 80 Cycles

8.3 The Q-Factor

The specimens subjected to the Freeze-Thaw cycles in the Rapid Freeze-Thaw cabinet apparatus also were tested until failure or until the data could no longer be obtained. The quality factor for both sets of concrete specimens decreased over the duration of the Freeze Thaw testing. Figure 8.3 shows the Q-factor plotted against the number of F/T cycles. The high potassium batch typically produced lower Q-factors than the control batch. Figure 8.4 reveals that the high potassium batch also decreases at an exponentially higher rate than the control samples. The coefficients of determination are very good for the exponential fit to the data. The Q-factor also provides good correlation with the expansion data and the relationship is plotted in Figure 8.5. An exponential relationship shows a very good fit to the data, with the high potassium batch having a slightly higher decay constant.

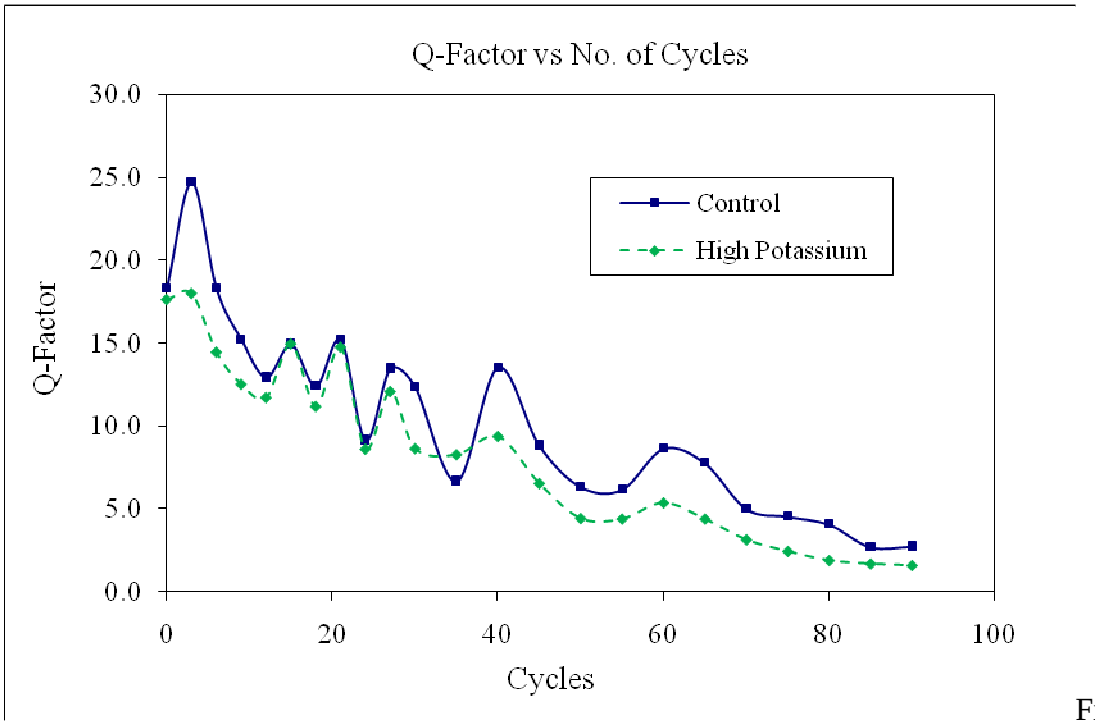

Figure 8.3: The Q-factor vs. No. of Freeze-Thaw Cycles

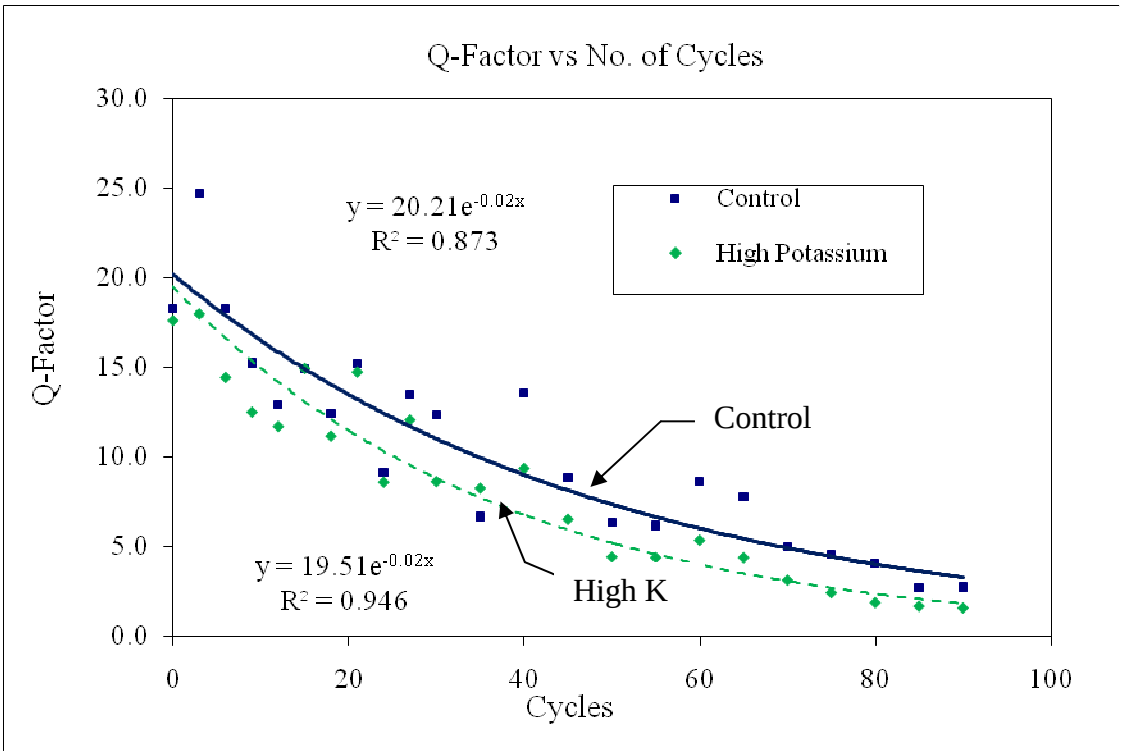

Figure 8.4: The Q-factor Variation during Freeze-Thaw Testing

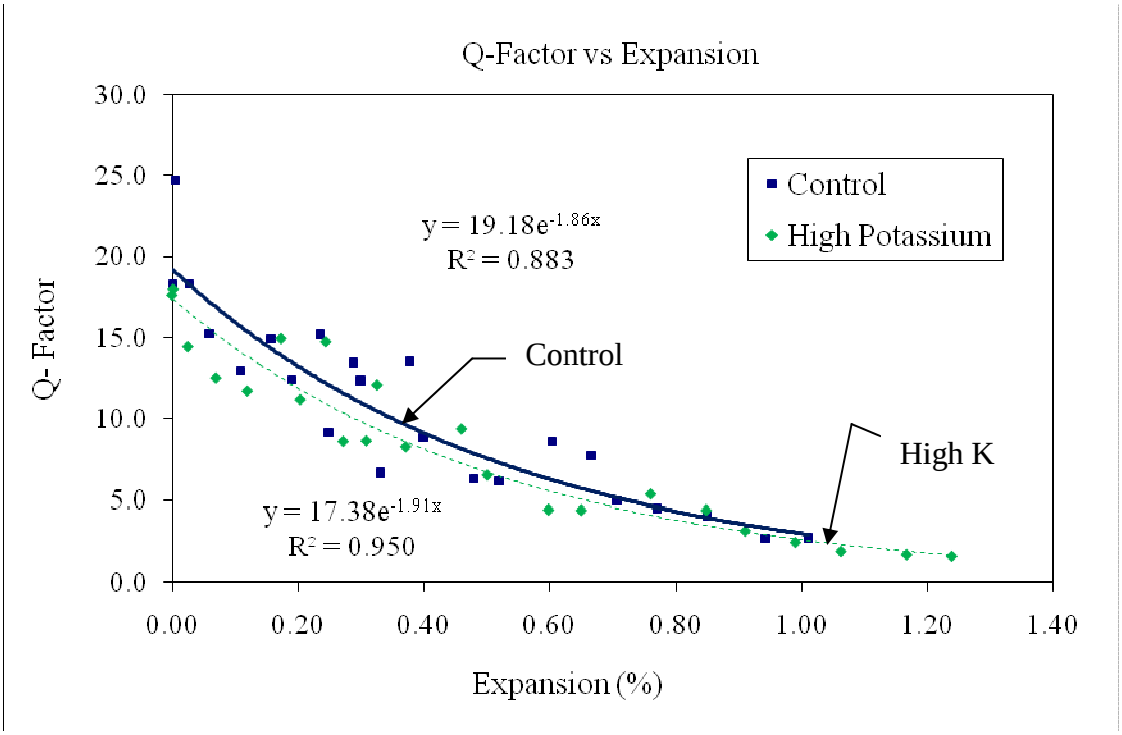

Figure 8.5: The Q-factor vs. Expansion for Freeze-Thaw Specimens

8.4 Non-Linear Analysis – Lorentzian Mismatch Analysis

As damage increases, the concrete begins to develop non-linear effects which distort the shape of the response spectrum. The Q-factor is capable of capturing the increase in damping associated with the increase in damage, manifested by the widening of the response spectrum. However, the Lorentzian analysis is capable of capturing the increase in non-linear effects manifested by the distortion of the response spectrum. Figure 8.8 plots the variation of the Lorentzian area ratios against the number of cycles during the testing. The exponential fit to the data provides the best coefficients of determination. The data typically shows lower Lorentzian area ratios for the high potassium batch from the beginning of the test. Both sets of data approach the asymptote at a similar number of cycles and since the control batch started at higher area ratios it therefore has a higher decay constant. Both sets of concrete were made with the same air entrainment treatment and the same aggregate and so would be expected to survive the same number of Freeze Thaw cycles.

In all the plots of the Lorenztian mismatch analysis, the area under the data is shaded while the area under the Lorentzian fit is blank/white. The Lorentzian area ratio is the ratio of the area under the Lorentzian fit to the data to the area under the data.

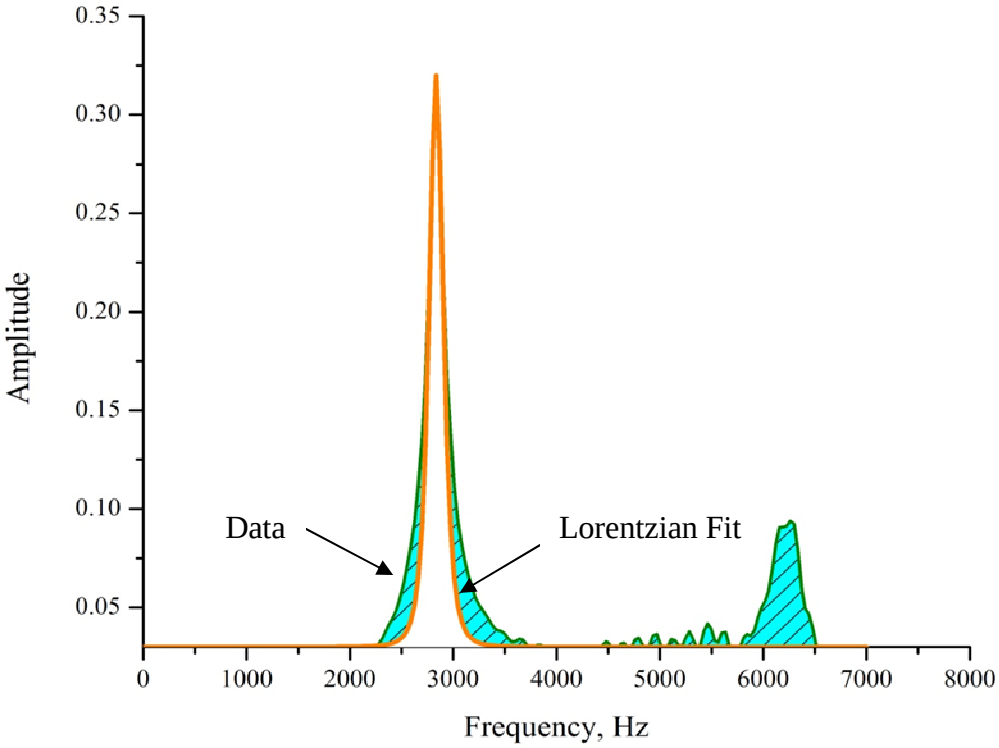

Figure 8.6 - Undamaged F/T Specimen @ 3 cycles

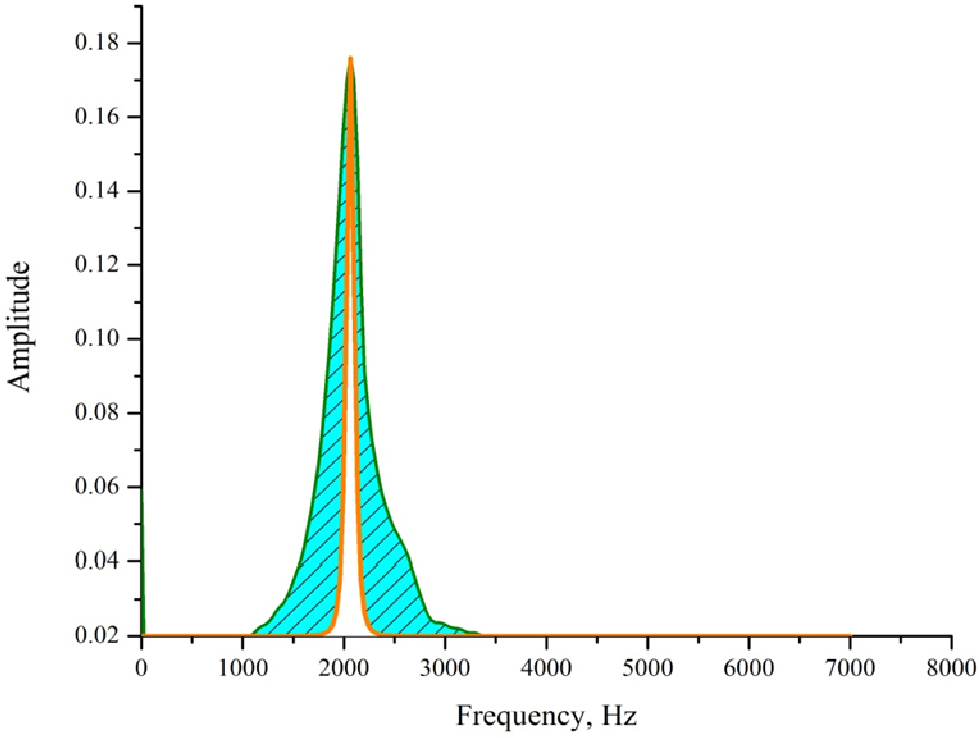

Figure 8.7 - Damaged F/T Specimen @ 24 cycles

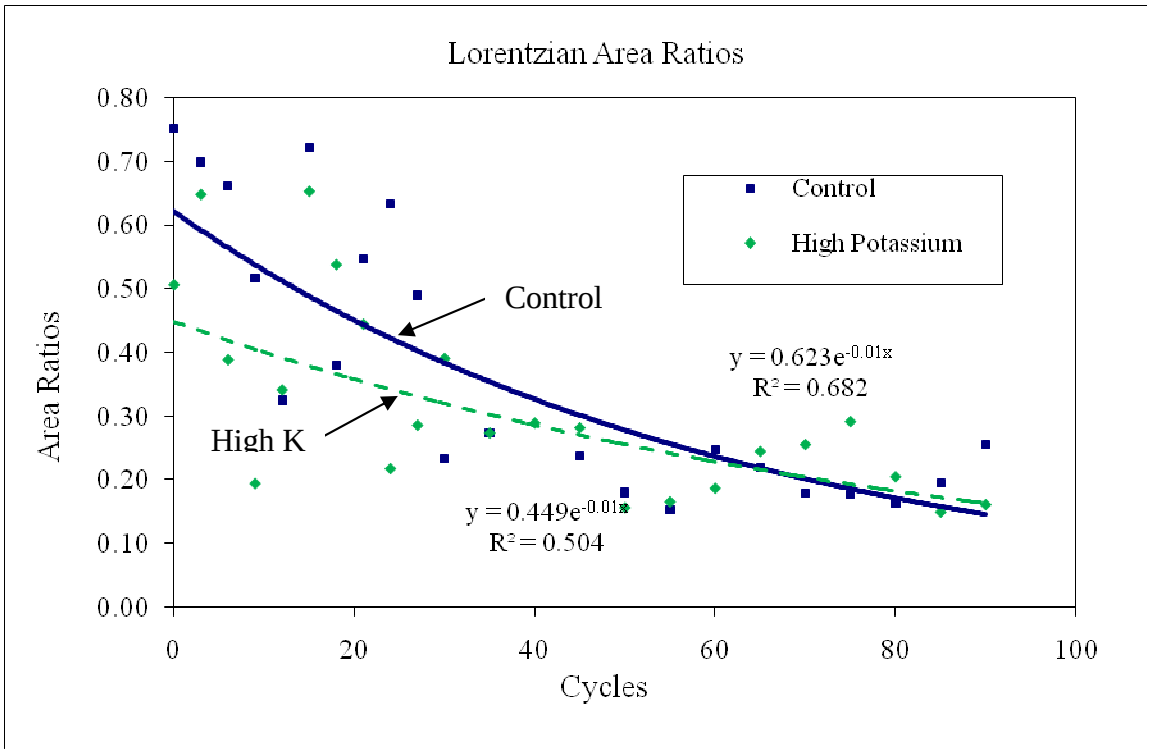

Figure 8.8: Lorentzian Area Ratios vs. No. of Freeze-Thaw Cycles

8.5 Non-Linear Analysis – Harmonic Ratios

Micro-cracking, especially in the interfacial transition zone, is responsible, in theory, for acoustic non-linearity in concrete. As the amount of micro-cracking increases, more of the fundamental frequency is expected to be transformed into higher order harmonics.

The ratios of the amplitude of the second harmonic to the square of the amplitude of the first harmonic are plotted in Figure 8.8 against the number of Freeze Thaw cycles. At around 50 cycles the high potassium batch begins a distinct

separation from the control batch and follows the expected increase reaching a maximum of approximately four times the ratio for the control data before failing.

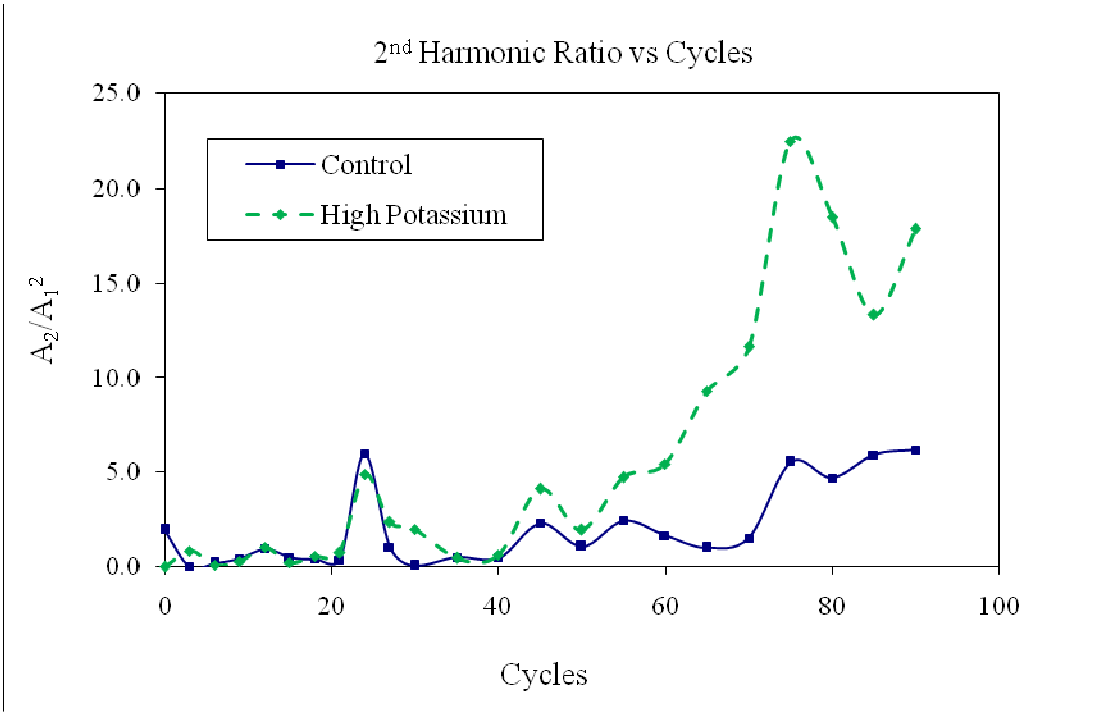

Figure 8.9: Change in 2nd Order Harmonics with F/T cycles

8.6 Summary and Discussion

It is clear that the addition of potassium carbonate to the concrete mix significantly aided the deterioration of the concrete samples. In each of the investigative signal analysis methods the high potassium batch reported data that highlighted its deterioration.

The Q-factor results obtained from the impact echo testing highlighted the deterioration caused by the increased potassium in the concrete mix. However, though consistent, the distinction between the control and the high potassium data was not very distinct. Figure 8.4 shows that though the high potassium batch

produces continuously lower Q-factors the decay of Q-factors is not significantly different from the control data. With increasing damage of the Freeze Thaw cycles the non-linear effects begin to appear. The Q-factor only seems to be capturing the effects of the macro damage caused by the Freeze Thaw tests which is similar for both sets of specimens due to the lack of air entrainment.

In an attempt to quantify the non-linearity and the distorted shape of the response spectra, a Lorentzian analysis was performed to compare the ratios of the areas of the distorted spectra to that of undamaged, undistorted spectra. From the beginning of the test the high potassium batch displays a less congruent fit to the undamaged spectra than the control data. The Lorentzian mismatch is capturing, from a very early stage, the micro-structural damage. This early stage damage may be associated with the high potassium content prior to its manifestation as micro-cracking, which is a larger scale phenomenon. In Figure 8.6 both the control and high potassium data sets approach the asymptote at a similar number of cycles and since the control batch started at higher area ratios it therefore has a higher decay constant.

Classic material non-linearity results in second order harmonic generation. As micro-cracking increases a larger portion of the fundamental wave is expected to be converted into higher order harmonics. High intensity ultrasound is required to detect third order harmonics but the impact echo energy levels were sufficient for second order harmonics to be generated. Woodward et al. suggest that casting direction has a significant influence on the second harmonic where harmonic growth is substantially greater when the wave was propagating in the casting direction rather than against it. This is thought to be due in part to condensation on the bottom side of the aggregate

and the formation of bleed water on the top surface. In general, the harmonic ratio $A_2/(A_1)^2$ is sensitive to micro-structural changes and micro-cracking in the interfacial transition zone while the third harmonic ratio, $A_3/(A_1)^3$ is more sensitive to micro-cracking. These are not mutually exclusive, however, since both deterioration mechanisms contribute to both harmonic ratios. Figure 8.9 then shows that the micro-structural changes and micro-cracking significantly increased for the high potassium batch of concrete, whereas the control samples may just be suffering from the micro-cracking brought about by the Freeze-Thaw tests.

Chapter 9: Summary and Conclusions

9.1 Summary

The original goal of this research lay in investigating the distributed damage associated with delayed ettringite formation[2], by using linear acoustic methods. That goal has metastasized into the investigation of distributed damage in general by using linear and non-linear ultrasonic techniques. The nondestructive determination of early deterioration of concrete is difficult. Deterioration is usually accompanied by micro-cracking which may be caused by stress, creep and shrinkage, ASR and/or DEF. Presently there is no applicable field method for the non-destructive determination of this sort of damage in concrete, especially in its early stages. Consequently, this research was performed with field applicability in mind. The impact echo method proved most suitable in achieving these goals.

In order to achieve the goals stated above concrete specimens were prepared in the laboratory. The primary goal here was to produce concrete samples in which distributed damage could be accelerated whether by DEF, ASR or Freeze Thaw cycling. Additionally a baseline for the determination of the damage had to be set and so a control batch of concrete was also prepared that would be free from the effects of distributed damage. Accelerated damage was achieved on a couple of levels.

From a compositional level, Portland cement type III was used throughout the entire study which exceeds all the threshold values suggested by researchers. In 1994, Taylor outlined threshold values at 0.83% for equivalent Na_2O, 0.22% for Na_2O,

[2] Wolter, S. refers to DEF as the cancer of concrete.

3.6% for SO3 and 1.6 + 0.2% for MgO. Manufactured Frederick Stone Sand conforming to ASTM C33 was used throughout the research. For the concrete batches, Calcitic Limestone ASTM # 57 was used for the coarse aggregate. These materials have been proven to accelerate damage in concrete (Ceesay 2006, Ramadan 2000).

The concrete specimens were then separated by the type of deteriorating cycles that they would undergo. The UMD Modified Duggan Cycle, which is effectively a heat cycle, has been proven to accelerate deterioration in concrete by initiating cracking and ettringite formation (Ceesay, 2007) and takes nine days to complete. Prior to the Duggan cycle the specimens were steam cured, which again is a proven method for initiating DEF in concrete with type III Portland cement. A second set of samples were subjected to Freeze-Thaw cycles in accordance with the relevant ASTM standard. The samples subjected to Freeze thaw cycles were not steam cured. While Freeze Thaw cycles do not necessarily promote DEF they certainly induce distributed damage and micro-cracking.

The progress of damage related parameters was monitored using several tests. The specimens subjected to the Duggan Cycle were tested for expansion, weight change and fundamental frequency in accordance with ASTM C215, every three to five days after the Duggan Cycle. Those specimens subjected to Freeze Thaw cycles in the Rapid Freeze-Thaw Cabinet apparatus were tested every three cycles for the first 30 cycles and every five cycles until failure or until meaningful results could no longer be obtained. Compression strength tests were carried out on specimens subjected to the Duggan Cycle in accordance with ASTM C39. These compression

tests were performed at 7, 30, 90, 120, and 150 days after the completion of the heating regime. Both the Duggan and Freeze Thaw specimens were also subjected to Scanning Electron Microscopy (SEM) and Energy dispersive x-ray analysis (EDAX). This destructive test determined the actual contributors to the distributed damage that is either DEF and/or ASR.

The results of the non-destructive impact echo tests were of primary importance. These results were analyzed using novel and cutting edge signal processing techniques. The Q-factor has been proven to be a useful tool to quantify the linear effects of distributed damage on concrete. The Q-factor is derived from the response spectrum of the specimen after a Fast Fourier Transform has been performed on the waveform from the impact echo test. As damage increases, however, non-linear effects dominate the response. A novel technique was developed to quantify these non-linear effects; the Lorentzian mismatch technique. Also, recent exploration of the second and third harmonics has proved to be useful in quantifying the non-linear effects of damage in concrete.

9.2 Summary of Results

In this research work, all the concrete samples made with additional 1.5% potassium exhibited excessive expansion and a significant reduction in strength.

The results of the tests used to monitor the progress of distributed damage are summarized in Tables 9.1 and 9.2. Chapters 5 and 6 contain the detailed results of these tests.

Table 9.1 - Summary of Test Results of Steam Cured Concrete Specimens Subjected to Duggan Cycle

Test		Control	High Potassium
Expansion (Max)		0.015%	0.076%
Weight Change (Max)		0.678%	0.697%
Resonant Frequency, Hz (Max)		3267	3003
Compressive Strength, psi	37 days	1854	2001
	150 days	5739	3115
SEM Analysis	100 days	No ettringite	Ettringite balls
	150 days	Random ettringite.	Numerous ettrigite balls
	200 days	Ettringite crystals	Numerous ettringite balls

Table 9.2 - Summary of Test Results for Concrete Specimens Subjected to Freeze-Thaw Cycles

Test		Control	High Potassium
Expansion (Max)		1.250%	1.350%
Weight Change (Max)		1.852%	1.696%
Resonant Frequency, Hz (Max)		3240	3227
SEM Analysis	100 days	Minor ettringite	Ettringite balls
	150 days	Random ettringite.	Numerous ettrigite balls
	200 days	Ettringite crystals	Numerous ettringite balls

The results of the signal processing of the impact echo data yielded more reasonable results for the specimens subjected to Freeze Thaw testing than for the specimens subjected to the Duggan Cycle. Chapters 7 and 8 provide detailed discussion on the results of each analysis technique.

The Q-factor results of the specimens subjected to the Duggan cycle proved to be heavily influenced by their storage condition of limewater. Though there was a distinct difference in the control data versus the high potassium data, there was not significant change in the results over time outside the parameter of standard deviation. The continued hydration increased the damping property of the cement and masked the decrease in damping contributed by the distributed damage. For the Freeze Thaw specimens, the distinction between the control and high potassium results was consistent. However, the Q-factor only seems to be capturing the effects of the macro damage caused by the Freeze Thaw tests which is similar for both sets of specimens due to the lack of air entrainment.

The Lorentzian mismatch analysis explored the deviation from the Lorentzian ideal of the response spectrum of an undamaged concrete specimen to that of the actual response spectrum of a damaged concrete specimen. For the Duggan cycle specimens though distinct differences exist between the control and high potassium data, the results are not conforming to what is expected. Again the storage solution may be contributing to the distortion of the results by filling the voids in the concrete and not allowing the response spectra to truly represent the distorted shape of the spectra for the damaged specimens. The transient stress waves depend on the voids in the concrete to report the state of the specimen. The specimens subjected to Freeze

Thaw cycles displayed, through the Lorentzian mismatch analysis, early stage indication of damage that may be associated with the high potassium content and its manifestation as micro-cracking.

The samples subjected to the Duggan cycle did not reveal a consistent trend in the variance of the second harmonic ratio. In most cases this is because the second harmonic is of negligible magnitude. Attenuation is a major factor influencing the magnitude of the second harmonic ratio, and though these samples display significant expansion, they were not noticeably cracked at the end of testing. In general, the harmonic ratio $A_2/(A_1)^2$ is sensitive to micro-structural changes and micro-cracking in the interfacial transition zone. The high potassium samples subjected to Freeze Thaw cycling showed that the micro-structural changes and micro-cracking significantly increased as represented by the approximate exponential increase of the second harmonic ratio which is depicted in Figure 8.9. The control samples displayed far less of an increase of the second harmonic ratio and might only be suffering from the micro-cracking brought about by the Freeze-Thaw tests.

9.3 Conclusions

Based on the results of this research the following conclusions were obtained:

1. The addition of potassium carbonate accelerated deterioration in concrete prisms causing an increase in expansion of specimens subjected to the Duggan and the Freeze Thaw Cycles. The Duggan cycle specimens displayed more exaggerated expansion.
2. The weight changes of these specimens were not significantly affected for both the Duggan and Freeze Thaw cycles.
3. The addition of potassium definitively affected the compressive strength of concrete samples subjected to the Duggan cycle.
4. Based on SEM morphology, the steam curing and the Duggan cycle enhanced DEF but were not critical for its formation. DEF was also observed in the Freeze Thaw specimens.
5. SEM results correlated with expansion results to show that DEF was a major player in the distributed damage observed. SEM results did not detect ASR at any stage.
6. The storage condition of limewater for Duggan specimens helped to mask the detection of distributed damage when signal processing techniques were used for the impact echo data.
7. Second order harmonics proved very useful in detecting micro-structural changes in specimens subjected to Freeze Thaw cycles.

8. The novel Lorentzian mismatch technique was also useful in distinguishing distributed damage in Freeze thaw specimens.
9. The Q-factor is useful only when significant non-linear effects are not present.
10. As micro-cracking increases larger portions of the fundamental wave are converted to higher harmonics.

9.4 Recommendations for Future Work

1. Investigate the effect of varying the specimen size on the signal processing techniques discussed herein.
2. Investigate the effect of air entrainment on the Freeze Thaw samples in producing results over a greater number of cycles.
3. Expand the research to include field tests.
4. Investigate the effect of reinforcement on the signal processing techniques.
5. Optimize the technique for scaling the Lorentzian fit of the undamaged specimen.

Bibliography

1. ASTM C215, “Standard Test Method for Fundamental Transverse, Longitudinal, and Torsional Frequencies of Concrete Specimens,” (2002) *ASTM International*, West Conshohocken, PA.
2. ASTM C192, “Standard Practice for Making and Curing Concrete Specimens in the Laboratory,” (2002) *ASTM International*, West Conshohocken, PA.
3. ASTM C666, “Standard Test Method for Resistance of Concrete to Rapid Freezing and Thawing,” (2002) *ASTM International*, West Conshohocken, PA.
4. ASTM C597, “Standard Specification for Pulse Velocity Measurements in Concrete,” (2002) *ASTM International*, West Conshohocken, PA.
5. Kesner, K., Sansalone, M.J., and Poston, R.W. (2004) "Detection and Quantification of Distributed Damage in Concrete Using Transient Stress Waves", *ACI Materials Journal,* Vol. 101, Issue 4, pp. 318-326.
6. Livingston, R.A., Ormsby, C., Amde, A.M., Ceary, M., McMorris, N., and Finnerty, P., (2006) "Field Survey of Delayed Ettringite Formation Related Damage in Concrete Bridges in the State of Maryland", *Seventh CANMET/ACI Conference on Durability of Concrete, SP-234*, Ed.V.M. Malhotra, ACI, Detroit, MI. pp. 251-268.
7. Clarke, S.L.,(1991) "Improved Method for Non-destructive testing of Concrete Prisms, in Mechanical Engineering". *MSc. Thesis*, U. Washington, Seattle, WA
8. Janssen, D. and Snyder, M., (1994) "Resistance of Concrete to Freezing and Thawing, SHRP-C-391", *Strategic Highway Research Program*, Washington D.C.
9. Malhotra, V.M. and Sivasundaram, V., (2004) "Resonant Frequency Methods", *Handbook on Nondestructive Testing of Concrete*, Eds.V.M. Malhotra and N.J. Carino, , CRC Press: Boca Raton, FL. pp. 7-1 7-18.
10. McMorris, N., Amde, A.M., and Livingston, R.A., (2007) "Improved impact-echo method for quantification of distributed damage in concrete", *Recent Advances in Concrete Technology*, Eds. A.M. Amde, G. Sabnis, and J.S.Y. Tan, DEStech: Washington, DC. pp. 185-194.
11. Zheng, Y., Maev, R.G., and Solodov, I.Y. (1999) "Nonlinear Acoustic Applications for Material Characterization: A Review ", *Can. J. Phys*., Vol. 77, pp. 927-967.
12. Ceesay, J., Amde, A.M., Azzam, A., Livingston, R.A., and Newman, J.W., “Investigations of Modifications to the Duggan Test for Delayed Ettringite

Formation," (2007) *Recent Advances in Concrete Technology*, A.M. Amde, G. Sabnis, and J.S.Y. Tan, Editors. DEStech: Washington, DC. p. 299-311.
13. Lijeron, C., (2008) "Correlating Q-Factor Measurements to Other Parameters in Deteriorated Concrete", *MSc. Thesis*, U. Maryland: College Park, MD.
14. Stauffer, J., Woodward, C., and White, K.R. (2005) "Nonlinear Ultrasonic Testing with Resonant and Pulse Velocity Parameters for Early Damage in Concrete", *ACI Materials Journal*, Vol. 102, Issue 3, pp. 118-121.
15. Livingston, R., McMorris, N., Lijeron, C., and Amde, A. (2008) "Non-Linear Frequency Domain Techniques for Processing Impact Echo Signals for Distributed Damage", *7th International Symposium on Non-Destructive Testing*, NDTCE 09 conference.
16. Brown, P.W., and Bothe, J.V., Jr., (1993) "The stability of ettringite," *Advances In Cement Research*, Vol. 5, No. 18, pp. 47-63.
17. Cheng, C., and Sansalone, M., (1994) "Determining the Minimum Crack Width that can be Detected Using the Impact-Echo Method, Part I: Experimental Study," *RILEM Journal of Materials and Structures*," Vol. 276, pp. 274-285.
18. Day, R., (1992) "The Effect of Secondary Ettringite Formation on the Durability of Concrete: A Literature Analysis," *Research and Development Bulletin RD108T*, Portland Cement Association, 115 pp.
19. Detwiler, R. and Powers-Couche, L., "Effect of Sulfates in Concrete on its Resistance to Freezing and Thawing," (1997) *Presentation at 1997 American Concrete Institute Spring Convention*, Portland Cement Association Research and Development Serial No. 2090.
20. European Committee for Standardization, Concrete (1989) "Performance, Production, Placing and Compliance Criteria," *Final Draft*, European Prestandard.
21. Fu., Y. and Beaudoin, J., (1996) "Mechanisms of Delayed Ettringite Formation in Portland Cement Systems," *ACI Materials Journal*, Vol.93, No. 4, July-August 1996, pp.327-333.
22. Fu, Y., et al., (1994) "Effect of Temperature on Sulphate Adsorption/Desorption by Tricalcium Silicate Hydrates," *Cement and Concrete Research*, Vol. 24, No. 8, pp. 1548-1432, 1994.
23. Grabowski, E., et al., (1992) "Rapid Test of Concrete Expansivity Due to Internal Sulfate Attack," *ACI Materials Journal*, Vol. 89, No. 5, September-October 1992, pp. 469-480.
24. Gress, D., "Early Distress of Concrete Pavements," Federal Highway Administration, Publication No. FHWA-SA-97-045, 53 pp.
25. Heinz, D., and Ludwig, U., (1987) "Mechanisms of Secondary Ettringite Formation in Mortars and Concretes Subjected to a Heat Treatment," Bryant

and Katherine Mather Symposium, American Concrete Institute SP-100, Scanlon, J., Editor, pp. 2059-2071.
26. Kennerley, R., (1964) "Ettringite Formation in Dam Gallery," *Journal of the American Concrete Institute*, Proceedings Vol. 62, No. 5, May 1964, pp. 559-574.
27. Krautkramer, J., and Krautkramer, H., " Ultrasonic Testing of Materials" 4th Ed. Springer-Verlag, Berlin, 1990.
28. Lawrence, C.D. , (1994) "Delayed Ettringite Formation: An Issue?," *Material Science of Concrete IV* , J. Skalny, Editor, The American Ceramic Society, Inc., Westerville, OH 1994, pp.113-154.
29. Livingston, R. A. and Amde, A. M. (2000). "Nondestructive Test Field Survey for Assessing the Extent of Ettringite-Related Damage in Concrete Bridges" *10th Int. Symposium on Nondestructive Characterization of Materials*, Elsevier Science, Ltd., Karaizawa, Japan.
30. Mehta, P. "Concrete Structures, Properties and Materials," Prentice Hall Inc., Englewood Cliffs, NJ, 1986, 450 pp.
31. Mehta, P., "Mechanism of Expansion Associated with Ettringite Formation," *ACI Materials Journal* Vol. 3, No. 1, 1973, pp.1-6.
32. Mielenz, R., Marusin, S., Hime, W., and Jugovic, Z., "Investigation of Prestressed Concrete Railway Tie Distress,", *Concrete International*, Vol. 17, No. 12, Dec. 1995, pp.62-68.
33. Neville, A, and Brooks, J., "Concrete Technology" John Wiley and Sons, Inc., New York, NY, 1987, 438 pp
34. "Portland Cement: Past and Present Characteristics," *PCA Concrete Technology Today*, Vol. 17/ Number 2, July 1996.
35. Ramadan, E. O., Amde, A. M., Livingston, R. A. (2000), "The Effect of Potassium and Initial Curing Concrete Expansion Associated with Delayed Ettringite Formation," *ACI Materials Journal* Vol. 17, No. 12, Dec. 2000, pp.62-68
36. Sansalone, M. and Carino, N., (1987) "Impact-Echo: A Method for Flaw Detection in Concrete Using Transient Stress Waves" NSBIR 86-3452, National Bureau of Standards, Gaithersburg, MD, Sep., 1987, 222 pp.
37. Sansalone, M., and Streett, W., (1997) "Impact-Echo Nondestructive Evaluation of Concrete and Masonry," Bullbrier Press, Ithaca, NY, 1997, 339 pp.
38. Taylor, H.F.W., (1984) "Delayed Ettringite Formation," *Advances in Cement and Concrete*, New Hampshire Conference, American Society of Civil Engineers, NY 1994, pp. 121-131.
39. Tepponen, P., and Eriksson, B., (1987) "Damages in Concrete Railway Sleepers in Finland," *Nordic Concrete Research*, No. 6, 1987, pp. 199-207.

40. Williams, T.J., et al., (1997) "Nondestructive Evaluation of Masonry Structures using the Impact-Echo Method," *The Masonry Society Journal*, Vol. 15, No. 1, June 1997.
41. Wolter, S., (1997) “Ettringite: The Cancer of Concrete”, Burgess Publishing, St. Paul, MN.
42. Yang, R., Lawrence, C., and Sharp, J, (1996) “Delayed Ettringite Formation in 4-Year Old Cement Pastes”, *Cement and Concrete Research*, Vol. 26, No. 11, pp. 1649-1659.
43. Ekolu, S.O., Thomas, M.D.A., Hooton, R.D. (2006). “Implications of pre-formed microcracking in relation to the theories of DEF mechanisms”. Elsevier Ltd., *Cement and Concrete Research* Vol.37, 161-165.
44. El-Korchi, T., Gress, D., Baldwin, K., and Bishop, P. (1989), “Evaluating the Freeze-Thaw Durability of Portland Cement-Stabilized-Solidified Heavy Metal Waste Using Acoustic Measurements”. *Environmental Aspects of Stabilization and Solidification of Hazardous and Radioactive Wastes*. ASTM STP 1033, P.L. Cote and T. M. Gilliam, Eds., American Society for Testing Materials. Philadelphia, pp.184-191.
45. Amick, H., and Monteiro, P., (2006). “Experimental Determination of Modal Damping in Concrete Beams”. *ACI Materials Journal* Vol. 103, No. 3
46. Stauffer, J., Woodward, C., and White, K., (2005). “Non-linear Ultrasonic Testing with Resonant and Pulse Velocity Parameters for Early Damage in Concrete”. *ACI Materials Journal*, Vol. 102, No. 2.
47. Ceesay, J. (2004). “The Influence of Exposure Conditions on Delayed Ettringite Formation in Mortar Specimens”. *M.S. Thesis*, University of Maryland, College Park, USA
48. Coppola, J. A., and Bradt, R.C., (1973) “Thermal Shock Damage in SiC,” *Journal of the American Ceramic Society,* Vol. 56, No.4, pp. 214-218.